

APPLICATION OF CELLULOSE NANOCRYSTALS AND ZINC OXIDE AS A GREEN
FIRE RETARDANT SYSTEM IN HIGH DENSITY POLYETHYLENE

A Thesis
Submitted to the Graduate Faculty
of the
North Dakota State University
of Agriculture and Applied Science

By

Ghazal Vahidi

In Partial Fulfillment of the Requirements
for the Degree of
MASTER OF SCIENCE

Major Program:
Mechanical Engineering

May 2019

Fargo, North Dakota

North Dakota State University
Graduate School

Title

Application of Cellulose Nanocrystals and Zinc Oxide as a Green Fire-
Retardant System in High Density Polyethylene

By

Ghazal Vahidi

The Supervisory Committee certifies that this *disquisition* complies with North Dakota
State University's regulations and meets the accepted standards for the degree of

MASTER OF SCIENCE

SUPERVISORY COMMITTEE:

Dr. Dilpreet Bajwa

Chair

Dr. Long Jiang

Dr. Nicole Stark

Approved:

7/1/2019

Date

Dr. Chad Ulven

Department Chair

ABSTRACT

Polymeric materials are widely used in diverse applications. However, a major weakness in majority of the thermoplastic polymers is their lack of ability to resist fire. Most of the chemicals and additives currently used to improve fire retardancy have deleterious effects on the environment. This research focuses on developing an environmentally safe and effective fire-retardant system for high density polyethylene (HDPE), using cellulose nanocrystals (CNCs) and zinc oxide (ZnO). The effect of CNCs coated with nano ZnO has been investigated for improving the fire resistance properties of the HDPE. Improved dispersion of CNCs into HDPE matrix was achieved by employing maleic anhydride as a coupling agent. It was found that addition of CNCs-ZnO can introduce a reasonable level of flame retardancy in HDPE matrix in addition to improving the maximum tensile strength and elongation at break.

ACKNOWLEDGEMENTS

I would like to especially thank my adviser Dr. Dilpreet Bajwa for providing me an opportunity to work within his research group for the last two years and for the guidance he has shown me along the way. Many thanks to my committee members as well, Dr. Long Jiang and Dr. Nicole Stark for their time, patience and direction on this project.

I would like to thank the USDA-NIFA for providing funding for this thesis research project; without USDA's investment, this research would not be possible. I would also like to thank US Forest Products Lab for supplying cellulose nanocrystals and testing fire properties of the composites.

I would like to acknowledge several other members of the North Dakota State University team for their assistance in this project, Jamileh Shojaeiarani, Amir Darabi, Chad Rehovsky, Joshua Liaw, and Ashkan Eslaminejad. Thank you for assistance in completing this project and helping me to learn a variety of testing techniques and research practices which have formed the basis for my research career.

The last but not the least, I would like to thank my family for their support, love, and inspiration along my way in my whole life.

DEDICATION

To my Husband:

Amir

To my Family:

Behzad, Mahvash, Zari

Thank you for your unconditional love and support.

TABLE OF CONTENTS

ABSTRACT.....	iii
ACKNOWLEDGEMENTS.....	iv
DEDICATION.....	v
LIST OF TABLES.....	ix
LIST OF FIGURES.....	x
LIST OF ABBREVIATIONS.....	xiii
LIST OF SYMBOLS.....	xv
CHAPTER 1. INTRODUCTION.....	1
1.1. Polymer nanocomposites.....	1
1.2. Fire hazard.....	1
1.3. Flame retardants.....	2
1.4. Commercial flame retardants.....	2
1.5. Green fire retardants.....	3
1.6. Zinc oxide.....	3
1.7. Cellulose nanocrystals.....	4
1.8. ZnO-CNCs flame retardant system.....	5
1.9. High Density Polyethylene.....	5
1.10. Compatibilizers and coupling agents.....	6
1.11. Summary.....	7
1.12. Research objectives.....	7
CHAPTER 2. LITERATURE REVIEW ON FLAME RETARDANCY.....	9
2.1. Thermal limitations of the polymers.....	9
2.2. Fire triangle.....	9
2.3. Flame retardancy mechanisms.....	10

2.4. Traditional flame retardants.....	11
2.4.1. Halogenated materials.....	11
2.4.2. Phosphorous materials	12
2.5. Nanosized fire retardants	13
2.5.1. Nanoclays.....	14
2.5.2. Metal oxides.....	16
2.5.3. Bio based products	18
2.6. Characterization methods of flammability	21
2.6.1. Limiting oxygen index (LOI).....	22
2.6.2. UL-94	22
2.6.3. Cone calorimetry.....	23
2.6.4. Thermogravimetric analysis.....	24
2.6.5. Summary	24
CHAPTER 3. MATERIALS AND METHODS	26
3.1. Design of experiment.....	26
3.1.1. Synthesis of the nano-sized zinc oxide	26
3.1.2. Synthesis of nanocomposites, Method 1: Template approach via solvent exchange .	27
3.1.3. Synthesis of nanocomposites, Method 2: Physical attachment of PEO on CNCs.....	29
3.1.4. Synthesis of nanocomposites, Method 3: Direct feeding with coupling agent.....	30
3.2. Nanocomposite characterization methods	35
3.2.1. Fourier transform infrared (FTIR) spectroscopy	35
3.2.2. Fractured surface morphology	35
3.2.3. Melt flow index (MFI)	35
3.2.4. Differential scanning calorimetry (DSC).....	36
3.2.5. Mechanical properties (Tensile Test).....	36

3.2.6. Dynamic mechanical analysis (DMA).....	37
3.2.7. Rheological properties	38
3.2.8. Thermogravimetric analysis (TGA).....	38
3.2.9. Horizontal burn test.....	39
3.2.10. Statistical analysis.....	40
CHAPTER 4. RESULTS AND DISCUSSION.....	41
4.1. PEO physical attachment method.....	41
4.1.1. Fourier transform infrared (FTIR)	41
4.1.2. Differential scanning calorimetry (DSC).....	42
4.1.3. Mechanical properties (Tensile Test).....	43
4.1.4. Dynamic mechanical analysis (DMA).....	44
4.2. Direct feeding with coupling agent method.....	45
4.2.1. Fourier transform infrared (FTIR) spectroscopy	45
4.2.2. Fractured surface morphology	47
4.2.3. Melt flow index (MFI).....	51
4.2.4. Mechanical properties (Tensile test).....	54
4.2.5. Dynamic mechanical analysis (DMA).....	56
4.2.6. Rheological properties	60
4.2.7. Thermogravimetric analysis (TGA).....	66
4.2.8. Horizontal burn test.....	73
CHAPTER 5. CONCLUSION AND FUTURE WORK.....	77
REFERENCES	80

LIST OF TABLES

<u>Table</u>	<u>Page</u>
2.1. Common halogenated FRs, chemical structure and additional information.....	12
2.2. List of common nano flame retardants in polymer composites.....	14
2.3. Classification of materials for the UL94 Vertical Burn test.	23
3.1. PEO treatment formulations.	30
3.2. Direct feeding formulations, CNCs-ZnO – HDPE-MA (separately used).	33
3.3. Direct feeding formulations, CNCs-ZnO – MAPE1 (without initiator).	33
3.4. Direct feeding formulations, CNCs-ZnO – MAPE2 (with initiator).	34
3.5. Direct feeding formulations, CNC-ZnO– PHDPE-MA (powder HDPE).....	34
4.1. Tensile properties of composite samples in PEO treatment.	44
4.2. Tensile properties of composite samples and original polymers in direct feeding method.....	56
4.3. Dynamic mechanical properties of HDPE and nanocomposites obtained from DMA.	57
4.4. Thermal properties of HDPE, PHDPE, and their nanocomposites.....	69
4.5. Fire characteristic of composite samples with HDPE-MA from horizontal burn test.....	76
4.6. Fire characteristic of composite samples with MAPE1 from horizontal burn test.....	76
4.7. Fire characteristic of composite samples with MAPE2 from horizontal burn test.....	76
4.8. Fire characteristic of composite samples with PHDPE-MA from horizontal burn test.....	76

LIST OF FIGURES

<u>Figure</u>	<u>Page</u>
1.1. The chemical structure of the cellulose molecule.....	4
1.2. Chemical structure of HDPE	6
1.3. Maleic anhydride grafted on polyethylene polymer	6
1.4. Chemical structure of PEO	7
2.1. Schematic of Emmon's fire triangle and polymer pyrolysis	10
2.2. Flame retardancy mechanism of phosphorous FR in epoxy resin [45].....	13
2.3. Representation of a cellulose fiber showing its organization.	20
2.4. Kinetic model for cellulose pyrolysis by Broido [81]. k_1 , k_2 , and k_3 represent different kinetic energies existed for each step of the model.....	20
3.1. Zinc oxide in a) sol gel form before drying and b) powder form after drying under the hood.....	27
3.2. Solvent exchange process in reflux condenser.	28
3.3. PEO-modified ZnO coated CNCs a) solution form, b) powder form after cryogenic grinder	30
3.4. a) CNCs powder b) ZnO powder c) CNCs-ZnO film before grinding.	31
3.5. a) Twin-screw extruder b) Mini-Jector injection molding machine.	34
3.6. Melt flow indexer.....	36
3.7. Tensile testing apparatus and loaded sample.	37
3.8. Three-point loading configuration of a flexural sample in DMA test.	38
3.9. Thermogravimetric analyzer.....	39
3.10. Horizontal burn test set up base on ASTM D635.	40
4.1. FTIR spectra of PEO modified ZnO-coated CNCs in HDPE matrix in absorbance mode.....	42
4.2. Representative DSC curves for PEO treatment during second heating scan of composite pellets.....	43

4.3.	DMA curves for PEO treatment, Storage modulus vs. temperature.....	44
4.4.	DMA curves for PEO treatment, Loss modulus vs. temperature.	45
4.5.	FTIR spectra of HDPE, MAPE1, MAPE2, PHDPE and their nanocomposites in absorbance mode.....	47
4.6.	SEM micrographs of HDPE-MA nanocomposites 1) HDPE-MA-3CNCs-3ZnO-P, 2) HDPE-MA-3CNCs-3ZnO-F, 3) HDPE-MA-5CNCs-5ZnO-P, 4) HDPE-MA-5CNCs-5ZnO-F at three magnifications a) 90X, b) 300X, c) 1000X	49
4.7.	SEM micrographs of MAPE2 nanocomposites 1) MAPE2-3CNCs-3ZnO-P, 2) MAPE2-3CNCs-3ZnO-F, 3) MAPE2-5CNCs-5ZnO-P, 4) MAPE2-5CNCs-5ZnO-F at three magnifications a) 90X, b) 300X, c) 1000X.....	50
4.8.	SEM micrographs of PHDPE-MA nanocomposites 1) PHDPE-MA-3CNCs-3ZnO-P, 2) PHDPE-MA-5CNCs-3ZnO-P at three magnifications a) 90X, b) 300X, c) 1000X.....	51
4.9.	Comparison of the melt flow index of virgin HDPE vs. HDPE-MA and MAPE2. Addition of MA increased viscosity and adding initiator increased it even further.	52
4.10.	Comparison of the melt flow index of HDPE-MA vs. different nanofiller loadings. Addition of nanofillers decreased viscosity.	53
4.11.	Comparison of the melt flow index of PHDPE vs. different nanofiller loadings. Addition of nanofillers decreased viscosity.....	53
4.12.	Comparison of the melt flow index of MAPE2 vs. different nanofiller loadings. Addition of nanofillers increased MFI.....	54
4.13.	Representative storage modulus vs. temperature curves for HDPE-MA and nanocomposites.....	58
4.14.	Representative storage modulus vs. temperature curves for MAPE2 and nanocomposites.....	59
4.15.	Representative storage modulus vs. temperature curves for PHDPE-MA and nanocomposites.....	60
4.16.	Complex viscosity for a) HDPE-MA and nanocomposites b) MAPE2 and nanocomposites c) Powder HDPE and nanocomposites.	62
4.17.	a) Storage modulus for HDPE- MA and its nanocomposites b) Loss modulus for HDPE- MA and its nanocomposites.	64
4.18.	a) Storage modulus for MAPE2 and its nanocomposites b) Loss modulus for MAPE2 and its nanocomposites.	65

4.19.	a) Storage modulus for PHDPE and its nanocomposites b) Loss modulus for PHDPE and its nanocomposites.....	66
4.20.	TGA and DTG curves for HDPE-MA composites.....	70
4.21.	TGA and DTG curves for MAPE1 composites.....	71
4.22.	TGA and DTG curves for MAPE2 composites.....	72
4.23.	TGA and DTG curves for PHDPE composites.....	73

LIST OF ABBREVIATIONS

ATH	Aluminum Trihydrate.
CNCs.....	Cellulose Nanocrystals.
CNF.....	Cellulose Nanofibers.
DMA	Dynamic Mechanical Analyzer.
DSC.....	Differential Scanning Calorimetry.
DTG	Derivative Thermogravimetric.
EPDM	Ethylene-Propylene-Diene Monomer
FR.....	Fire retardant.
FTIR.....	Fourier-Transform Infrared Spectroscopy.
HDPE	High Density Polyethylene.
IFR	Intumescent Flame Retardant.
GPC.....	Gel Permeation Chromatography.
LOI.....	Limited Oxygen Index.
MAPE	Maleic Anhydride grafted Polyethylene.
MFI	Melt Flow Index.
MH	Magnesium Hydroxide.
PBS	Poly (1,4-butanediol succinate).
PEO.....	Poly Ethylene Oxide.
PHDPE.....	Powder High Density Polyethylene.
pHRR	Peak Heat Release Rate.
PLA.....	Poly (lactic acid).
PP	Polypropylene.
PVC.....	Polyvinyl Chloride.
SEM	Scanning Electron Microscopy.

T_{onset} Initial Decomposition Temperature.

T_{endset} Temperature at the End of the Thermal Degradation.

TGAThermogravimetric Analysis.

UV.....Ultra Violet.

ZnOZinc Oxide.

LIST OF SYMBOLS

°C	Celsius.
kg	Kilogram.
kJ/m ²	Kilojoule/square meter.
kN	Kilo Newton.
mm	Millimeter.
mm/min	Millimeter/minute.
MPa	Mega Pascal.
T _{onset}	Initial Decomposition Temperature.
T _g	Glass Transition Temperature.
T _m	Melting Temperature.
W%	Total Weight-loss.
wt%	Weight Percent.
T _{endset}	Temperature at the End of the Thermal Degradation.

CHAPTER 1. INTRODUCTION

1.1. Polymer nanocomposites

Polymer nanocomposites, tailored material with enhanced characteristics, have attracted a lot of interests as a vital alternative for traditional metallic materials over the recent decades. Polymer nanocomposites are polymer matrices containing homogeneously dispersed nano-sized reinforcing fillers (1-100 nm at least in one dimension) [1, 2]. They broadly involve science, engineering, and technology and are used in various industrial sectors especially in automotive, building products, and aerospace sector [3]. Thermoplastics such as polyolefins and polyamides are among the most representative choices as a matrix in polymer nanocomposite owing to their ease of processing, recyclability, good mechanical properties, and cost-effective manufacturing methods [4]

Despite the vast potential of thermoplastic nanocomposites, compatibility, environmental impacts, and high flammability have limited their applications in safety-oriented segments. High susceptibility to combustion under fire, thermal degradation and decomposition, and release of toxic gases under combustion are considered as the major weaknesses of these polymeric materials [5].

1.2. Fire hazard

Fire hazard is a general term that is a combination of different factors, including ignitability, amount of heat release, ease of extinction, weight-loss, flame spread, smoke index, and toxicity [6]. Modern life is surrounded by a wide variety of readily combustible materials such as cellulosic materials and man-made polymers [7]. Synthetic polymers alone may not be a fire hazard, but they are factors that contribute to ignition and the rapid spread of fire in vehicles, residential buildings, and other facilities [8].

According to the USA Fire Administration annual report [9] during 2017 in the US alone there were more than 1 million residential fires, injuring 14,000 people and killing more than 3,000 people along with billions of dollars financial loss.

1.3. Flame retardants

In order to meet fire safety requirements and diminish fire hazards, different solutions have been developed. For polymers in particular, various chemical and physical strategies have been evolved to prevent burning, or at least slow it down [10]. Recently, flame retardants (FRs) have been widely recognized as fire safety tools capable of lowering the number of fire injuries and deaths. Thus, adding flame retardants to polymers, fibers, and papers has become more prevalent to protect the final product from burning [11].

Therefore, it is clear that flame retardants are an important part of polymer composite formulations, especially for applications where the polymer has a significant chance of being exposed to an ignition source such as in electronic and electrical applications, where polymers are easily ignitable like in plastic bottles, or with building and transportation materials where the rapid spread of fire may cause issues during evacuation [12].

1.4. Commercial flame retardants

Halogenated and phosphorous flame retardants are well-known in various fire retardancy applications that can augment fire performance of the polymers under combustion. However, it is worth noting that widely used halogenated FRs contain chemicals that are hazardous to human health and are environmentally deleterious [13] because they are considered as persistent organic pollutants, which are hard to break and oxidize in the environment [11].

1.5. Green fire retardants

To improve the fire retardancy of the polymer composites and to ensure human health safety and eco-friendliness, a renewed interest is emerging for the development of sustainable and safe solutions of FRs in polymeric composites. The most common FRs falling in this definition are saccharide-based products, bio-based aromatic products, minerals, and proteins. When added in polymers, bio-based fire retardants such as lignin and cellulose are able to generate an insulating char layer on the surface of the polymers during their thermal decomposition. This barrier layer can reduce the amount of smoke release and oxygen flow as a result of its condensed phase action. Mineral flame retardants, such as aluminum trihydroxide (ATH) and zinc oxide, are very efficient in decreasing the fire hazard and they are widely used in commercial applications due to the fact that they do minimal when it comes to harming the human body or the ecosystem [10].

1.6. Zinc oxide

Among different mineral FRs, zinc oxide (ZnO) is known to be one of the most promising options due to the low cost, high surface reactivity, large number of active sites, and non-toxicity. ZnO particles can reduce the thermal impact in polymers because of their high heat capacity [14, 15]. Nano-sized ZnO can be synthesized through simple, fast, and cost effective laboratory methods [16]. Due to the high excitation bonding energy along with the large width of band, these nanoparticles have lots of potential applications. Current applications of ZnO are mostly in inflammatory, wound healing, and antioxidant properties [17, 18]. Smaller size and larger specific area of nano-sized ZnO over micro-sized options can result in stronger interfacial interactions while compounding with other components [19].

1.7. Cellulose nanocrystals

Cellulose is one of the most abundant organic materials in the world that has attracted a lot of interests in the recent years due to its sustainability and also its potential to be a rich feedstock for extracting various chemicals and high value products. Cellulose is a condensation linear homopolymer composed of β -1,4-linked glucopyranose units (Figure 1.1). Cellulose in fiber form can be found in the cell wall of various plants. These fibers can turn into nano-sized products in different sizes and shapes by using various methods such as acid hydrolysis, which attack the amorphous regions of the cellulose fibers while crystalline regions remain intact. This results in production of cellulose nanocrystals (CNCs).

CNCs are considered as promising nanofillers in polymeric matrices because of their high crystallinity, high aspect ratio, and resulting superior mechanical and thermal properties [20, 21]. However, CNCs alone are not able to improve the thermal stability of the polymers [10]. Even though the charring effect of CNCs can significantly reduce the weight-loss of the polymers during combustion [10], additional fire retardants is still essential to improve the fire performance of polymer nanocomposites.

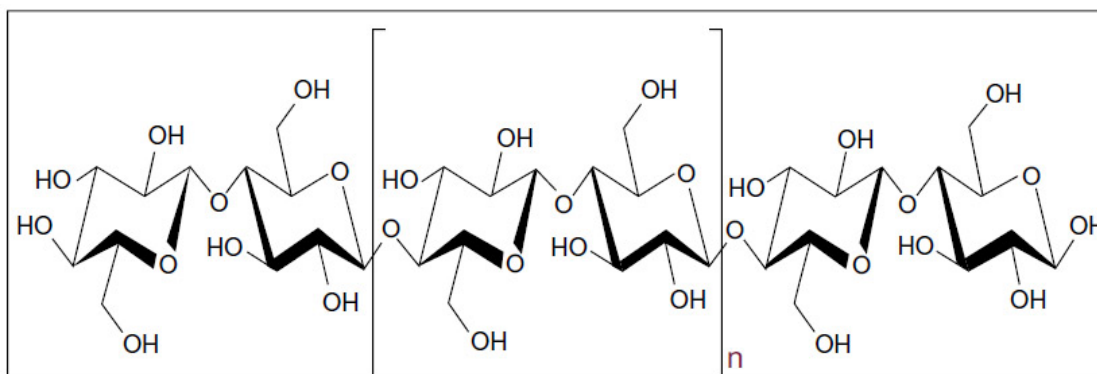


Figure 1.1. The chemical structure of the cellulose molecule.

1.8. ZnO-CNCs flame retardant system

Zinc oxide can be deposited on CNCs surface due to similar polarities in their nature. Incorporating ZnO-coated CNCs in the polymer matrix can lead to higher thermal stability and fire retardancy of the polymer nanocomposites through uniform dispersion of ZnO coated CNCs in the polymer [22]. Strong interfacial interaction between ZnO coated CNCs and polymer matrix as well as uniform dispersion of nanofillers is highly desirable in order to obtain superior mechanical and thermal properties of the composite. Hydrophilic nature of cellulose nanocrystals due to the presence of numerous hydroxyl groups on their surface limits their uniform dispersion through hydrophobic polymers [23]. Therefore, various methods have been presented for chemical modification of CNCs surface [24, 25]. However, large scale industrial production of cellulose nanocomposites typically avoids laboratory procedures and time consuming methods and involves direct mixing approaches such as melt extrusion [23].

1.9. High Density Polyethylene

High Density Polyethylene (HDPE) is one of the most commonly used thermoplastic polymers that is produced from the monomer ethylene in an addition polymerization process (Figure 1.2). Low cost, high strength to density ratio, and recyclability make this polymer an attractive candidate for a diverse range of applications. However, high flammability and fast flame spread rate have become of the main concerns while employing polyethylene polymer in safety oriented applications [26]. Reinforcement of HDPE with nano-sized materials have been a field of interest to achieve higher mechanical and thermal properties [1]. Although, highly hydrophobic nature of HDPE has prevented nanoparticles to disperse uniformly as mentioned before.

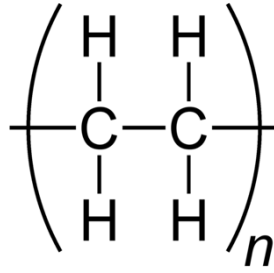


Figure 1.2. Chemical structure of HDPE.

1.10. Compatibilizers and coupling agents

Since direct mixing of nanofillers in a polymer matrix was more commercially viable, a lot of research is dedicated to find proper compatibilizers in order to enhance the interfacial attractions [27]. Maleic anhydride (MA) is one of the most promising options. It helps to enhance the interactions between CNCs and HDPE via an esterification reaction and hydrogen bonding of MA functional groups (-COOH and -C=O) and cellulose hydroxyl groups (-OH) [28]. MA modified HDPE is normally prepared by free radical grafting of the MA on HDPE backbone in the presence of peroxide initiator either in solution or melt [29] (Figure 1.3).

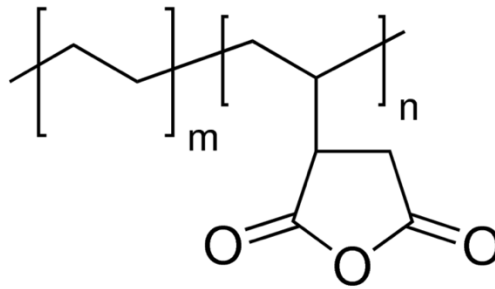


Figure 1.3. Maleic anhydride grafted on polyethylene polymer.

Polyethylene oxide (PEO) is among common dispersion agents that also can be employed to increase the adhesion between the fillers and the polymer. Physical attachment of PEO to the polymer backbone can happen by decreasing the surface tension through non-chemically bonded and dipole-dipole interactions [20].

feeding of HDPE and maleic anhydride (MA) coupling agent with ZnO-coated CNCs via melt-extrusion.

Research objectives and hypothesis of this thesis are as follows;

1. The first objective is to synthesize nano-sized ZnO particles and to coat them on CNCs' surface, hypothesizing that using a simple laboratory method will result in successful production of nano-sized ZnO.
2. The second objective is to incorporate ZnO coated CNCs in an HDPE matrix through physical or mechanical methods, hypothesizing that using these methods will assist uniform dispersion of the nanofillers in the HDPE matrix.
3. The third objective is to evaluate the fire performance and mechanical properties of the polymer nanocomposites, hypothesizing that incorporation of nanosized fillers will improve HDPE mechanical and thermal performance.

CHAPTER 2. LITERATURE REVIEW ON FLAME RETARDANCY¹

2.1. Thermal limitations of the polymers

Polymers are large organic molecular chains comprising of a series of repeating monomers that have expressively contributed to the quality of daily life. Natural occurring polymers such as cellulose, rubber, and wool abound in the nature, while synthetic polymers were introduced into the market in the 1800s. Generally, polymers are found in an extensive range of applications including automotive industry, food packaging, textiles, and biomedical devices, due to their light weight, corrosion resistant structure, and unique behavior [30, 31]. Beside these advantages, the specific structure of the polymers limits their applications when they are exposed to heat [32]; most thermoplastic polymers undergo significant thermal degradation [33], which has a substantial effect on their service life and limit their applications in different fields. In particular, polymers need to be qualified for long-term service in inhospitable environments. Understanding the principal elements of fire and polymer thermal degradation process will benefit developing methods to boost fire performance and thermal stability of polymers.

2.2. Fire triangle

The life cycle of a flame is a fundamental step in understanding polymer pyrolysis. There are three crucial elements that a fire needs to be ignited: fuel, heat, and oxidizing agent (generally oxygen) [34]. Combustible polymers, which can act as fuel, will catch on fire in the presence of heat and oxygen. At elevated temperatures higher than polymers' decomposition temperature, chemical bonds start to break in the molecular level and free radicals with lower molecular weights

¹ The materials of this chapter were co-authored by Ghazal Vahidi, Dilpreet S. Bajwa, and Jamileh Shojaeiarani. Ghazal Vahidi wrote this chapter in consultation with Dilpreet S. Bajwa and Jamileh Shojaeiarani. Ghazal Vahidi was the primary collector of the material of this chapter, and also drafted and revised all versions of this chapter. Dilpreet S. Bajwa also served as proofreader and supervised findings of this work.

will be formed to create mostly combustible gases. In the presence of sufficient oxygen and energy sources, combustion of polymers will initiate. This process can become self-sustaining if it produces enough energy and risen flames can easily propagate [35].

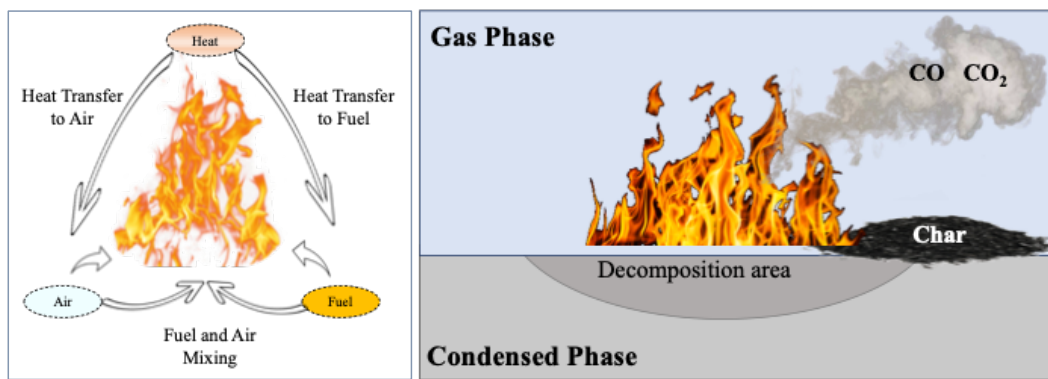


Figure 2.1. Schematic of Emmon's fire triangle and polymer pyrolysis.

2.3. Flame retardancy mechanisms

According to their specific mechanisms, fire retardants interrupt polymer pyrolysis process in one or more steps. Three of the most common flame retardancy mechanisms are listed as below [35, 36].

1. Gas phase inhibition mechanism; the FRs that act in this stage, react with the polymer under combustion in the gas phase. These free radical scavengers bond with the existent hydroxyl or oxygen agents at the molecular level and extinguish the combustion. Halogenated and phosphorous FRs are common in this category.
2. Cooling mechanism; some of the halogen-free components such as hydrated minerals make up a class of FRs that decompose in an endothermic reaction when exposed to fire. They release water molecules that cool down the combustion environment of polymers.
3. Solid phase char formation mechanism; there are two types of FRs that act in this stage. FRs with charring effect (e.g. Silicon or carbon family FRs [37]) or FRs which cross-

link to the polymer matrix in elevated temperatures and create a barrier layer that hinders the heat transfer and release of additional gasses. Intumescent FRs such as melamine compounds and phosphorous compounds are from this category. They react to form a porous carbonaceous 3D-char layer that insulate the polymer surface and slow down the pyrolysis [38, 39].

2.4. Traditional flame retardants

2.4.1. Halogenated materials

As discussed before, halogenated flame retardants interrupt in the gas phase stage by producing free radicals in a continuous stream. High energy OH^* and H^* radicals that are generated during the combustion of the polymer (R^*) react with halogen radicals (X^*), which are released from halogenated hydrocarbon (RX) as in equations (2.1-2.4) [40].

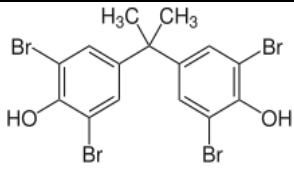
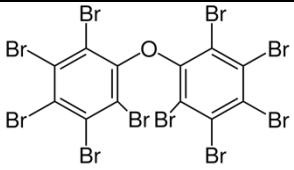
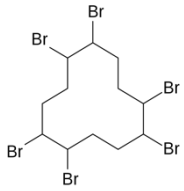
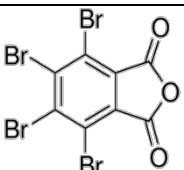


Type of the halogen in halogenated FRs is the key that determines their effectiveness. Bromine and chlorine based halogenated FRs bond with polymers' carbon atoms in low bond energies [40]. As a result, they can take part in the combustion process easily following the mechanism discussed earlier.

However, more thermally stable types of FRs such as fluorine compounds are not very common when it comes to polymer fire retardancy. This is due to the reason that they won't release halogen radicals in the same range or below the decomposition temperatures of most of the polymers since they are more thermally stable [41]. Iodine-based compounds are also not very

common in plastics because they have weak thermal stability and they release halogen radicals usually in processing temperature range of polymers [35, 40, 41]. The most commonly used halogenated FRs [13, 42] are listed in Table 2.1.

Table 2.1. Common halogenated FRs, chemical structure and additional information.

Halogenated FR	Code	Chemical formula	Additional info.
Tetrabromobisphenol A	TBBPA		Most common halogenated FR, reactive FR in epoxy resins
Polybromodiphenylether	PBDE		Contains 10 bromine atoms, FR additives in styrene polymers, polyolefins, polyesters and nylons.
Hexabromocyclododecane	HBCD		cycloaliphatic halogenated FR, expanded or compact PS and textiles
Tetrabromophthalic anhydride	TBPA		FR additive in unsaturated polyesters, base material for other FRs

2.4.2. Phosphorous materials

Halogen-free phosphorous-based FRs are recognized as the most available alternate for halogen-containing components. These FR additives can be assigned to the polymer chains during polymerization and take place in combustion process in gas and/or solid phase among cooling effect. These compounds include a wide range of products: phosphates and red phosphates, phosphines and phosphine oxides, phosphonates and phosphonium compounds. Dehydration and

char formation are two major mechanisms of act for these components, especially in combustion of the oxygen-containing polymers e.g. cellulose, polyamides, etc. [43, 44].

Most of the phosphorus-based FRs can provoke dehydration of polymer chain ends and char formation by liberating moisture during phosphoric acid condensation into pyrophosphate and water (during thermal decomposition). This inherent flame-retardant mechanism can be carried as that in Figure 2.2 for epoxy resin composite [45]. It is worth mentioning that delivering water can also cause dilution of the oxidizing gas phase. However, condensation and dehydration can induce stress corrosion cracking in some applications. Moreover, some studies have indicated that phosphorous-based FRs act as neurotoxicants (substances capable of causing adverse effects in the central and peripheral nervous system, and in sense organs) after they break in the environment [41].

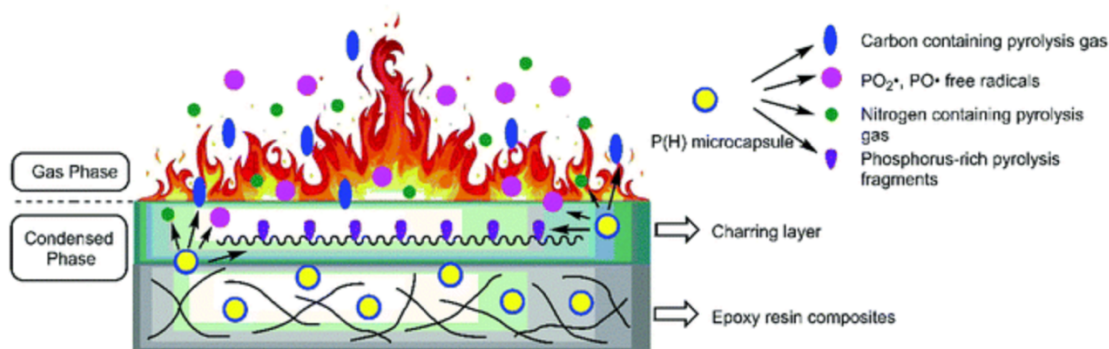


Figure 2.2. Flame retardancy mechanism of phosphorous FR in epoxy resin [45].

2.5. Nanosized fire retardants

With the advent of nanotechnology in the past few decades, the prospects of polymer-based nanocomposites in the application of flame retardant have progressed rapidly. Although nanofillers do not show excellent fire retardance [46], incorporation of a low amount of nanofillers in nanocomposites inherently tend to provide drastic improvement in thermal stability and flame

retardancy [47], smoke release amount [48], peak heat release rate (PHRR) and the speed at which flames spread throughout the nanocomposites [46].

The main mechanism of fire retardancy for nanocomposites, which happens in the condensed phase, depends on different factors such as structure, chemical composition of the nanofillers [49], and nanofiller dispersion [50]. In general, the presence of nanofillers in polymer matrix can alter the overall response of nanocomposites in the exposure to flame.

A list of the most common employed nanofillers in nanocomposites with the aim of fire retardancy is summarized in Table 2.2. Fire retardancy mechanism and selected works reported by the literature were discussed for some of the nano flame retardants in the following paragraphs.

Table 2.2. List of common nano flame retardants in polymer composites.

Nanofiller		Nanofiller loading	Polymer matrix	Reference
Nanoclay		5, 10, and 15 wt. %	polyurethane	[51]
Graphene		2 wt%	polyurethane	[52]
Carbon nanotube		5-40 wt%	polyketone	[53]
Metal oxides	ZnO ₂ nanowires	10-40 wt%	polypropylene	[54]
	SnO ₂ . MnO ₂	2 wt%	Epoxy	[55]
	Zinc borate	30 wt%	polypropylene	[56]
	Zinc oxide	1 wt%	polypropylene-ethylene-propylene-diene monomer	[57]
Cellulose nanocrystals (treated)		10 wt%	Poly(lactic acid)	[58]

2.5.1. Nanoclays

Nanoclays are ubiquitous nanofillers and isolated from naturally occurring clays through energetic stirring, followed by centrifugation and freeze-drying, centrifugation and cross-flow filtration, and ultracentrifugation. Nanoclays are composed of stacked mineral silicate layers, forming complex clay crystallites. Three main mechanisms have been reported for fire retardancy

in composite materials containing clay particles, including migration [59], barrier [60], and paramagnetic mechanisms [61].

In the combustion process of the composites containing clay particles, the formed bubbles during polymer degradation push the clay nanoparticles from interior layers to the surface of the composites. The clay migration into the outer surface is mainly attributed to the difference in surface free energy between polymer and polymer-clay blend, the temperature and viscosity gradient during directional heating, and the formation of rising gasses as combustion process [62]. Aggregation of the clay particles, due to the degradation of the organic treatment on the clay interlayers, makes the clay particles more hydrophilic and less compatible. This, in turn, would result in formation of a clay-rich barrier that reduce the rate of weight-loss in composite combustion [59].

Barrier mechanism, which occurs in condensed phase, suggests that the formation of char layer prevents the mass transport of the degradation products to the surface of the degrading polymer and acts as a thermal barrier. This, in turn, would limit further exposure to the heat and oxygen and hinder burning process [63].

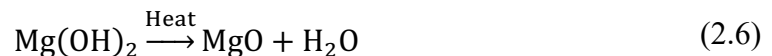
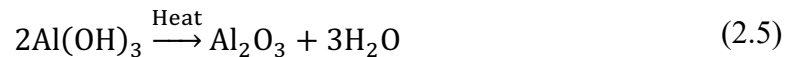
Paramagnetic radical trapping mechanism is another suggested mechanism in providing fire retardancy through incorporating nanoclay into different polymers. This mechanism proposes that structural metals in clay particles such as iron, can trap the formed radicals during polymer combustion and reduce the degradation rate [61].

Nanoclays are widely used as flame retardant additives in polymer nanocomposites, owing to their incombustible properties. Contributions of nanoclays can result in superior fire retardancy in polymer matrices through noticeable improvements in peak heat release rate, time to ignition, and fire growth index [64]. Ahmed *et al.* observed a protective char layer on the surface of

polystyrene upon the incorporation of nanoclay that resulted higher fire retardancy and the lesser emission of smoke, CO, and CO₂ compared to the virgin polystyrene [49]. Achieving nano-dispersion of the clay in the polymer matrices is an essential parameter, affecting the fire retardancy of polymer-clay nanocomposites. Lu *et al.* reported different methods in improving the nano dispersion of clay in LLDPE-PA6 blends. They observed that the blends with clay localized in the LLDPE phase, rather than PA6 phase, exhibited better flame retardancy [65].

2.5.2. Metal oxides

Metallic nanoparticles have received considerable attention for their applications as flame retardants. They exhibit different reactions against fire regarding their structure; some metallic nanoparticles utilize hydrated minerals and release water molecules as they decompose and provide an endothermic reaction. In this turn, the cooling effect would increase the self-extinguish ability in nanocomposites. Aluminum tri-hydroxide (ATH) and magnesium hydroxide (MH) are two non-halogen fire retardant additives that undergo endothermic reaction and interfere with the combustion process as the exposure to the heat [66].



The noticeable increase in limiting oxygen index (LOI) as a result of yielding a barrier on the surface of FR materials is another factor that can lower the heat flux provided by flame and the higher the non-flammability in nanocomposites.

The formation of char is another mechanism in some fire retardant materials such as alumina trihydrate (ATH) that delay ignition and development of a fire [67]. Phosphates are used as additives due to their ability of char formation.

In addition, at an elevated temperature, some metal containing fire retardants decompose to release water, which leads to the cooling of the substrate below the flash point. Water formation, in turn, favors the dilution of combustible gases, reduces the oxygen effect, and decreases the rate of the spread of the flame. Xi *et al.* reported a flame-retardant behavior in polyurethane foams due to the endothermic decomposition and water release reaction from ATH. They also reported that the water released from ATH reacted with the decomposition products and formed polyphosphate and increased the barrier effect of the char layer to heat and flame [68]. However, contradictory results were reported for the release of ammonia and water owing to the incorporation of ATH in polymer matrices, which led to an earlier degradation of EVA [69] and poly(1,4-butanediol succinate) (PBS) [70] due to hot water hydrolysis.

2.5.2.1. Zinc oxide

Zinc oxide (ZnO) is one of the most popular photocatalyst metallic compounds because of its advantages such as cost efficiency, numerous active sites, high surface reactivity and low environmental impacts. In fact, it is listed as safe by the US food and drug administration given that zinc is an essential trace element [16]. ZnO particles have high thermal conductivity as well as great heat capacity. Therefore, associating them into polymeric compounds will result in absorbing the heat transmitted from the surroundings and retarding the direct thermal impact to the polymer backbone. In other terms, they act as an inhibitor to slow down the flame spread rate [11, 71].

With recent advancements in nanotechnology, nano-sized zinc oxides are among emerging high value inorganic products with significant features (such as high catalyst effect, effective antibacterial properties, high UV absorption, and chemical and physical stability) that have many applications as solar cells, sensors, semiconductors, and transparent electrodes [72].

It is common to use high concentration of inorganic mineral fillers such as $\text{Al}(\text{OH})_3$ up to 20 wt% to modify flame retardancy of polyvinyl chloride (PVC) [73]. However, it is reported that addition of only 0.635 wt% of ZnO and 9 wt% of $\text{Al}(\text{OH})_3$ combination into PVC can significantly increase its LOI value (up to 30%) [74].

ZnO-intumescent flame retardant (IFR) system has been reported to be effective in flame retardancy property of the polypropylene-ethylene-propylene-diene monomer (PP-EPDM) polymer blend [57]. Addition of the 1 wt% ZnO and 29 wt% IFR showed the best fire performance as that formulation exhibited an LOI value of 35.6% compared to 17% LOI of original PP-EPDM blend. Furthermore, a heat release peak (pHRR) appeared for the formulation containing ZnO, reflecting the better barrier effect of the char layer compared to the original polymer blend and also formulations containing just IFR. Uniformly dispersed ZnO particles assist the IFR to have a more homogenous and compact char layer. Moreover, great heat capacity of them would result in absorbing the heat transferred from the combustion and creation of a more effective char layer [57].

2.5.3. Bio based products

In addition to inorganic fire retardants, certain plants have developed defense mechanism against fire invasions. Bio based compounds in these plants owe their intrinsic fire retardancy advantages to their molecular structure, which creates a thermally stable char layer when they are exposed to fire. Char formation mechanisms initiate when the water stored in the wood starts to be liberated during the thermal decomposition of wood components (lignin, cellulose, etc.) and encourage the formation of an insulator layer for the underlying wood [10, 75].

Biomass is the largest resource for bio-based materials, and up to 75% of that is composed of saccharide-based products, while the rest is mostly energy storage components (e.g. starch),

proteins, and vegetable oils. A massive range of chemicals and biofuels are produced based on these biomass derivatives, and they owe their commercial attraction to their fast growth and reasonable pricing. Furthermore, their inherent ability of char formation and the resulting fire retardancy make them interesting for FR applications [76].

2.5.3.1. Cellulose nanofibers

Cellulose is the most abundant organic polymer. It is found in cell wall of plants as well as in fungi, bacteria and algae, and it has numerous glucose units with many degrees of polymerization based on its extraction method. Figure 2.3 represents a cellulose fiber organization [10, 77]. During its thermal decomposition, cellulose can produce an insulating char layer under certain conditions, depending on its extraction method and surface treatment. The amount of char and its thermal stability depends on the degradation condition and existing components in the combustion environment, considering the fact that char formation mechanism is very complicated in cellulosic materials. [78, 79].

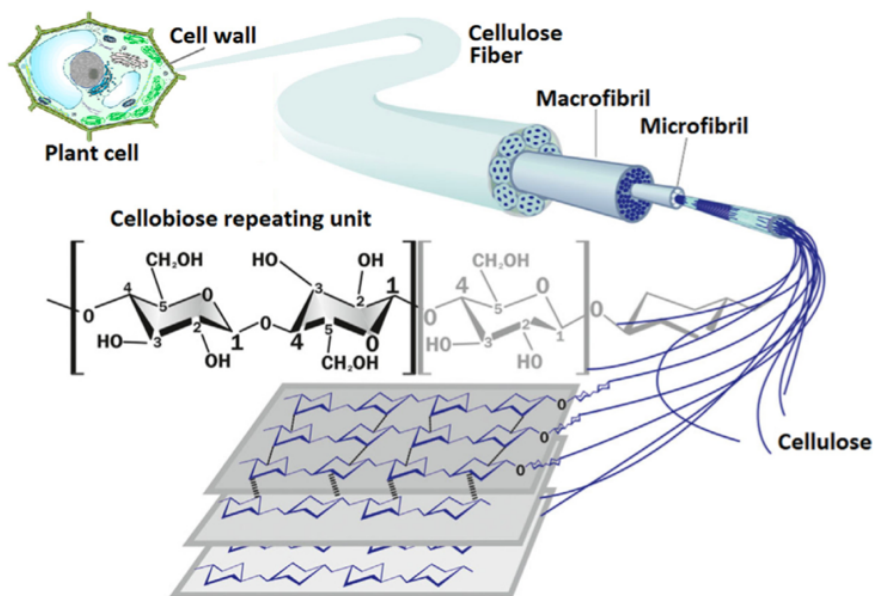


Figure 2.3. Representation of a cellulose fiber showing its organization.

Figure 2.4 represents a simplified model of cellulose pyrolysis. In low temperatures, degradation will lead to the formation of anhydrocellulose. As temperature goes up, the remaining cellulose will unzip into tar and anhydrocellulose will produce char and gas. Since cellulose is widely used in various industries, its fire performance is essential to eliminate its fire hazard. There has been much research carried out to improve cellulose's fire retardancy by applying chemical surface modifications or incorporating other fire retardants (e.g. phosphorous FRs) to improve its inherent char formation behavior [77, 80].

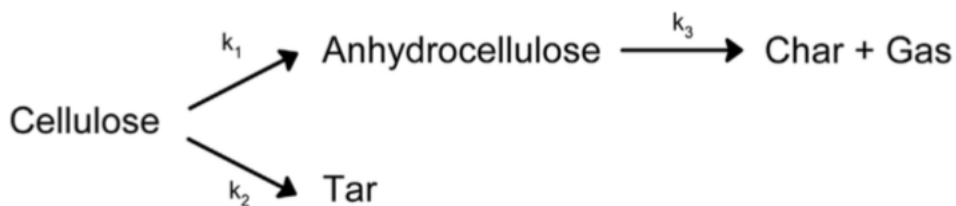


Figure 2.4. Kinetic model for cellulose pyrolysis by Broido [81]. k_1 , k_2 , and k_3 represent different kinetic energies existed for each step of the model.

Cellulosic nanomaterials, such as cellulose nanocrystals (CNCs) and cellulose nanofibers (CNFs), are generally used as nanofillers for various polymers in order to tailor their physical

and/or mechanical properties. They typically have a diameter between 5 nm to 500 nm and most of them are commercially available or can be extracted via well-known methods (e.g. acid hydrolysis) [20, 21]. Recently, flame retardancy potential of these nanofillers has attracted a lot of interests. There are numerous reports on flame retardancy performance of surface-modified cellulose nanocrystals or cellulose nanoparticles hybrid systems with other fire retardants [82-84].

10 wt.% of cellulose nanocrystals extracted with phosphoric acid hydrolysis has proven to increase the thermal stability of polylactic acid (PLA) by formation of a protective char layer [58]. Phosphoric acid has a well-known fire retardancy property [45]. Moreover, CNCs have a highly crystalline structure with well-packed chains and hard-to-break inter-chain hydrogen bonding which protect them from melting in high temperatures. Therefore, the incorporation of phosphoric acid treated CNCs in PLA matrix would enhance the thermal stability of the polymer by formation of the char layer and hindering the heat energy.

Cellulose nanofibrils-clay nanopaper composite has been reported as an effective flame retardant coating for wood [85]. The hybrid system was prepared as a “break and mortar” structure, where CNFs represent the mortar and clay nanopapers represent the brick. The thermal shielding provided by this system caused an 81% decrease in heat flux of the wood as reported by cone calorimetry test [85]. The char layer formed by this hybrid acted as an oxygen barrier insulating layer and increased the oxygen diffusion length. Additionally, CNF volatiles diffusion was hindered by clay char layer, resulting in formation of micro voids and further decline in thermal conductivity.

2.6. Characterization methods of flammability

Flame retardancy process can be characterized either in gas phase, by investigating the present pyrolysis species, or in solid phase, by studying the morphology and composition of the

char layer. There are numerous macro and micro fire characterization methods. The following paragraphs will discuss most commonly used laboratory test methods.

2.6.1. Limiting oxygen index (LOI)

This test is one of the primary methods that has been used for so many years to investigate the relative flammability of materials [86]. Since air consists of about 21% oxygen by volume, any material with an LOI less than 21% can burn easily in the air. In addition, a material with an LOI greater than 21% can reduce the flame after removal of igniting source [87].

LOI represents the minimum concentration of oxygen percentage in the oxygen-nitrogen mixture that maintains the flame combustion of the material for 3 min or consumes a length of 5 cm of the sample (based on ASTM D2863) as expressed in equation (2.7). According to the standard, specimens with dimension of 80 mm × 10 mm × 4 mm are placed vertically at the center of a glass chimney and the top of the sample is ignited with a burner.

$$\text{LOI} = \frac{[\text{O}_2]}{[\text{O}_2] + [\text{N}_2]} \times 100 \quad (2.7)$$

This test is very useful in the laboratory scale characterization of fire retardancy because it requires a cost-effective setup and small sample size. However, due to the high oxygen index simulation and small scale input heat, it is not very suitable for real extent fire performance [37].

2.6.2. UL-94

The UL-94 tests have been considered as flammability tests of plastics for parts in devices and appliances by Underwriters Laboratories based on the IEC 60695-11-10 standard. The most popular UL-94 test is UL94 vertical test which have been used as a method for determination of ignitability and flame spread rate of plastic materials. The flame resource is controlled to have a blue flame with 20 mm height and a constant power of 50 W. Top of the flame is located in a 10 mm distance from the bottom of the specimen. The bottom of the specimen is exposed to the flame

for 10 s and then the burner is removed. After-flame time t_1 is the time required for the flame to be extinguished. The bottom of the specimen is exposed to the flame for another 10 s after the first extinction. The time required for the flame to extinguish is noted as the after-flame time t_2 , and the time required for the fire to disappear is reported as the afterglow time t_3 . Five replications should be tested for each sample formulation [41, 88]. The sample is classified as V0, V1 or V2 according to the criteria listed in Table 2.3.

Table 2.3. Classification of materials for the UL94 Vertical Burn test.

Classification	Requirements
UL-94 V0	t_1 and t_2 less than 10 s for each specimen $t_1 + t_2$ less than 50 s for the five specimens $t_2 + t_3$ less than 30 s for each specimen No after-flame or afterglow. No burning drops
UL-94 V1	t_1 and t_2 less than 30 s for each specimen $t_1 + t_2$ less than 250 s for the five specimens $t_2 + t_3$ less than 60 s for each specimen No after-flame or afterglow up. No burning drops
UL-94 V2	t_1 and t_2 less than 30 s for each specimen $t_1 + t_2$ less than 250 s for the five specimens $t_2 + t_3$ less than 60 s for each specimen No after-flame or afterglow. Burning drops allowed

2.6.3. Cone calorimetry

This test is one the most important fire characterization methods for polymeric materials in bench scale and it is based on ASTM E 1354 and ISO 5660 standards. It measures the reducing oxygen concentration in the combustion gases of a specimen subjected to a given heat flux. After exposing the sample to a conical radiant electrical heater, the combustion is triggered by an electric spark. Variety of data such as heat release rate (HRR) as a function of time, peak of heat release rate (pHRR), total heat release rate (THR), effective heat of combustion (EHC), time to ignition (TTI), mass loss rate (MLR), and average specific extinction area (ASEA) can be reported by this test [88-90].

2.6.4. Thermogravimetric analysis

Thermo-gravimetric analysis (TGA) measures the changes in physical and chemical properties of materials (e.g. weight) as a function of temperature, based on ASTM E1131 and ISO 11358 standard. To analyze thermal properties of the materials, weight-loss at onset temperature (T_{onset}) and percentage of the weight that remains at the end of the heating process will be obtained by TGA. Materials that have higher T_{onset} , produce less fuel for the combustion and, therefore, have better flame retardancy properties. Also, char is considered as not readily combustible and provides an insulator barrier for underlying materials [91].

2.6.5. Summary

A relatively broad range of flame retardants including commercial non-organic FRs along with currently under development bio-based and mineral FRs have been discussed. It was attempted to highlight the recent efforts of researchers in the field of the fire suppression in plastics, considering the fact that polymeric materials are emerging in everyday life at an exponential rate. Since some of the traditional halogenated FRs are in the process of being banned due to their deleterious effect to human health and environment, discussing the functionality of green bio-based alternatives is of the significant importance. It is worth to mention that the complexities in the fire-retardant systems of different polymers and lack of systematic studies on various parameters (materials, mechanisms, methodologies, and techniques) in fire analysis have mostly led to qualitative observations.

It has been confirmed that the flammability of polymeric materials is a matter of convolution for which no sole solution can be found; especially considering the wide variety of polymer matrices. However, advancements of fire characterization techniques and a better

understanding of flammability phenomena have facilitated the selection of the most promising additives for fabrication of safe and fire resistant polymers.

CHAPTER 3. MATERIALS AND METHODS²

In this research, the polymer nanocomposite samples as well as the nano-sized zinc oxide were manufactured using three separate methods. Standard testing methodology used to characterize different mechanical and thermal properties of the polymer and polymer nanocomposites.

Three methods have been developed to improve the uniform dispersion of polar nanoparticles in apolar HDPE matrix and boost their interfacial bonding. To truly create a nanocomposite that performs better compared to its virgin polymer, it is important to achieve a uniform distribution of nanoparticles by eliminating agglomerations.

In this work, nanocomposites term refers to the polymer composite contacting up to 10 wt% CNCs and ZnO nanofillers.

3.1. Design of experiment

3.1.1. Synthesis of the nano-sized zinc oxide

3.1.1.1. *Materials*

Sodium hydroxide and Zinc acetate dehydrate were purchased from MilliporeSigma, Burlington, MA. Analytical grade methanol (99.8%) was supplied by Thermo Scientific, Waltham, MA.

² The materials of this chapter were co-authored by Ghazal Vahidi, Dilpreet S. Bajwa, Jamileh Shojaeiarani, and Nicole M. Stark. Ghazal Vahidi conceived and carried out the experiments. Ghazal Vahidi wrote this chapter in consultation with Dilpreet S. Bajwa, Jamileh Shojaeiarani, and Nicole M. Stark. Ghazal Vahidi was the primary developer of the methods that are advanced here. Ghazal Vahidi also drafted and revised all versions of this chapter. Dilpreet S. Bajwa also served as proofreader and supervised the proposed methods of this chapter.

3.1.1.2. Procedure

Zinc oxide nanoparticles were prepared following the procedure has been described in literature [16, 92]. Briefly, 13.17 g sodium hydroxide powder was dissolved in 300 ml methanol. Solution was heated to 50°C along with the continuous stirring for 1 hour. Then 9.6 g zinc acetate dehydrate, as the source of ZnO, was dissolved in 300 ml methanol by continuous stirring. The mixture was heated to 50°C while vigorously stirring for 30 minutes. The formation of zinc oxide nano-sol started by adding zinc acetate solution to sodium hydroxide solution drop-wised under continuous stirring for 30 minutes. Mixture was then heated to 50°C for 30 minutes and then stirred continuously for 2 hours in room temperature to crate the ZnO white sol gel (450 g sol gel, 9wt%). ZnO sol gel was dried under a fume hood to achieve a fluffy powder (Figure 3.1).

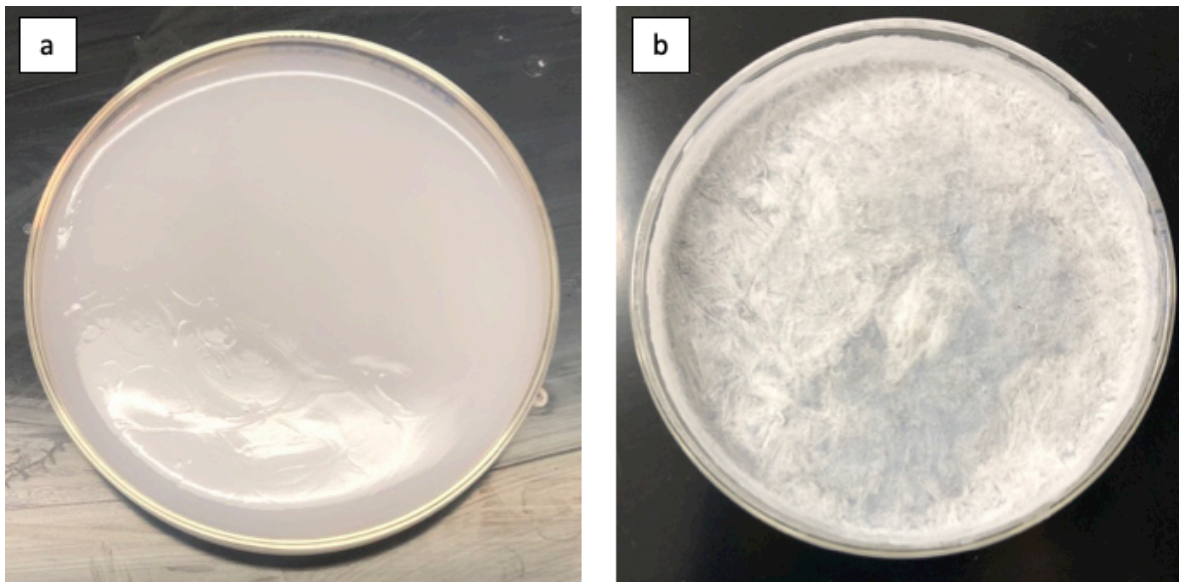


Figure 3.1. Zinc oxide in a) sol gel form before drying and b) powder form after drying under the hood.

3.1.2. Synthesis of nanocomposites, Method 1: Template approach via solvent exchange

3.1.2.1. Materials

High density polyethylene (HDPE Marlex-9006, MFI: 6 g/10 min, density: 0.953 g/cm³) was purchased from Chevron Philips chemicals, The Woodlands, TX. Cellulose nanocrystals

(CNCs, dimensions of 150 nm length and 7 nm width) were supplied by US forest product lab, Madison, WI. Acetone and toluene were provided by MilliporeSigma, Burlington, MA.

3.1.2.2. Procedure

CNCs with different concentrations were dispersed in water (5-10 wt%). To assist CNCs dispersion in water, sonification and homogenization were employed for 5 minutes, one at a time. Then, acetone was gently added on top of the aqueous dispersions in order to avoid rapid mixing. The organic layer formed on top of the aqueous dispersions was exchanged two times daily (850 mL each time). HDPE with different concentrations was dissolved in toluene (1-15 wt%) in 100°C.

Cellulose nanocrystal organogels were impregnated with different concentrations of HDPE-toluene solution. Impregnation happened in a round-bottom flask at 80°C in an oil bath with a reflux condenser, without stirring for 18 h to ensure complete equilibration (Figure 3.2). Then, Samples were dried under the hood. A significant phase separation of polar nanoparticles and apolar matrix was observed and composite synthesis was unsuccessful. Therefore, no further steps had taken, and next design of experiment was developed.



Figure 3.2. Solvent exchange process in the reflux condenser.

3.1.3. Synthesis of nanocomposites, Method 2: Physical attachment of PEO on CNCs

3.1.3.1. Materials

High density polyethylene (HDPE Marlex-9006, MFI: 6 g/10min, density: 0.953 g/cm³) was purchased from Chevron Philips chemicals, The Woodlands, TX. Cellulose nanocrystals (CNCs, dimensions of 150 nm length and 7 nm width) were supplied by US forest product lab, Madison, WI. Polyethylene oxide (PEO, Mn=10⁶ g mol⁻¹) was purchased from Sigma-Aldrich chemicals, St. Louis, MO.

3.1.3.2. Procedure

ZnO coated CNCs were obtained by adding ZnO sol gel to CNCs aqueous suspension (5 wt%) followed by homogenization and sonification for 5 minutes, respectively (50:50 weight ratio, CNCs:ZnO). PEO was used to enhance the interfacial bonding between the polar CNCs and the HDPE with highly hydrophobic nature. PEO was dissolved in distilled water (2 wt%) using magnetic stirring to obtain the aqueous polymer solution. PEO- modified CNCs were prepared by adding polymer solution to ZnO coated CNCs aqueous suspension (25:25:50 weight ratio, CNCs: ZnO: PEO). The mixture was dried under the fume hood and then was grinded in a cryogenic grinder with liquid nitrogen to obtain a fluffy powder (Figure 3.3). This step was necessary for a uniform dispersion of modified CNCs in the HDPE matrix. To eliminate any residual solvent, the samples were dried in an oven at 60°C temperature.

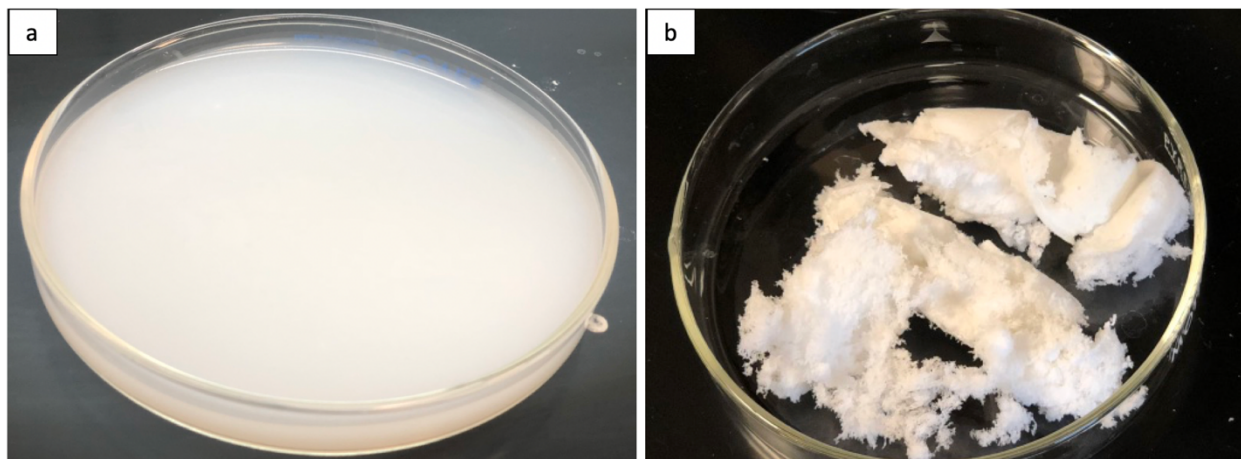


Figure 3.3. PEO-modified ZnO coated CNCs a) solution form, b) powder form after cryogenic grinder.

Polymer nanocomposites were prepared by diluting the HDPE with PEO-modified ZnO coated CNCs (CNCs content ranging from 0 to 3% based on HDPE content) in a twin-screw extruder (Krauss-Maffei Co., Florence, KY, USA). The screw speed was 160 rpm and temperatures were set to 160°C to 175°C (feed throat to die). Composites were extruded in filaments with 2 mm diameter and then chopped into small pieces with 2 mm length. Chopped nanocomposite were fed into a mini injection molding machine (Mini-Jector 45-OH, USA) to achieve samples in the standard dog-bone and flexural shapes. Table 3.1, summarizes the compositions of nanocomposite materials and the corresponding codes in this work.

Table 3.1. PEO treatment formulations.

Material formulation	HDPE (wt%)	CNCs (wt%)	ZnO (wt%)	PEO (wt%)
HDPE-0.75CNCs-0.75ZnO	97	0.75	0.75	1.5
HDPE-1.5CNCs-1.5ZnO	92.5	1.5	1.5	4.5
HDPE-3CNCs-3ZnO	70	3	3	24

3.1.4. Synthesis of nanocomposites, Method 3: Direct feeding with coupling agent

3.1.4.1. Materials

High density polyethylene (HDPE Marlex-9006, MFI: 6 g/10min, density: 0.953 g/cm³) was purchased from Chevron Philips chemicals, The woodland, TX. Powder HDPE (PHDPE,

RM341-U(UG), MFI: 3 g/10min, density: 0.941 g/cm³) was purchased from NOVA Chemicals SURPASS, Painesville, OH. Cellulose nanocrystals (CNCs, dimensions of 150 nm length and 7 nm width) were supplied by US forest product lab, Madison, WI. Maleic anhydride (MA, C₄H₂O₃, puriss ≥99.0% (NT), M_w=98.06 g/mol) and dibenzoyl peroxide as initiator (C₁₄H₁₀O₄, 75% remainder water, M_w=242.23 g/mol) were purchased from Sigma-Aldrich chemicals St. Louis, MI and Acros organics, Morris, NJ, respectively.

3.1.4.2. Procedure

CNCs and ZnO film were attained following previous fashion in 3.1.3.2. (50:50 weight ratio, CNCs: ZnO). The suspension was dried under a fume hood and the resulting films then were ground in a mortar and pestle to achieve a fine powder. Additionally, powder CNCs and powder ZnO were used directly to investigate the effect of making film in different properties of polymer nanocomposites (Figure 3.4). To eliminate moisture or any residual solvent, the samples were dried in an oven at 60°C temperature.

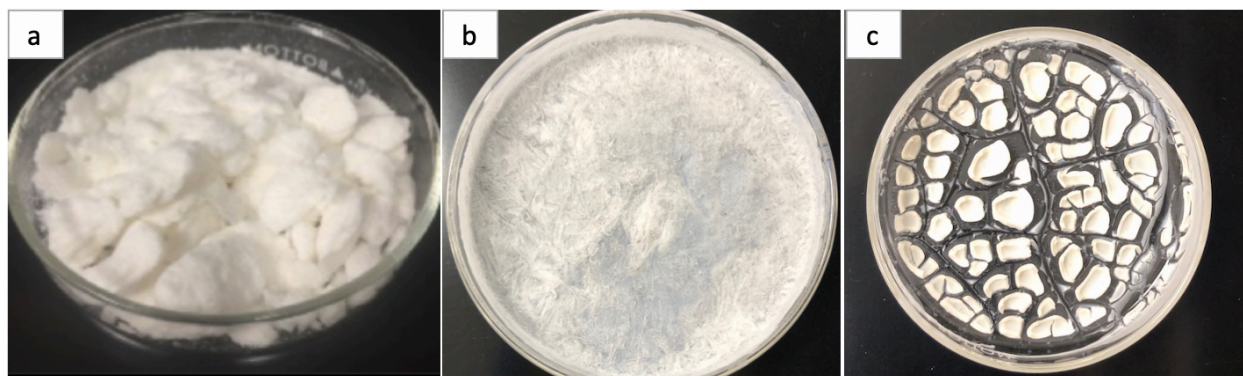


Figure 3.4. a) CNCs powder b) ZnO powder c) CNCs-ZnO film before grinding.

Two types of HDPE polymer were used in this method to be diluted by nano particles. In the first approach, HDPE pellets were fed to a twin-screw extruder directly with maleic anhydride (MA, 3 wt%), CNCs, and ZnO either in film or powder form (1.5-5 wt%, respectively). For the second approach, maleic anhydride grafted polyethylene (MAPE) was synthesized through in situ

polymerization. HDPE pellets with 3wt% of MA and 0.5wt% of dibenzoyl peroxide were fed to the extruder. The resulting MAPE polymer then was extruded again with nano fillers either in film or powder form (1.5-5 wt%, respectively). Additionally, to study the effect of polymer grain size in uniform dispersion of nanofillers, two extra batches were prepared using powder HDPE (PHDPE). PHDPE was fed to the extruder with 3% MA and CNCs and ZnO in powder form (3-5 wt%, respectively).

Prior to feeding the materials into the twin-screw extruder (Krauss-Maffei Co., Florence, KY, USA), all materials were mixed thoroughly with an overhead stirrer to assist the particles to distribute uniformly (Figure 3.5). The extruder's screw speed was 160 rpm and temperatures were set to 160°C to 175°C (feeding throat to die). Extrudates were collected in filament form with 2 mm diameter and then chopped into small pieces with 2 mm length. Chopped nanocomposites were fed into a mini injection molding machine (Mini-Jector 45-OH, USA) to achieve samples in standard dog-bone and flexural shapes. The final composition and codification of the samples are shown in Table 3.2, Table 3.3, Table 3.4, and Table 3.5.

Table 3.2. Direct feeding formulations, CNCs-ZnO – HDPE-MA (separately used).

Material formulation	HDPE (wt%)	P-CNCs (wt%)	P-ZnO (wt%)	MA (wt%)
HDPE-MA-P-1.5CNCs-1.5ZnO	94	1.5	1.5	3
HDPE-MA-P-3CNCs-3ZnO	91	3	3	3
HDPE-MA-P-5CNCs-5ZnO	87	5	5	3
	HDPE (wt%)	F-CNCs (wt%)	F-ZnO (wt%)	MA (wt%)
HDPE-MA-F-1.5CNCs-1.5ZnO	94	1.5	1.5	3
HDPE-MA-F-3CNCs-3ZnO	91	3	3	3
HDPE-MA-F-5CNCs-5ZnO	87	5	5	3

P: Powder of CNCs and ZnO separately, F: Films of ZnO coated CNCs

Table 3.3. Direct feeding formulations, CNCs-ZnO – MAPE1 (without initiator).

Material formulation	HDPE (wt%)	P-CNCs (wt%)	P-ZnO (wt%)	MA (wt%)
MAPE1-P-1.5CNCs-1.5ZnO	94	1.5	1.5	3
MAPE1-P-3CNCs-3ZnO	91	3	3	3
MAPE1-P-5CNCs-5ZnO	87	5	5	3
	HDPE (wt%)	F-CNCs (wt%)	F-ZnO (wt%)	MA (wt%)
MAPE1-F-1.5CNCs-1.5ZnO	94	1.5	1.5	3
MAPE1-F-3CNCs-3ZnO	91	3	3	3
MAPE1-F-5CNCs-5ZnO	87	5	5	3

P: Powder of CNCs and ZnO separately, F: Films of ZnO coated CNCs

Table 3.4. Direct feeding formulations, CNCs-ZnO – MAPE2 (with initiator).

Material formulation	HDPE (wt%)	P-CNCs (wt%)	P-ZnO (wt%)	MA (wt%)	Initiator (wt%)
MAPE2-1.5CNCs-1.5ZnO-P	93.5	1.5	1.5	3	0.5
MAPE2-3CNCs-3ZnO-P	90.5	3	3	3	0.5
MAPE2-5CNCs-5ZnO-P	86.5	5	5	3	0.5
	HDPE (wt%)	F-CNCs (wt%)	F-ZnO (wt%)	MA (wt%)	Initiator (wt%)
MAPE2-1.5CNCs-1.5ZnO-F	93.5	1.5	1.5	3	0.5
MAPE2-3CNCs-3ZnO-F	90.5	3	3	3	0.5
MAPE2-5CNCs-5ZnO-F	86.5	5	5	3	0.5

P: Powder of CNCs and ZnO separately, F: Films of ZnO coated CNCs

Table 3.5. Direct feeding formulations, CNC-ZnO– PHDPE-MA (powder HDPE).

Material formulation	PHDPE (wt%)	P-CNCs (wt%)	P-ZnO (wt%)	MA (wt%)
PHDPE-MA-3CNCs-3ZnO-P	91	3	3	3
PHDPE-MA-5CNCs-5ZnO-P	87	5	5	3

P: Powder of CNCs and ZnO separately

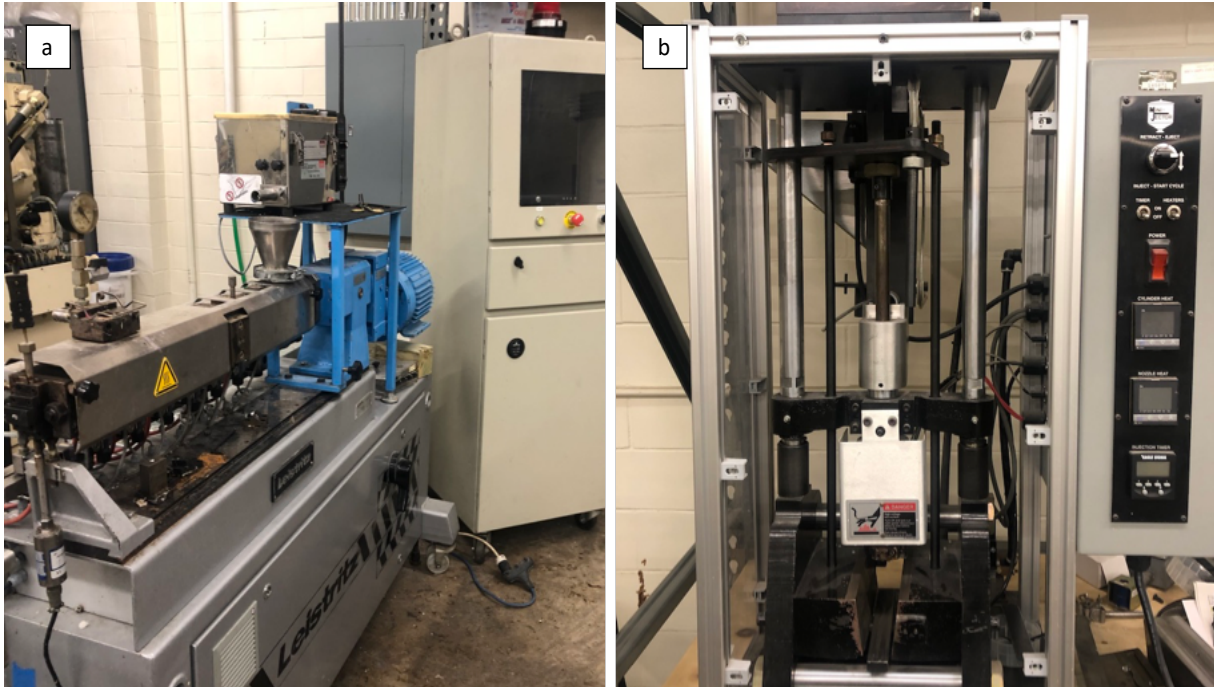


Figure 3.5. a) Twin-screw extruder b) Mini-Jector injection molding machine.

3.2. Nanocomposite characterization methods

Several tests were conducted to evaluate the performance of the nanocomposites compared to the virgin polymer to study the effect of incorporating CNCs and ZnO as nanofillers.

3.2.1. Fourier transform infrared (FTIR) spectroscopy

FTIR measurements of nanocomposite samples was carried out to monitor the modification of CNCs as well as the effect of MA as a coupling agent in nanocomposite samples with an absorbance mode in the range of 650 and 4000 cm^{-1} . A Thermo Nicolet 8700 spectrometer (Thermo Fisher, Waltman, MA, USA) equipped with an attenuated total reflectance (ATR) sampling accessory was used to record the spectra.

3.2.2. Fractured surface morphology

The morphology of HDPE and nanocomposites was studied using scanning electron microscopy (SEM). The impact-fractured surface was investigated using SEM (JEOL Inc., Peabody, MA, USA) working with an accelerating voltage of 20 kV at magnifications of 90X, 300X, and 1000X. The samples were sputter-coated with a layer of gold before SEM examination to avoid specimen excessive charging.

3.2.3. Melt flow index (MFI)

Tinius Olsen melt flow indexer (Model MP1200, Tinius Olsen, Horsham, PA) according to ASTM D1238 standard (D. ASTM, 2004) was used to evaluate melt flow index of composite pellet samples compared to the virgin polymer (Figure 3.6). HDPE, PHDPE, MAPE1, and MAP2 polymer pellets along with some CNCs-ZnO contained formulations were evaluated in order to measure the changes in MFI of HDPE due to the use of coupling agent and nanofiber loading. A fixed weight of 7 g at the melting temperature of 180°C was consistent for all of the samples.



Figure 3.6. Melt flow indexer.

3.2.4. Differential scanning calorimetry (DSC)

Differential scanning calorimetry experiment was conducted using a TA Instrument Q200 calorimeter (New Castle, DE, USA). A heating scan from 40 to 200°C at a heating rate of 10°C.min⁻¹, followed by a cooling process up to 25°C was applied. Hermetic Aluminum pans were used holding the sample. The weight of each sample was approximately 7-10 mg.

3.2.5. Mechanical properties (Tensile Test)

ASTM D638-14 is a standard test method for determining the tensile properties of the plastics. Mechanical characteristics of injection molded polymer and composite samples including ultimate tensile strength, strain at maximum tensile strength, and modulus of elasticity can be found from the tensile test. An Instron universal testing machine (Model 5567, MA, and USA) was used in room temperature (25°C) to investigate the mechanical properties of the composite samples compared to the original polymer (Figure 3.7). Instron machine was equipped with 2 KN load cell and 5 mm/min crosshead speed. Test was repeated for at least five specimens of each formulations.



Figure 3.7. Tensile testing apparatus and the loaded sample.

3.2.6. Dynamic mechanical analysis (DMA)

A dynamic mechanical analyzer (TA Instruments, DMA Q800, DE, USA) was used to investigate the viscoelastic behavior of nanocomposites. DMA was equipped with a dual cantilever clamp according to the ASTM D5026 to study viscoelastic behavior of the nanocomposite (Figure 3.8). Temperature was in the range of 40 to 120°C at a heating rate of 1°C.min⁻¹. The samples were prepared to run the DMA test with approximately 59 mm length, 13 mm width, and 3 mm thickness. Test was repeated for two specimens of each formulations.

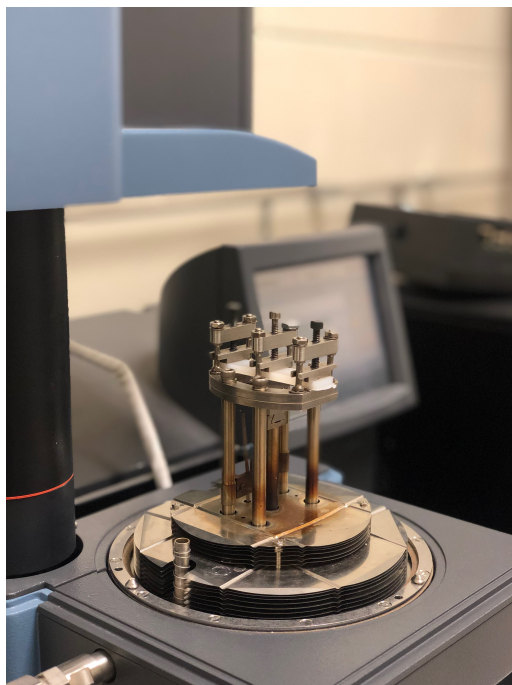


Figure 3.8. Three-point loading configuration of a flexural sample in DMA test.

3.2.7. Rheological properties

The flow properties (rheological properties) such as complex viscosity and shear moduli of the formulations were measured using a Rheometer AR 2000 (TA Instruments, New Castle, DE, USA). The rheological properties of HDPE and nanocomposites were measured in an oscillatory mode in frequency sweep test setup. The sample weighing 0.5 g was placed between two parallel plates with 25 mm diameter and a gap of 1 mm at 180 °C.

3.2.8. Thermogravimetric analysis (TGA)

Thermal stability of the samples was studied through thermogravimetric analysis and the corresponding derivative curves (DTG). Thermogravimetric analyses were carried out using a PerkinElmer thermogravimetric analyzer Pyris 1 in nitrogen (sample gas, flow rate 60 ml/min balance gas, flow rate 40 ml/m) (Figure 3.9). The weight of each sample would approximately be 10 mg. The temperature range was set from 25 °C to 600 °C with the heating rate of 10 °C/min.



Figure 3.9. Thermogravimetric analyzer.

3.2.9. Horizontal burn test

ASTM D635 is a standard test method for determining the rate of burning and/or extent and time of burning of plastics in a horizontal position. It was used to evaluate the fire performance of the composite samples as shown in Figure 3.10. The specimens were prepared to be approximately 59 mm long, 13 mm wide, and 3 mm thick.

To calculate the weight-loss percentage in one minute, nanocomposites were placed in the burn test setup that was adjacent to a flame source. The flame source was removed after 30 seconds, and composites continued to burn. The fire was extinguished after one minute and the remaining part of the samples were weighed. The weight-loss was calculated based on the difference of initial and final weights of the specimens.

$$\text{Weight loss (\%)} = \frac{W_1 - W_2}{W_1} \times 100 \quad (3.1)$$

In equation (3.1), W_1 and W_2 are the weight of the composite samples before and after the fire test, respectively.

In the second setup, the flame source was removed after 30 seconds and the flame spread through a 40 mm marked distance on the samples while time was being recorded. The flame spread rate (mm/s) was calculated in the second test based the time recorded during the test.

$$\text{Flame spread rate } \left(\frac{\text{mm}}{\text{s}} \right) = \frac{40\text{mm}}{t} \quad (3.2)$$

In equation (3.2), t is the required time for the flame to spread over 40 mm of the samples. The test was repeated for three specimens of each formulation.

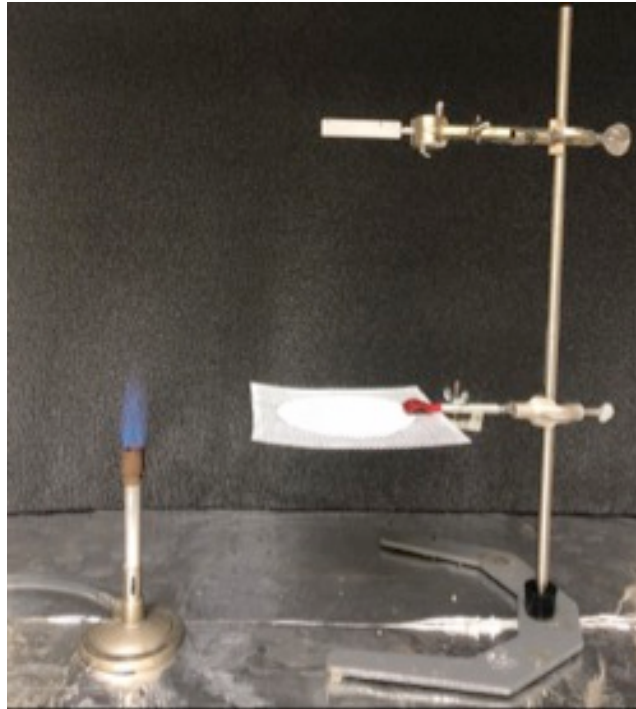


Figure 3.10. Horizontal burn test setup base on ASTM D635.

3.2.10. Statistical analysis

The mean values and standard deviations of the mechanical properties of the samples were statistically analyzed by ANOVA and Tukey's test ($\alpha=0.05$). The data was analyzed using Minitab software version 17 (Minitab Inc., State College, PA, USA).

CHAPTER 4. RESULTS AND DISCUSSION³

4.1. PEO physical attachment method

In PEO physical attachment method, CNCs were modified with PEO to enhance their interfacial bonding with HDPE matrix.

4.1.1. Fourier transform infrared (FTIR)

The FTIR spectra of the virgin HDPE and composite samples are shown in Figure 4.1. The changes in the peak intensity in FTIR is associated with the changes in the number of functional groups or new chemical bonding between the existing components, whereas a shift in peak position usually means the hybridization state or electron distribution.

Analysis revealed no substantial change in chemical bonding between components. However, one new peak (1110 cm^{-1} wave number) was observed in composite samples with 3% CNCs and 3% ZnO and 24% PEO. This peak can be assigned to C-O-C stretching between PEO and CNCs. The OH groups on CNCs can play the role of proton donors and the C-O-C group on PEO is a proton acceptor and hydrogen bonding can be established between the CNCs and PEO [93].

³ The materials of this thesis were co-authored by Ghazal Vahidi, Dilpreet S. Bajwa, Jamileh Shojaeiarani, and Nicole M. Stark. Ghazal Vahidi conceived and carried out the tests and analyzed the observed results. Ghazal Vahidi wrote this chapter in consultation with Dilpreet S. Bajwa, Jamileh Shojaeiarani, and Nicole M. Stark. Dilpreet S. Bajwa also served as proofreader and supervised findings of this work. Ghazal Vahidi was the primary developer of the conclusions that are advanced here. Ghazal Vahidi also drafted and revised all versions of this chapter.

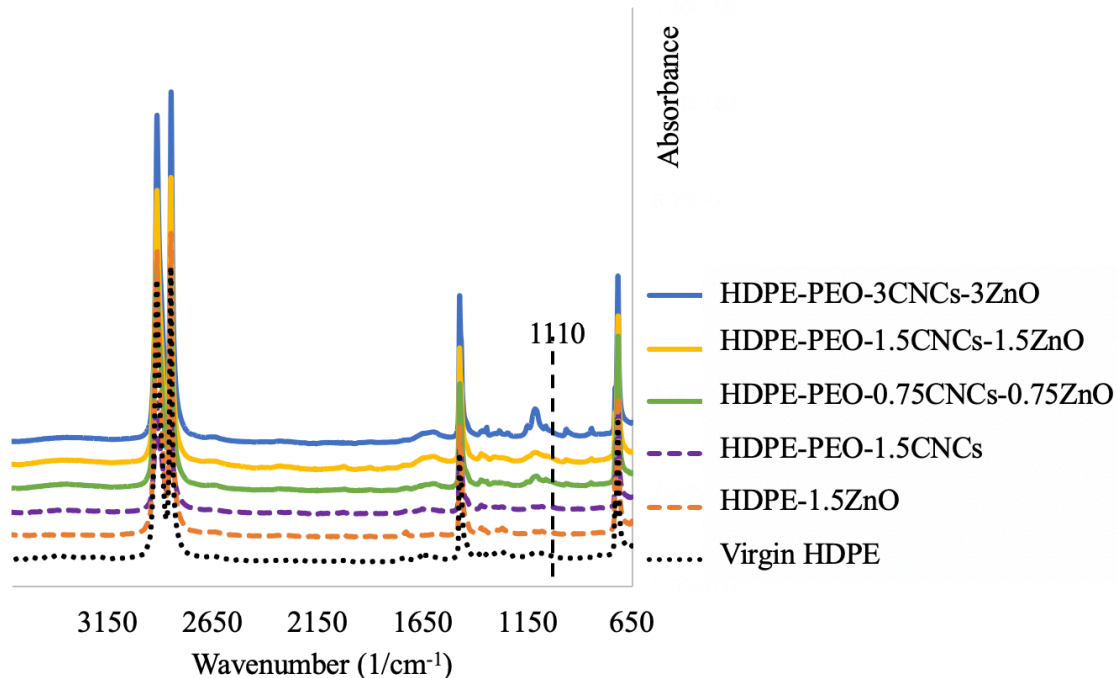


Figure 4.1. FTIR spectra of PEO modified ZnO-coated CNCs in HDPE matrix in the absorbance mode.

4.1.2. Differential scanning calorimetry (DSC)

Figure 4.2 illustrates the DSC thermograms of virgin HDPE and composites. Glass transition of HDPE happens in very low temperatures [94] and therefore, there is no sign of glass transition peak in this thermogram. All the composite samples possessed melting endotherms with similar melting temperatures same as virgin HDPE, which was around 130°C. This observation confirmed the presence of single homogeneous phase through the heating process for almost all the formulations. However, the formulation with the highest concentrations of CNCs, ZnO and PEO (HDPE-24PEO-3CNCs-3ZnO) exhibited a 2°C decrease in the melting point. This observation can be attributed to the increased chain mobility in the HDPE matrix as a result of chain shortening effect of CNCs-ZnO agglomerations; large clusters of CNCs and ZnO nanoparticles can as impurities causing the binding and shortening of the polymer chain [95]. A small melting peak around 65°C was observed in HDPE-4.5PEO-1.5CNCs-1.5 ZnO formulation,

and pure PEO melting peak is around 65°C as reported in the literature [96, 97]. Therefore, this peak can be assigned to the presence of PEO in a non-homogenous blend with other components of the composite in this specific formulation.

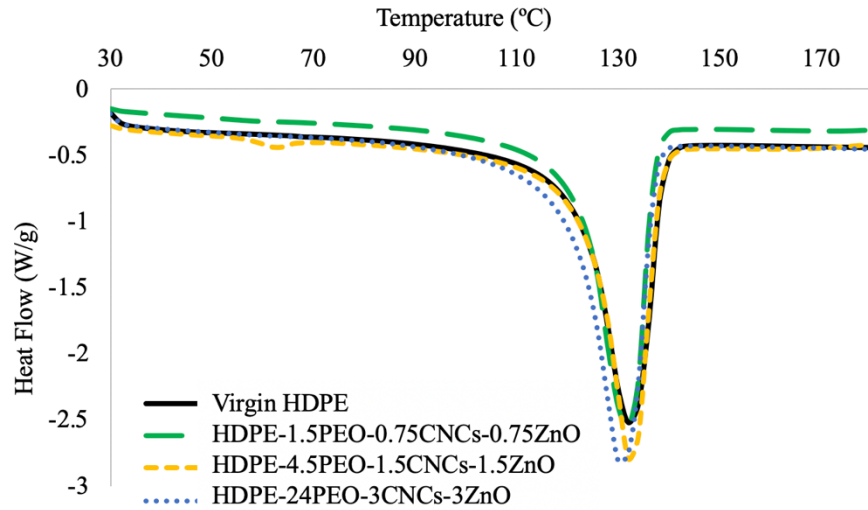


Figure 4.2. Representative DSC curves for PE treatment during the second heating scan of composite pellets.

4.1.3. Mechanical properties (Tensile Test)

The effect of CNCs-ZnO loadings on the tensile properties of the nanocomposite are summarized in Table 4.1. No significant change was observed in mechanical properties of HDPE composites. Elongation at maximum tensile strength experienced an increase while increasing the amount of nanofillers. In highest concentration of the CNCs-ZnO-PEO, Elongation at max tensile strength was 30% higher than the virgin polymer. This could be assigned to the plasticity of PEO more than the role of nanofillers [98]. Moreover, there was no change in Young's modulus and maximum tensile strength values compared to the original polymers.

Table 4.1. Tensile properties of composite samples in PEO treatment.

Material formulation	Young's modulus (MPa)	Maximum tensile strength (MPa)	Elongation at max tensile strength (%)
HDPE	537±36 ^a	22±2.3 ^a	12±1.00 ^a
HDPE-PEO-0.75CNCs-0.75ZnO	559±53 ^a	22±1.3 ^a	14.6±0.55 ^b
HDPE-PEO-1.5CNCs-1.5ZnO	527±28 ^a	22±1.5 ^a	15.1±0.35 ^b
HDPE-PEO-3CNCs-3ZnO	531±44 ^a	24±1.3 ^a	15.4±0.60 ^b

*Same superscript letters within the same column are not significantly different.

4.1.4. Dynamic mechanical analysis (DMA)

The storage and loss moduli of nanocomposites at elevated temperatures was evaluated through DMA test in compared to the virgin HDPE. Figure 4.3 and Figure 4.4 show the plots of storage and loss modulus vs temperature for virgin HDPE and the nanocomposites with different CNCs and ZnO loadings. Nanocomposite formulation possessed higher storage modulus compared to the virgin HDPE except for HDPE-1.5PEO-0.75CNCs-0.75ZnO formulation with lowest concentration of the PEO and the nanofillers. Same trend was observed for the loss modulus. This observation can be contributed to the improved dispersion of nanofillers in high percentages of PEO [99].

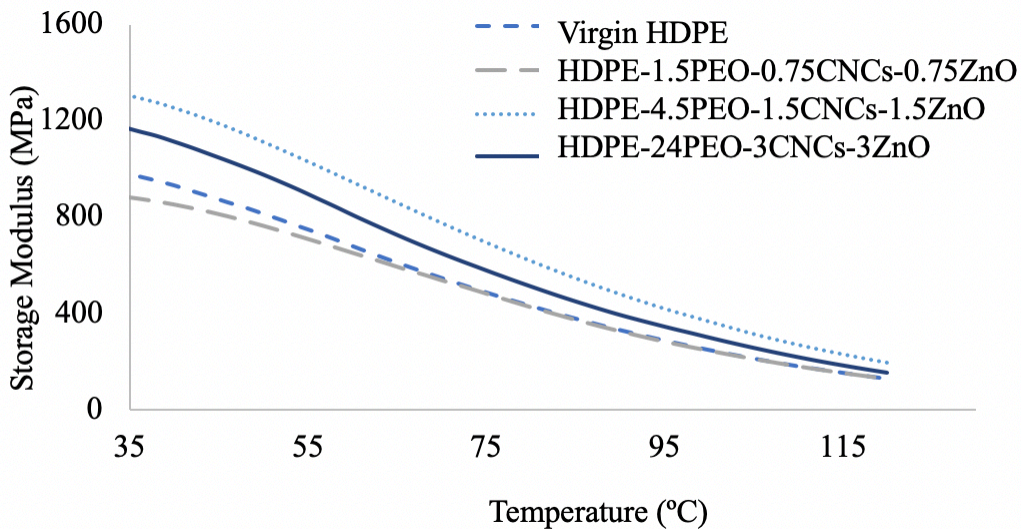


Figure 4.3. DMA curves for PEO treatment, Storage modulus vs. temperature.

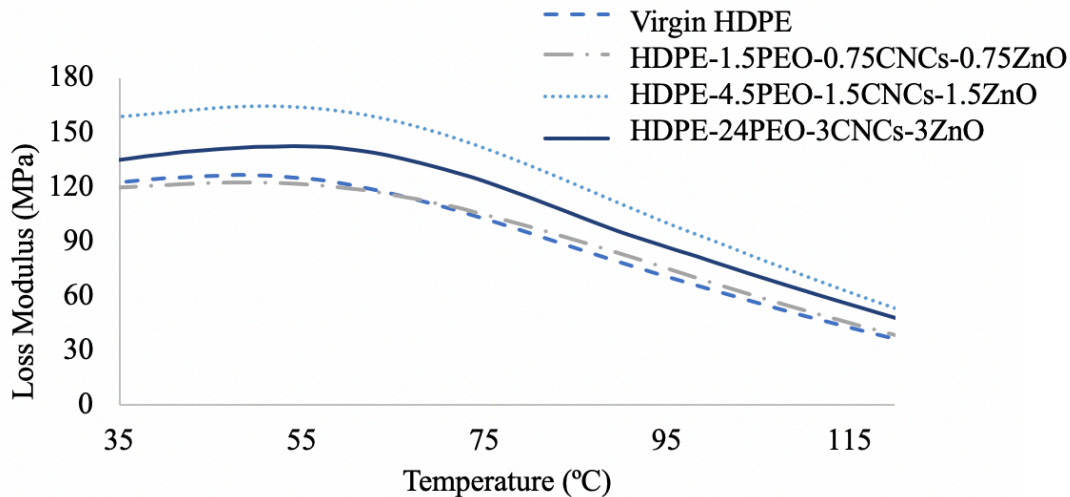


Figure 4.4. DMA curves for PEO treatment, Loss modulus vs. temperature.

4.2. Direct feeding with coupling agent method

In this method, MA was used as a coupling agent to enhance the uniform distribution of CNCs-ZnO nanoparticles in polymer matrix through direct feeding using an extruder.

4.2.1. Fourier transform infrared (FTIR) spectroscopy

The Fourier transform infrared (FTIR) absorption spectra were recorded for the determination of the new peaks as a sign of chemical bonding between the MA coupling agent with HDPE and CNCs-ZnO fillers (Figure 4.5). The C=O peak, specific to PE and MA chemical bonding, is found in the 1742 cm^{-1} wavenumber, which exists in the all formulations that contain MA. This observation suggested the successful interactions of HDPE with the coupling agent [100]; new bands at 1718 cm^{-1} to 1790 cm^{-1} wavenumbers belong to symmetric and asymmetric stretching of the carbonyl group (C=O) of MA [101]. In MAPE2 formulations spectra, a new peak at 1100 cm^{-1} was observed which is assigned to C-O bond in ether and alcohol functional groups or benzoic acid compound; this can be a sign of dibenzoyl peroxide decomposition producing either ether or benzoic acid groups [102, 103]. The 3350 cm^{-1} peak existed in MAPE2 formulations

is a sign of O-H band between HDPE backbone and peroxide molecule, which initiate the MA grafting process [104].

The FTIR spectra of the all the formulations with CNCs exhibited a broad band over 3100 to 3500 cm^{-1} , which can be attributed to the O-H stretching vibrations. The intensity of the peak was weaker in the MAPE1 and HDPE-MA compared to the MAPE2 formulation indicating that MA incorporation into CNCs was stronger in the first two formulations. By contrast, MAPE2 formulations had a peak intensity similar to the neat CNCs [105]. As shown in Figure 4.5, the band with the 2920 cm^{-1} wavenumber can be contributed to the C-H stretching vibrations existing in HDPE [106]. Additionally, The peaks with 1250 cm^{-1} wavenumber exhibited the bending vibrations of CH_2 saccharide structure in CNCs [107].

Finally, the new peak created by the successful grafting of ZnO on CNCs at 810 cm^{-1} is related to the out of plane deformations of carboxyl groups in CNCs [108], and this new peak was shifted and weakened compared to the FTIR spectra of the neat CNCs from literature [106, 109, 110].

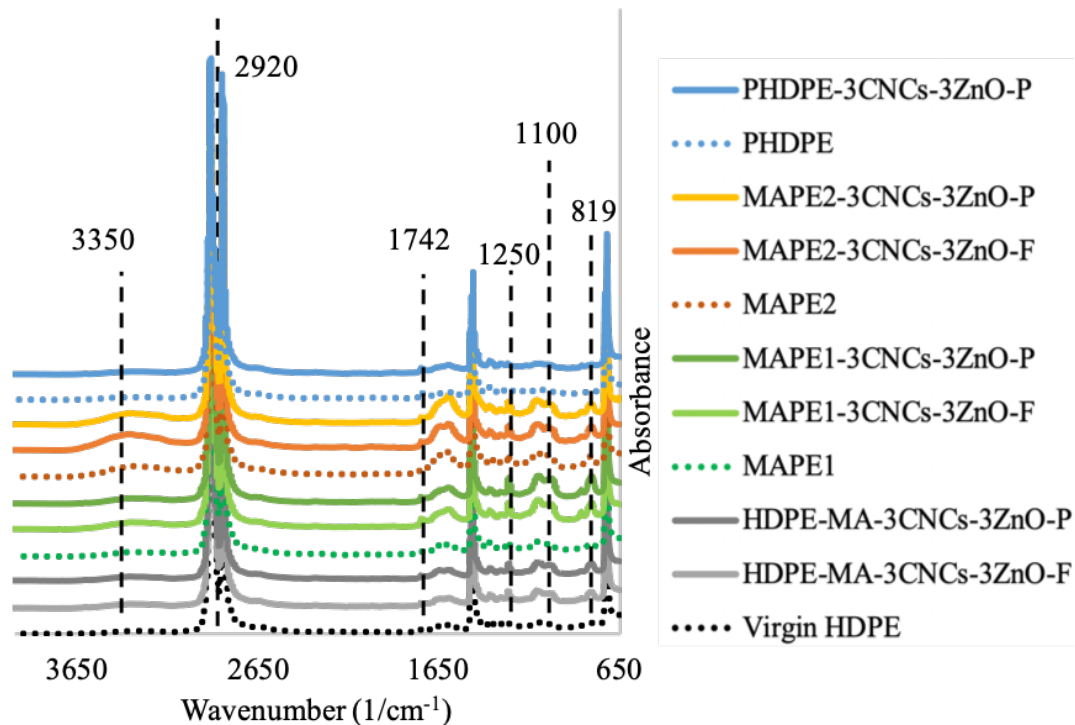


Figure 4.5. FTIR spectra of HDPE, MAPE1, MAPE2, PHDPE and their nanocomposites in absorbance mode.

4.2.2. Fractured surface morphology

The impact-fractured surface of the HDPE-MA, MAPE2, and PHDPE-MA nanocomposites are illustrated in Figure 4.6, Figure 4.7, and Figure 4.8, respectively. In the HDPE-MA nanocomposites, the formulations with 3 and 5 wt% nanofillers in powder form exhibited a rough surface with irregular patterns, indicating a higher toughness energy required for the fracture. On the other hand, in the formulations with 3 and 5 wt% nanofillers in film form, the fractured surface was laminated and smoother, suggesting a more brittle nature [111]. Meanwhile, the presence of CNCs-ZnO aggregates was more predominant in the film formulations, as one can see white chunks with some cavities around them, indicating relatively poor interactions between the HDPE and nanofillers in film form (Figure 4.6) [109]. Compared to HDPE-MA formulations, the occurrence of CNCs-ZnO aggregates in the MAPE2 nanocomposites were more prevalent in

both powder and film forms, as depicted in Figure 4.7. Generally, formulations with nanofillers in film form had more CNCs-ZnO clusters compared to the formulations with nanofillers in powder form. It is worth noting that the fractured surface in MAPE2 formulations was rougher and had more irregular patterns compared to the other formulations, suggesting a more ductile and less stiff nature.

As shown in Figure 4.8, there is relatively fewer traces of CNCs-ZnO aggregations in PHDPE, which can be attributed to the better dispersion of powder nanofillers in the powder HDPE matrix. Furthermore, the presence of the ZnO white layer surrounding the CNCs in the formulations with nanofillers in film form demonstrated that ZnO successfully coated the surface of the CNCs.

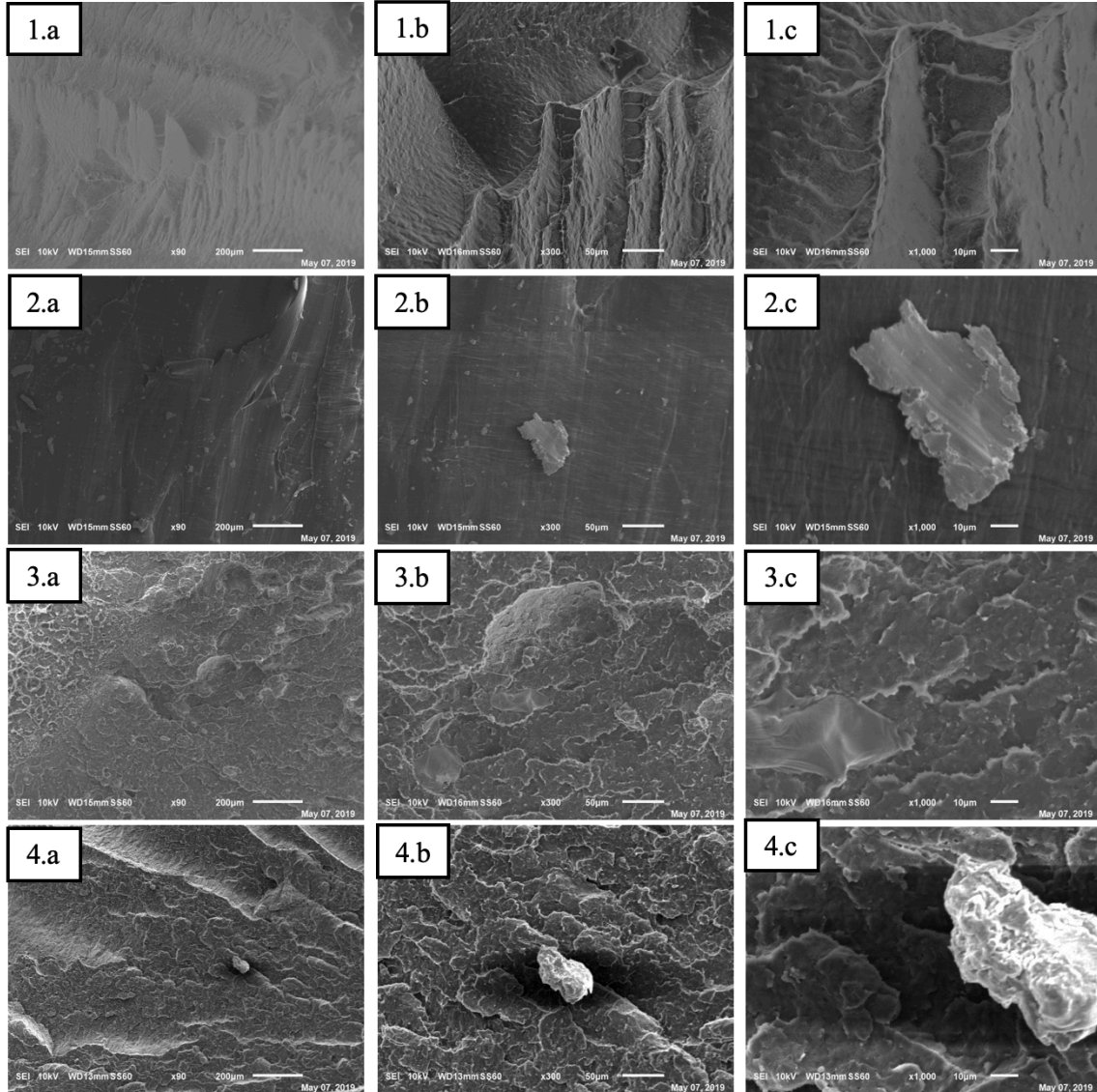


Figure 4.6. SEM micrographs of HDPE-MA nanocomposites 1) HDPE-MA-3CNCs-3ZnO-P, 2) HDPE-MA-3CNCs-3ZnO-F, 3) HDPE-MA-5CNCs-5ZnO-P, 4) HDPE-MA-5CNCs-5ZnO-F at three magnifications a) 90X, b) 300X, c) 1000X

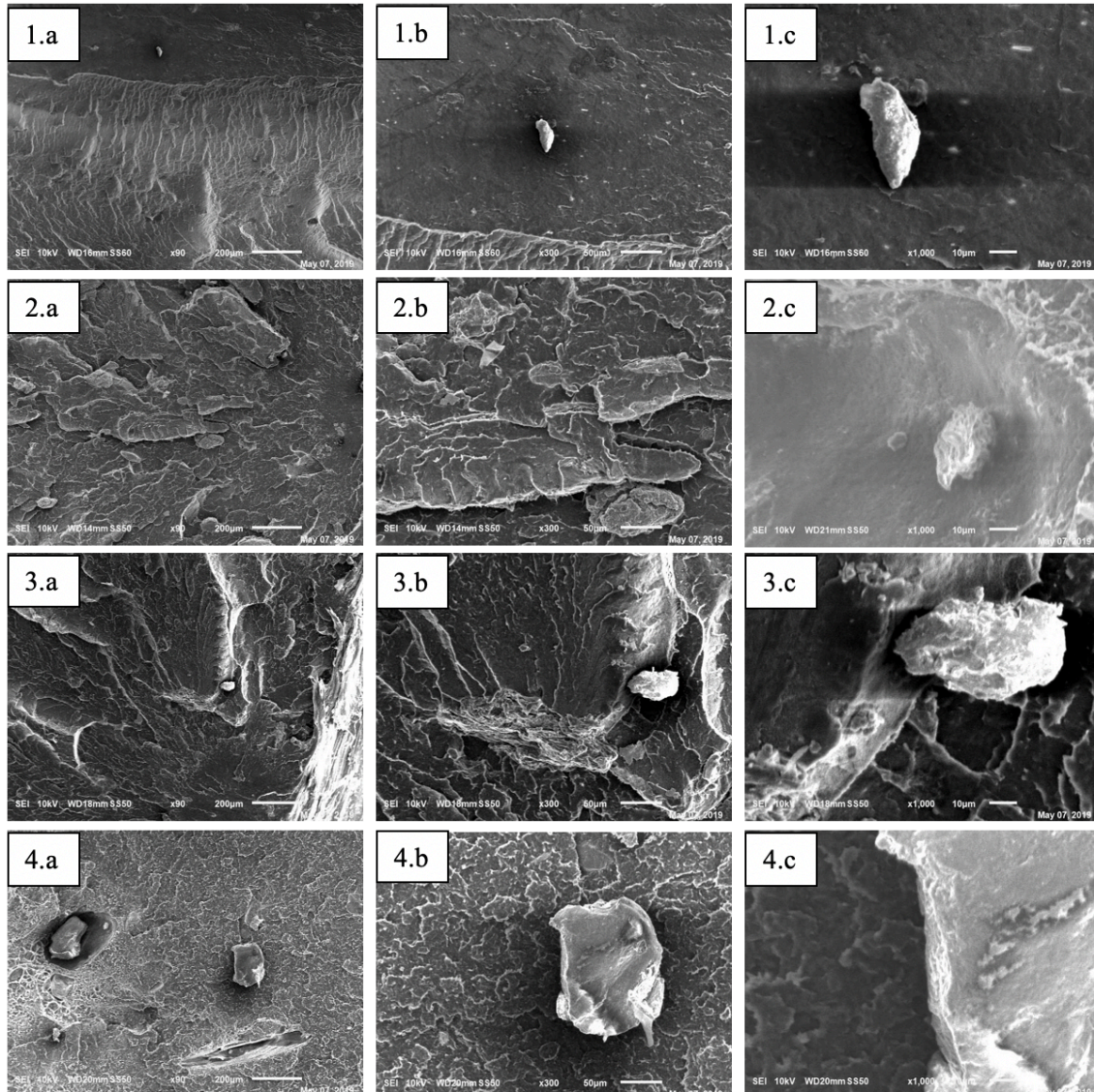


Figure 4.7. SEM micrographs of MAPE2 nanocomposites 1) MAPE2-3CNCs-3ZnO-P, 2) MAPE2-3CNCs-3ZnO-F, 3) MAPE2-5CNCs-5ZnO-P, 4) MAPE2-5CNCs-5ZnO-F at three magnifications a) 90X, b) 300X, c) 1000X

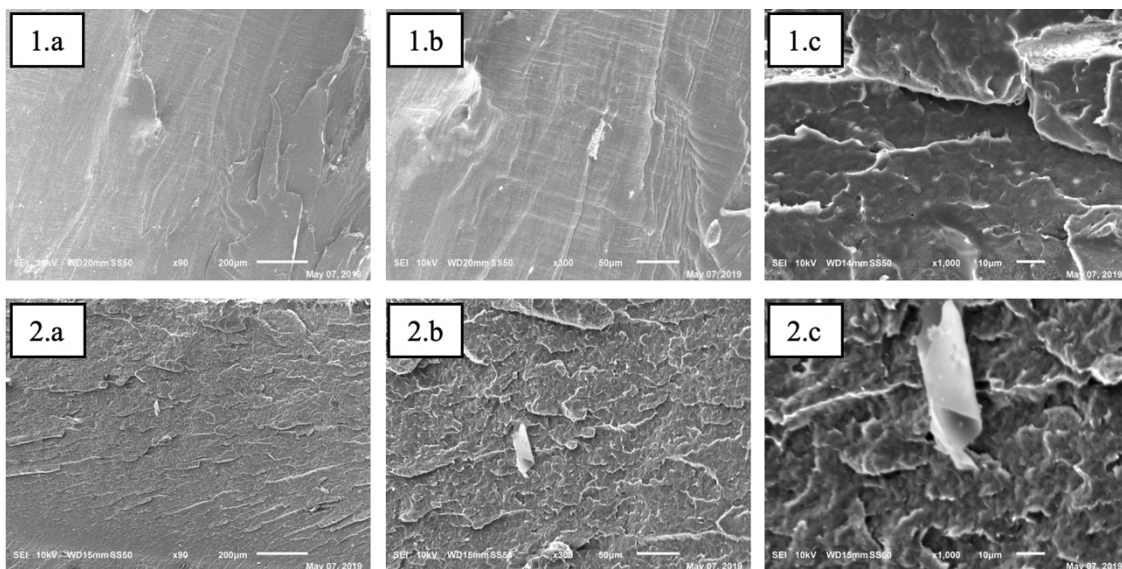


Figure 4.8. SEM micrographs of PHDPE-MA nanocomposites 1) PHDPE-MA-3CNCs-3ZnO-P, 2) PHDPE-MA-5CNCs-3ZnO-P at three magnifications a) 90X, b) 300X, c) 1000X

4.2.3. Melt flow index (MFI)

Melt flow index (MFI) is an indicator of the ease of flow for polymeric materials and is related to the molecular weight. Application of MA as a coupling agent in HDPE caused a 10% decline in MFI compared to the virgin polymer as represented in Figure 4.9. Since MA has a conjugated structure with a carbon double bond ($C=C$) and two carboxylate groups, which means it can be grafted onto the polyolefins' backbone while slightly increasing the degree of crosslinking for the polymer [112]. Cross-linking phenomena increases the molecular weight of the polymers, and this can result in a decrease in ability to flow [113]. Moreover, when an initiator is added to the coupling agent, the degree of reactivity of the $C=C$ bond and the polymer increases significantly, which results in an even more cross-linked structure for the polymer [114]. A 35% decline in MFI of MAPE2 compared to HDPE-MA was observed, most likely due to this highly cross-linked structure.

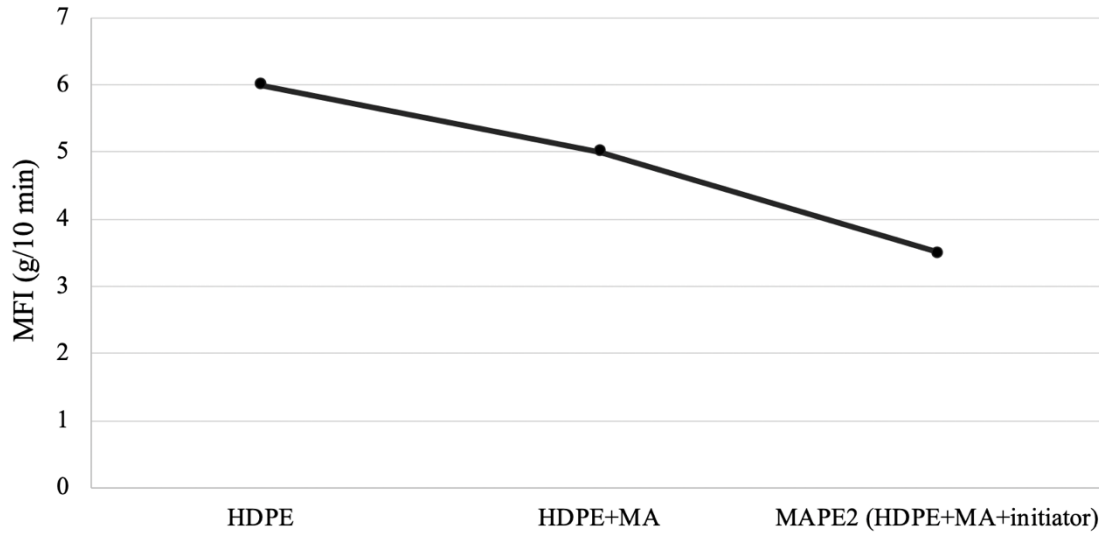


Figure 4.9. Comparison of the melt flow index of virgin HDPE vs. HDPE-MA and MAPE2. Addition of MA increased viscosity and adding initiator increased it even further.

A slight increase in MFI was recorded after adding CNCs and ZnO nanofillers to both HDPE-MA and P-HDPE polymers (Figure 4.10 and Figure 4.11). This could be a result of increased fiber-matrix interaction, which can be accomplished via a more uniform dispersion of nanofillers in the polymer. In contrast, fiber-fiber interactions decrease the fluidity of the composite samples while increasing the viscosity and flow resistance [115]. Because these two factors work against one another, increment in MFI was relatively smooth.

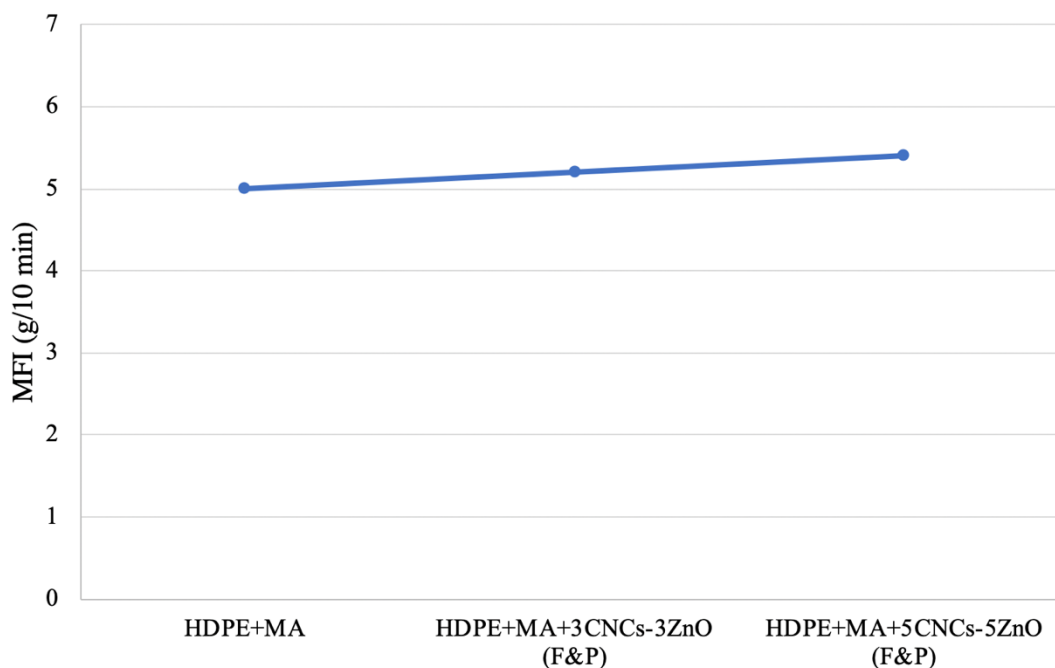


Figure 4.10. Comparison of the melt flow index of HDPE-MA vs. different nanofiller loadings. Addition of nanofillers decreased viscosity.

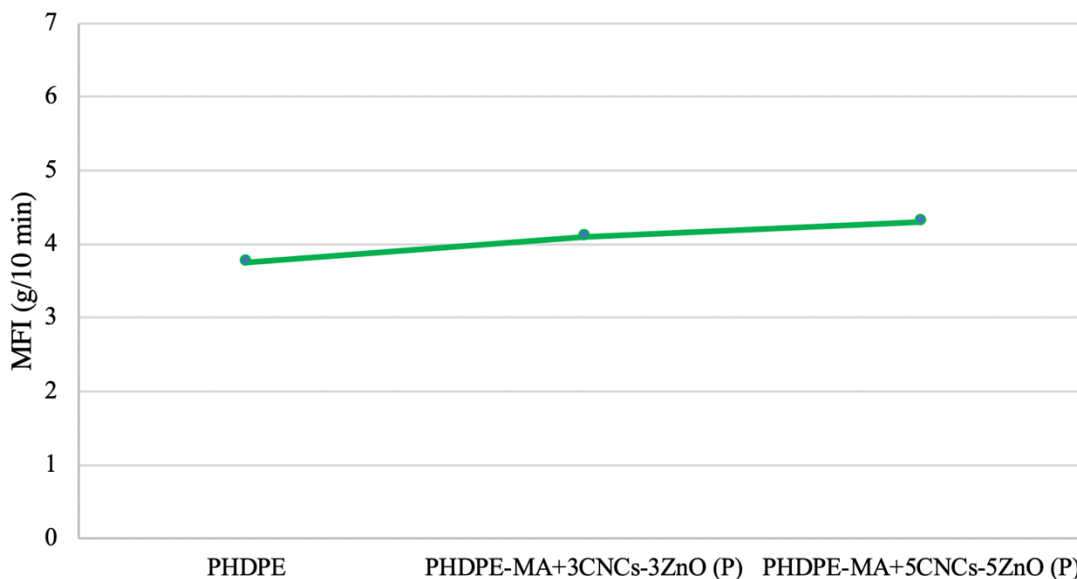


Figure 4.11. Comparison of the melt flow index of PHDPE vs. different nanofiller loadings. Addition of nanofillers decreased viscosity.

Incorporation of the nanofillers in MAPE2 composite samples resulted in 30% increase in MFI compared to MAPE2 polymer (Figure 4.12). This result can be an indicator of a chain scission reaction after adding the nanofillers in the highly cross-linked polymer more than fiber matrix

interactions. Chain scission reaction happens in polymers as a result of the oxygen attacking the polymer chain and abstracting a hydrogen atom from HDPE backbone. This will lead to a decrease in the molecular weight of the HDPE and formation of the carbonyl end groups [116-118]. Melt extrusion of the HDPE formulations will initiate the chain breakage. The addition of nanofillers will further impact the chain scission and increase the flowability. Furthermore, presence of the initiator in MAPE2 formulations assisted the oxidation during the MFI test, resulting an increase in the chain scission and subsequently, a decrease in viscosity [119]. This phenomena was more predominant in these formulations and overpowered the fiber-fiber interactions that usually increase the viscosity [120].

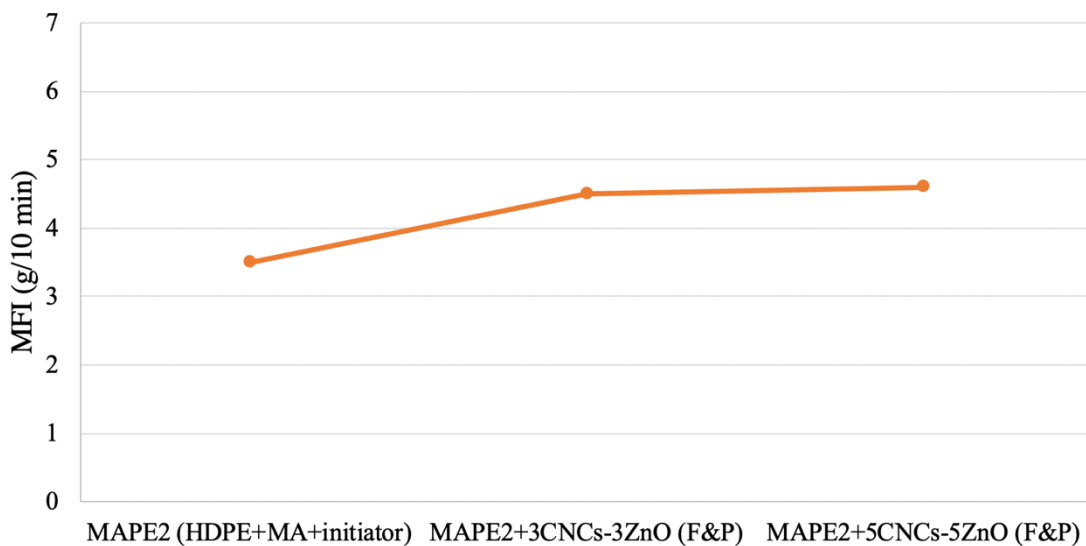


Figure 4.12. Comparison of the melt flow index of MAPE2 vs. different nanofiller loadings. Addition of nanofillers increased MFI.

P: Powder of CNCs and ZnO separately, F: Films of ZnO coated CNCs

4.2.4. Mechanical properties (Tensile test)

The mechanical properties of the samples were evaluated through tensile test and the results are summarized in Table 4.2. HDPE-MA composites showed relatively constant values for all three mechanical properties (Young’s modulus, maximum tensile strength, and elongation at

maximum tensile strength) compared to the virgin polymer. Same trend was also observed in PHDPE-MA composites.

As a benchmark, mechanical properties of MAPE1 and MAPE2 were evaluated against the virgin HDPE. Results showed no significant changes in the maximum tensile strength and the elongation at maximum tensile strength, indicating that any changes in these properties of the composites can be assigned to the role of nanofillers. However, Young's moduli of MAPE2 and MAPE1 were higher than the virgin polymer. This can be assigned to the crosslinking effect of MA, which resulted in a higher chain entanglement density and a stiffer network structure [121].

In formulations where MAPE was used as the polymer instead of direct feeding of HDPE with MA and nanofillers, a considerable increase was noted in elongation at maximum tensile strength and tensile strength with increasing the amount of fillers. This increase was up to 33% for maximum tensile strength and up to 22.5%, for percentage of the strain at maximum tensile strength. Several studies have suggested that agglomerations of the nanosized impurities in a neat polymer can increase its mechanical strength by binding between the polymer chains [122-124]. In MAPE formulations, poorly dispersed nanofillers in the polymer matrix may act as a cluster of impurities and result in an increase in maximum tensile strength. Meanwhile, for MAPE2 formulations Young's modulus showed a decline up to 20%. This result could be attributed to the poor interactions between the nanofillers and the matrix, considering the fact that MAPE2 polymer exhibited a higher young modulus than the virgin HDPE [125, 126]. The decline in the values for nanocomposites suggested the polymer chain scission reaction and weak interfacial bonding between the nanofillers and the matrix.

These observations were confirmed in following paragraphs with DMA test results where addition of the nanofillers in MAPE2 matrix have caused a reduction in the stiffness of the

composite samples. Generally, samples with lower stiffness have higher toughness energy and higher percentage of the strain [127, 128].

Table 4.2. Tensile properties of composite samples and polymers in direct feeding method.

Formulations	Maximum tensile stress (MPa)	Young's modulus (MPa)	Elongation at max tensile strength (%)
Virgin HDPE	22±2.3 ^a	537±36 ^a	12±1.0 ^{ab}
MAPE1	18±1.3 ^a	570±15 ^{ab}	13±0.6 ^a
MAPE2	19±0.8 ^a	585±10 ^b	14±0.9 ^a
Virgin PHDPE	16±0.5 ^c	437±26 ^c	11±0.9 ^d
HDPE-MA-3CNCs-3ZnO-P	21±2.6 ^a	568±47 ^a	13±1.0 ^a
HDPE-MA-5CNCs-5ZnO-P	20±1.5 ^a	572±50 ^a	13±0.3 ^a
HDPE-MA-3CNCs-3ZnO-F	19±1.7 ^a	575±31 ^a	13±2.0 ^b
HDPE-MA-5CNCs-5ZnO-F	21±2.0 ^a	571±55 ^a	12±0.6 ^a
MAPE1-1.5CNCs-1.5ZnO-P	24±0.8 ^a	434±54 ^a	15±0.7 ^{cb}
MAPE1-3CNCs-3ZnO-P	24±1.7 ^a	460±42 ^a	15±0.7 ^{cb}
MAPE1-5CNCs-5ZnO-P	25±1.0 ^b	521±39 ^a	14±0.7 ^b
MAPE1-1.5CNCs-1.5ZnO-F	26±1.1 ^b	431±70 ^a	16±1.4 ^c
MAPE1-3CNCs-3ZnO-F	25±1.0 ^b	513±24 ^a	15±1.0 ^{cb}
MAPE1-5CNCs-5ZnO-F	23±2.0 ^a	509±27 ^a	13±0.5 ^b
MAPE2-1.5CNCs-1.5ZnO-P	19±1.6 ^{ab}	383±55 ^c	14±0.7 ^b
MAPE2-3CNCs-3ZnO-P	17±1.5 ^{ab}	466±62 ^{ab}	13±1.0 ^b
MAPE2-5CNCs-5ZnO-P	18±1.0 ^b	451±50 ^{bc}	15±1.2 ^c
MAPE2-1.5CNCs-1.5ZnO-F	25±0.2 ^b	438±55 ^{bc}	16±0.7 ^c
MAPE2-3CNCs-3ZnO-F	25±0.5 ^b	503±48 ^a	15±0.2 ^c
MAPE2-5CNCs-5ZnO-F	27±0.9 ^b	559±18 ^a	15±0.3 ^c
PHDPE-MA-3CNCs-3ZnO-P	17±0.37 ^c	442±22 ^c	12±0.7 ^d
PHDPE-MA-5CNCs-3ZnO-P	17±0.5 ^c	486±24 ^d	13±0.4 ^{ad}

*Same superscript letters within the same column are not significantly different.

4.2.5. Dynamic mechanical analysis (DMA)

The DMA test studies the viscoelastic properties of the nanocomposite samples subjected to a periodic loading in various temperature ranges. Interactions between the nanofillers and polymer chains can result in a different viscoelastic behavior compared to the virgin polymer. The storage modulus of the polymer is associated with its elastic behaviors (Young's modulus), while the loss modulus is related to the viscous behaviors of the polymer and the energy dissipated because of the chain mobility. $\tan \delta$ is the ratio of the loss modulus to the storage modulus and represents the contribution of either of those behaviors in the viscoelastic materials [129]. For

comparison, the storage modulus of all samples at two different temperatures, loss modulus at 50°C, and tan δ peak intensity are shown in Table 4.3.

Table 4.3. Dynamic mechanical properties of HDPE and nanocomposites obtained from DMA.

Formulations	Storage modulus (MPa)		Loss modulus (MPa)	Tan δ peak intensity
	50 (°C)	100 (°C)	50 (°C)	
Virgin HDPE	759	178	118	0.32
MAPE2	778	220	122	0.32
Virgin PHDPE	590	150	100	0.27
HDPE-MA-3CNCs-3ZnO-P	791	228	130	0.28
HDPE-MA-5CNCs-5ZnO-P	771	223	140	0.29
HDPE-MA-3CNCs-3ZnO-F	866	248	126	0.30
HDPE-MA-5CNCs-5ZnO-F	860	210	140	0.32
MAPE2-3CNCs-3ZnO-P	766	228	100	0.29
MAPE2-5CNCs-5ZnO-P	794	247	115	0.31
MAPE2-3CNCs-3ZnO-F	650	184	113	0.31
MAPE2-5CNCs-5ZnO-F	717	211	125	0.32
PHDPE-MA-3CNCs-3ZnO-P	526	130	90	0.29
PHDPE-MA-5CNCs-3ZnO-P	549	139	92	0.29

Figure 4.13 illustrates that storage modulus of the HDPE-MA formulations were higher compared to the virgin HDPE. This trend was consistent even at high temperatures. This can be attributed to the enhanced interactions and modified stress and load transfers between fibers and matrix and reinforcing effect of the CNCs [93, 130]. As the percentage of nanofillers increased, the moduli started to decrease as a result of weaker interactions and agglomerations of the CNCs-ZnO in HDPE [131]. The small decline in tan δ values as increasing the concentration of nanofillers was most likely due to the increased interactions between the polymer chains and CNCs-ZnO, promoting some restrictions in the amorphous chains' mobility [132].

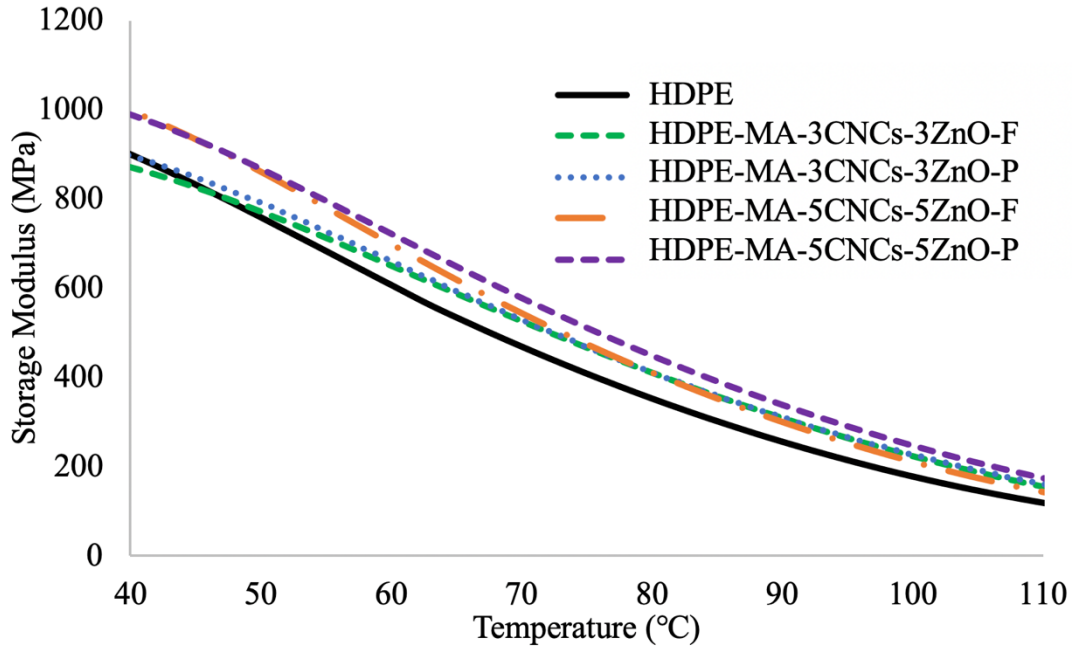


Figure 4.13. Representative storage modulus vs. temperature curves for HDPE-MA and nanocomposites.

As shown in Figure 4.14, the incorporation of nanofillers in MAPE2 slightly reduced the values of the storage modulus compared to the neat MAPE2, especially for the formulations that CNCs-ZnO used as film. This was an indicator of the decrease in the stiffness of the nanocomposites. It also correlates with the results obtained from tensile testing, where a small decrease in Young's modulus was observed in the same formulations. A slight reduction in peak intensity indicates the immobilization of polymer chains in the presence of the nanofillers and reduced dissipation energy. It is worth mentioning that a higher storage modulus of MAPE2 compared to neat HDPE could be contributed to the chain mobility restrictions of the polymer due to the interactions with MA molecule [133].

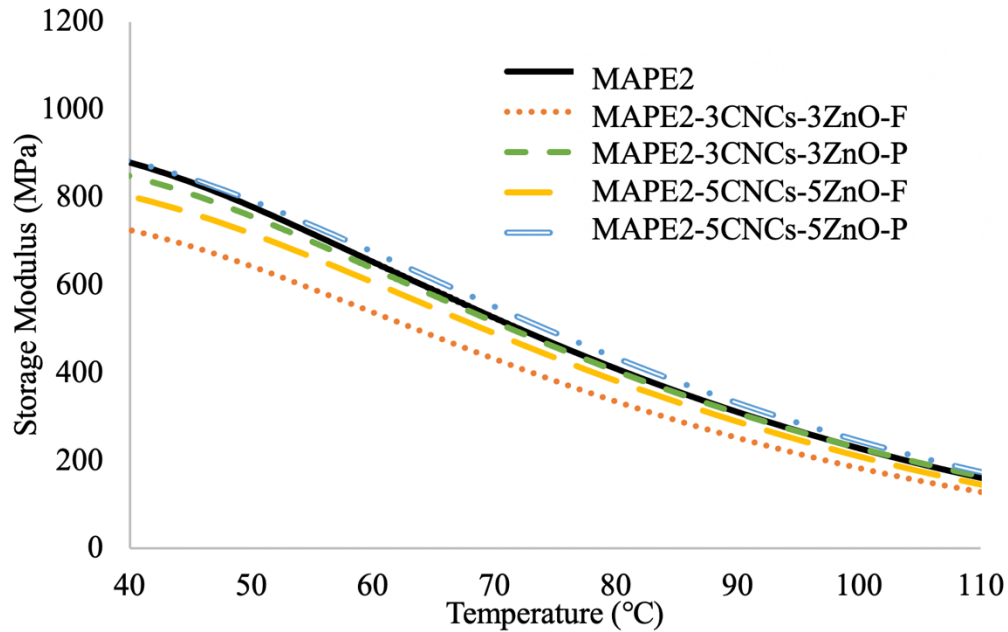


Figure 4.14. Representative storage modulus vs. temperature curves for MAPE2 and nanocomposites.

In the case of PHDPE-MA nanocomposites (Figure 4.15), a slight decrease in the storage modulus and increase in $\tan \delta$ was observed compared to the virgin PHDPE. This observation suggests weaker interactions between nanofillers and polymer, and also more energy dissipation potential because of the higher $\tan \delta$ in nanocomposite samples.

It is noticeable that the DMA test results are generally in good correlation with the tensile testing results. Formulations with higher storage modulus exhibited higher Young's modulus in the tensile test, indicating stronger fiber and matrix interactions. Having the correlation between both the mechanical test results proved the uniformity of the samples within a formulation.

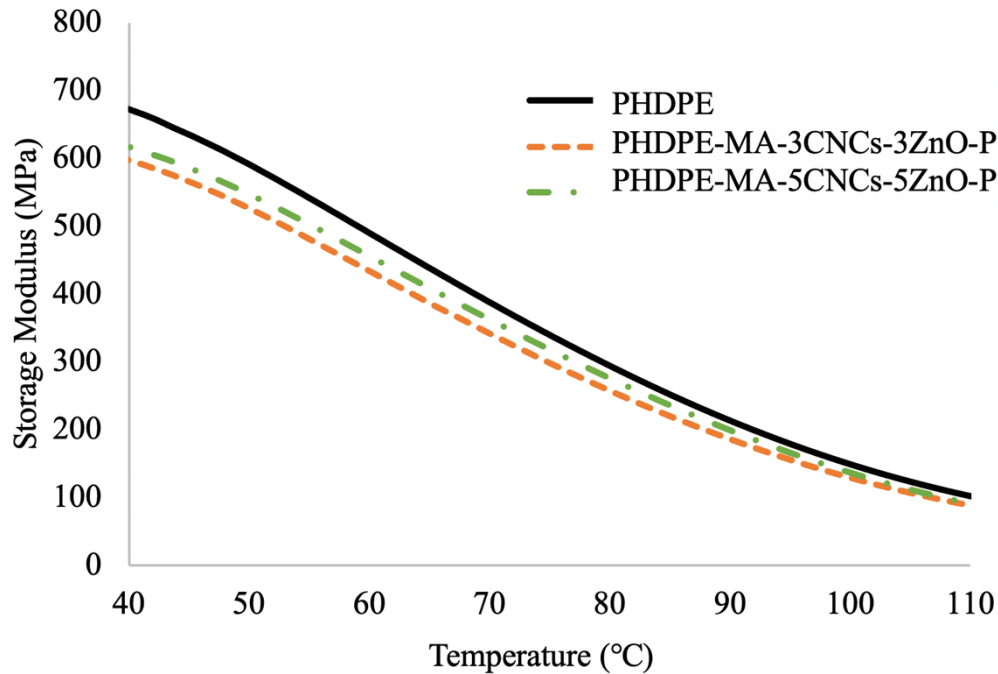


Figure 4.15. Representative storage modulus vs. temperature curves for PHDPE-MA and nanocomposites.

4.2.6. Rheological properties

The dynamic oscillatory shear measurements were carried out at 180°C to study the rheological properties and dynamic shearing response of the HDPE-MA, MAPE2, PHDPE-MA, and their different formulations of the nanocomposites. Representative complex viscosity (η^*) curves for different formulations are shown in Figure 4.16. The addition of nanofillers into HDPE increased the complex viscosity, indicating a higher melt strength in the nanocomposites compared to the virgin polymer. This behavior can be attributed to both the interactions between the matrix and nanofillers and also the formation of the network-like structures, which is most likely due to the MA cross-linking effect [134]; a network structure shows greater resistance to the applied stress. At higher concentrations of nanofillers, overall higher values for the complex viscosity was observed. The presence of nanofillers and their increased interactions with the matrix restricted the polymer chains' mobility in the molten state, and this in turn resulted in higher viscosity for the nanocomposite compared to the virgin polymer [135].

It's worth mentioning that the polymer chain structure significantly governs the rheological properties and melt strength of the polymers. By increasing the operating frequency, η^* values started to decline for all the formulations submitting a non-Newtonian behavior that is called shear thinning effect in molten state [136]. A similar trend was observed for complex viscosity of the PHDPE-MA nanocomposites; frequency dependent η^* values represented an increase in higher nanofillers loading signifying an improved fiber-matrix interaction. Conversely, the addition of ZnO-CNCs into MAPE2 decreased the complex viscosity values. This behavior can be ascribed to the poor fiber-matrix interactions in these formulations. Highly cross-linked structure of MAPE2 exhibited a higher viscosity compared to the formulations with the nanofillers, which addition of the nanofillers caused a chain scission reaction in the matrix and decreased the viscosity [137]. The short polymer chains produced during the chain scission reaction are more mobile and therefore, they can flow more easily [119]. It is concluded that the presence of the peroxide in these formulations caused oxidation and degradation of the CNCs and subsequently, the chain scission of the HDPE.

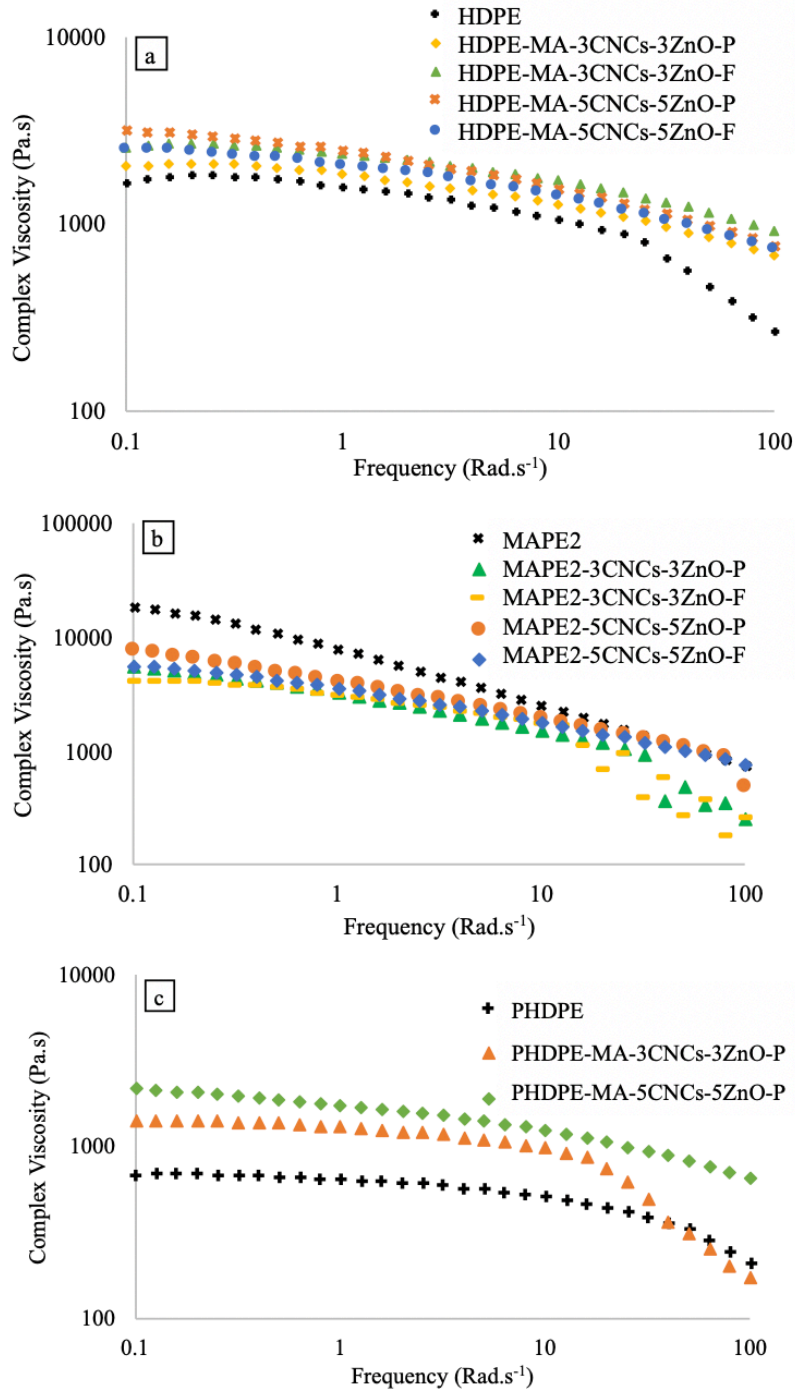


Figure 4.16. Complex viscosity for a) HDPE-MA and nanocomposites b) MAPE2 and nanocomposites c) Powder HDPE and nanocomposites.

Rheological behaviors of HDPE and its different formulations was also studied through shear moduli as a function of angular frequency at 180°C. Figure 4.17 depicts storage and loss modulus values for HDPE-MA compared to its nanocomposites. Both storage and loss modulus

exhibited an improvement upon addition of nanofillers to the virgin HDPE, suggesting the formation of relatively good interactions between the matrix and the nanofillers and resulting stress transfers from matrix to the fibers. At higher nanofiller loadings, higher storage and loss modulus were observed, most likely due to the enhancements in chain entanglements of the polymers [120].

On the contrary, addition of the nanofillers in MAPE2 polymer resulted in a reduction in both storage and loss moduli (Figure 4.18). This observation could be attributed to the fewer interactions between the nanofibers and the matrix in these formulations and lower viscosity as expected from the previous results. These formulations showed the similar pattern in DMA and tensile test as they were not as stiff as virgin MAPE2 and had lower Young's modulus.

Both storage and loss moduli increased in PHDPE-MA formulations with addition of the nanofillers (Figure 4.19), indicating the stronger interactions. Similar to HDPE-MA formulations, highest value for storage and loss modulus happened in the highest concentrations of the CNCs-ZnO, submitting the improved load transfer between the matrix and nanofibers.

An increasing trend was observed for storage and loss moduli by increasing the angular frequency for all three types of the formulations; this was due to the fact that at lower frequencies, entangled chains can relax over a larger period of time resulting in lower moduli. On the other hand, entangled chains don't have enough time to relax back at higher frequencies, and this would result in an increase in the moduli [138]. Furthermore, general values for loss modulus was higher than storage modulus for all formulations signifying an overall viscous behavior of the polymer nanocomposites.

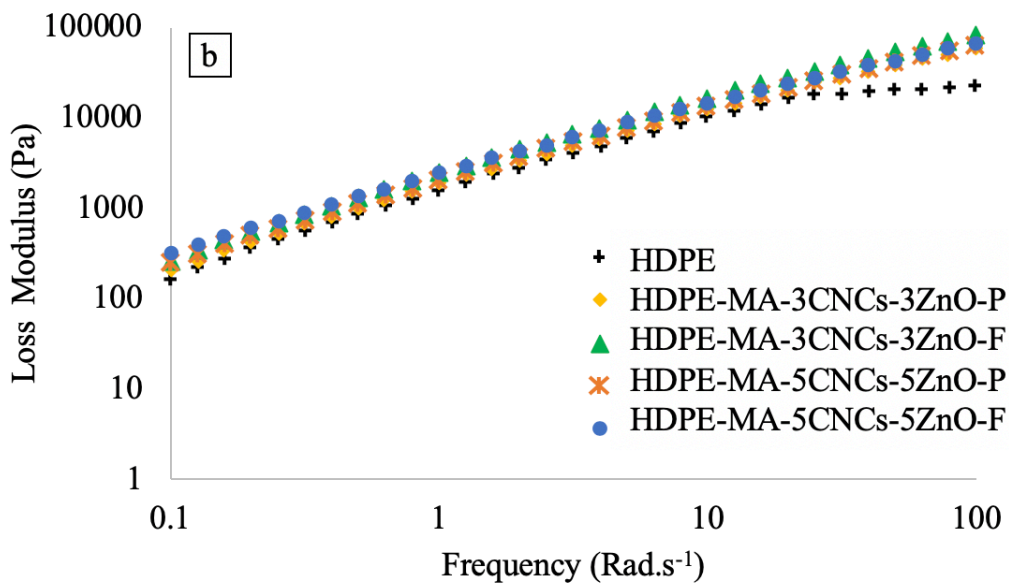
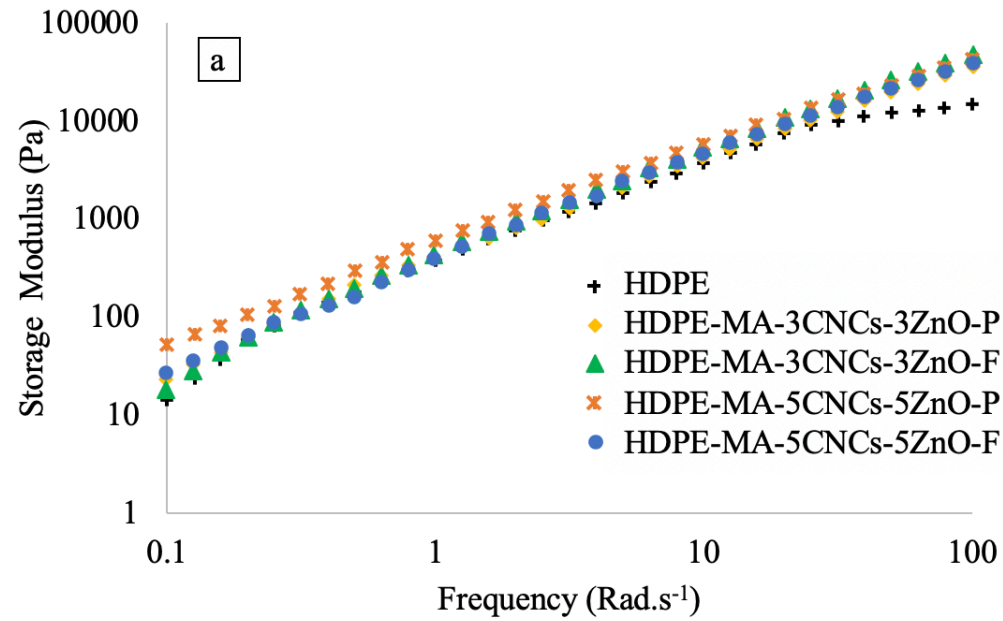


Figure 4.17. a) Storage modulus for HDPE- MA and its nanocomposites b) Loss modulus for HDPE- MA and its nanocomposites.

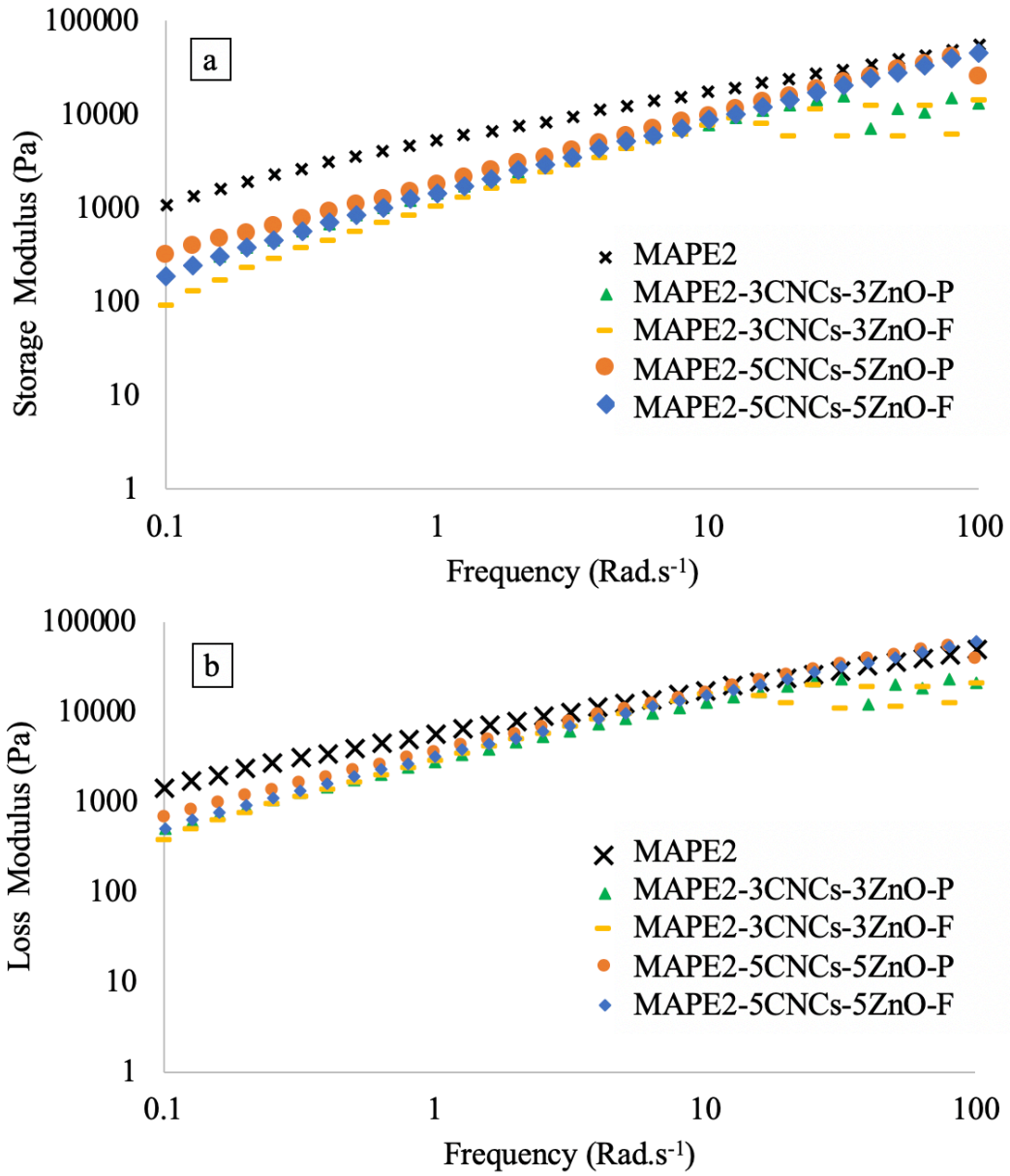


Figure 4.18. a) Storage modulus for MAPE2 and its nanocomposites b) Loss modulus for MAPE2 and its nanocomposites.

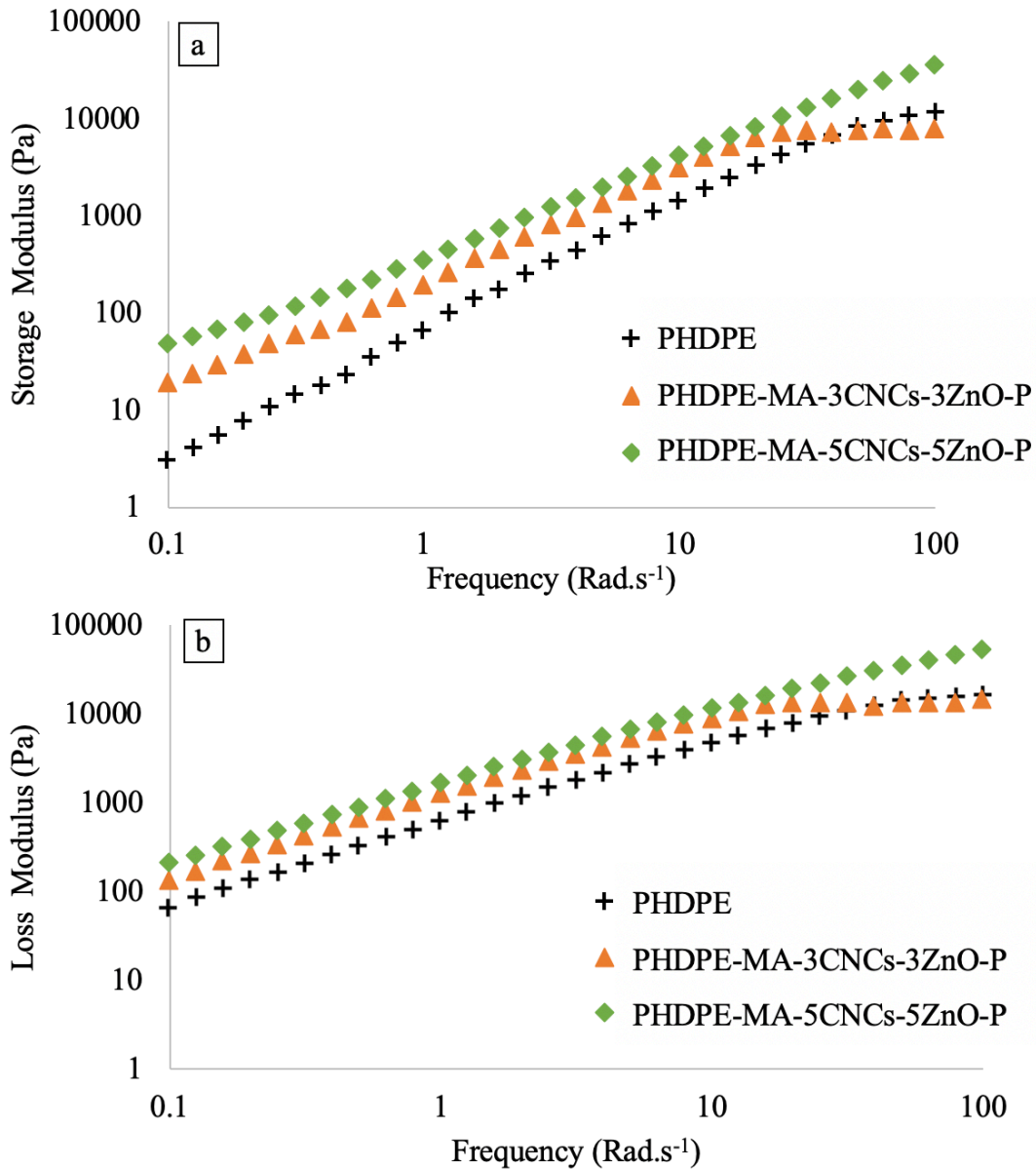


Figure 4.19. a) Storage modulus for PHDPE and its nanocomposites b) Loss modulus for PHDPE and its nanocomposites.

4.2.7. Thermogravimetric analysis (TGA)

Thermal stability of samples was studied through weight-loss (TGA) and the corresponding derivative curves (DTG). Thermal properties of the polymer nanocomposites including initial decomposition temperature (T_{onset}), peak decomposition (T_{peak}), and final degradation temperatures (T_{endset}) are summarized in Table 4.4.

Considering the weight-loss profiles for virgin HDPE, MAPE1, MAPE2, and PHDPE-MA nanocomposites, thermal decomposition of all samples was in typical one-step degradation pattern.

The thermal properties of HDPE composites were characterized against control samples. Virgin HDPE with 3 wt% CNCs, HDPE-MA with 3 wt% CNCs, and HDPE-MA with 3 wt% ZnO composite formulations were evaluated through TGA. It was observed that HDPE-MA-3 wt% ZnO formulation had a 10°C increase in T_{onset} compared to the virgin polymer, and the weight-loss was around 95.7%. This could be attributed to the heat dissipation and absorption role of ZnO nanoparticles [11]. The other two control formulations with 3 wt% CNCs experienced a decrease up to 20°C in T_{onset} compared to the virgin HDPE. T_{endset} in HDPE-MA-3wt% CNCs formulation had an 11°C increase, whereas in virgin HDPE with 3 wt% CNCs composite the increase was up to 5°C. This observation suggested that the presence of MA assisted the dispersion of CNCs in the HDPE matrix and resulted in a higher thermal stability due to the CNCs char formation and improving the fire retardancy due to barrier mechanism [10]. T_{peak} was also the highest (10°C increase) in this formulation compared to all the control samples, confirming the improved dispersion of the CNCs. Moreover, weight-loss was 96.5 % in HDPE-MA-3CNCs, whereas in virgin HDPE-3CNCs weight-loss was almost similar to the value for the virgin HDPE.

Overall for nanocomposite formulations, the total mass loss values were lower than the virgin HDPE. However, in nanocomposites that HDPE and MA were directly used, all thermal characteristics shifted to higher values, indicating higher thermal stability for nanocomposite compared to HDPE (Figure 4.20). T_{onset} and T_{endset} of the virgin HDPE were 421°C and 495°C, respectively. T_{onset} and T_{endset} of the neat CNCs are 253°C and 302°C, respectively, as it has been shown by Shojaeiarani *et al* [24]. However, in HDPE-MA composites, T_{onset} and T_{endset} increased up to 20°C and 30°C for the formulation with 3 wt% CNCs and 3 wt% ZnO in powder form. This

is related to the uniform distribution of nanofillers in the polymer, which boosted thermal stability of composites in this group of formulations [139], especially in the lower percentages of nanofillers.

Nano ZnO particles absorb the heat transmitted from the surroundings and reduce the thermal impact on the polymers [14]. In the meantime, charring effect of the CNCs protect the polymer from combustion by creating a barrier char layer [19]. The synergetic effect of CNCs and ZnO in the HDPE matrix boosted their flame retardancy mechanism and resulted in higher thermal stability for the nanocomposites compared to both virgin polymer and neat CNCs. Another important observation in these formulations was a 15°C increase in the T_{peak} compared to the virgin polymer in the formulation with 5wt% CNCs and 5wt% ZnO in powder form. Minimum weight-loss happened in the highest concentration of nanofillers because of the increased char residue, which inhibits the inner layer degradation.

Same trend was observed in PHDPE-MA nanocomposites; composite samples showed a significant increase in thermal properties by increasing the percentage of the nanofillers, indicating the uniform dispersion of CNCs and ZnO in HDPE matrix (Figure 4.23). T_{onset} was modified by 50°C and T_{endset} had a shift of 30°C compared to the virgin polymer. Moreover, maximum weight-loss happened at 485°C for virgin PHDPE, whereas in composites with 5 % loading of CNCs-ZnO maximum weight-loss was in 497°C.

In MAPE1 and MAPE2 composites, generally both T_{onset} and T_{endset} experienced a decrease. This observation can be an indicator of poor interfacial bonding between the nano fillers and the matrix [140] (Figure 4.21 and Figure 4.22). HDPE polymer in these formulations was pre-extruded to manufacture MAPE1 and MAPE2; this induced thermal history could result in polymer chains degradation and lower the thermal stability in terms of T_{onset} and T_{endset} . Moreover, presence

of 0.5 wt% dibenzoyl peroxide (initiator) in MAPE2 composites caused oxidization and degradation of the CNCs and ZnO and negated their flame retardancy effect. Weight-loss decreased in some of the formulations in higher loadings of CNCs, indicating the charring effect of nanofillers.

Table 4.4. Thermal properties of HDPE, PHDPE, and their nanocomposites.

Formulations	T _{onset} (°C)	T _{endset} (°C)	T _{peak} (°C)	Weight-loss (%)
Virgin HDPE	421.2	494.6	485.4	99.8
Virgin PHDPE	417.5	494.9	485.0	99.0
Virgin HDPE-3CNCs	401.2	502.2	490.1	99.3
HDPE-MA-3CNCs	400.7	510.3	496.0	96.5
HDPE-MA-3ZnO	430.2	501.5	487.5	95.7
MAPE2-1.5CNCs-1.5ZnO-P	404.3	458.0	442.5	98.7
MAPE2-3CNCs-3ZnO-P	416.2	466.3	445.1	95.8
MAPE2-5CNCs-5ZnO-P	415.0	461.3	444.6	94.7
MAPE2-1.5CNCs-1.5ZnO-F	410.9	461.7	444.0	98.8
MAPE2-3CNCs-3ZnO-F	406.2	460.1	443.0	98.8
MAPE2-5CNCs-5ZnO-F	407.1	464.2	444.5	97.7
MAPE1-1.5CNCs-1.5ZnO-P	422.5	466.5	441.0	99.1
MAPE1-3CNCs-3ZnO-P	404.3	458.9	442.4	97.1
MAPE1-5CNCs-5ZnO-P	403.7	457.5	444.5	93.5
MAPE1-1.5CNCs-1.5ZnO-F	406.2	460.2	443.0	99.3
MAPE1-3CNCs-3ZnO-F	405.4	458.1	440.6	98.7
MAPE1-5CNCs-5ZnO-F	404.5	462.4	442.4	97.5
HDPE-MA-3CNCs-3ZnO-P	440.6	512.4	492.3	97.9
HDPE-MA-5CNCs-5ZnO-P	400.2	499.6	500.0	94.6
HDPE-MA-3CNCs-3ZnO-F	430.0	527.3	475.2	98.8
HDPE-MA-5CNCs-5ZnO-F	427.2	510.2	496.9	94.2
PHDPE-MA-3CNCs-3ZnO-P	466.9	514.7	486.8	94.0
PHDPE-MA-5CNCs-3ZnO-P	447.2	527.4	497.2	91.0

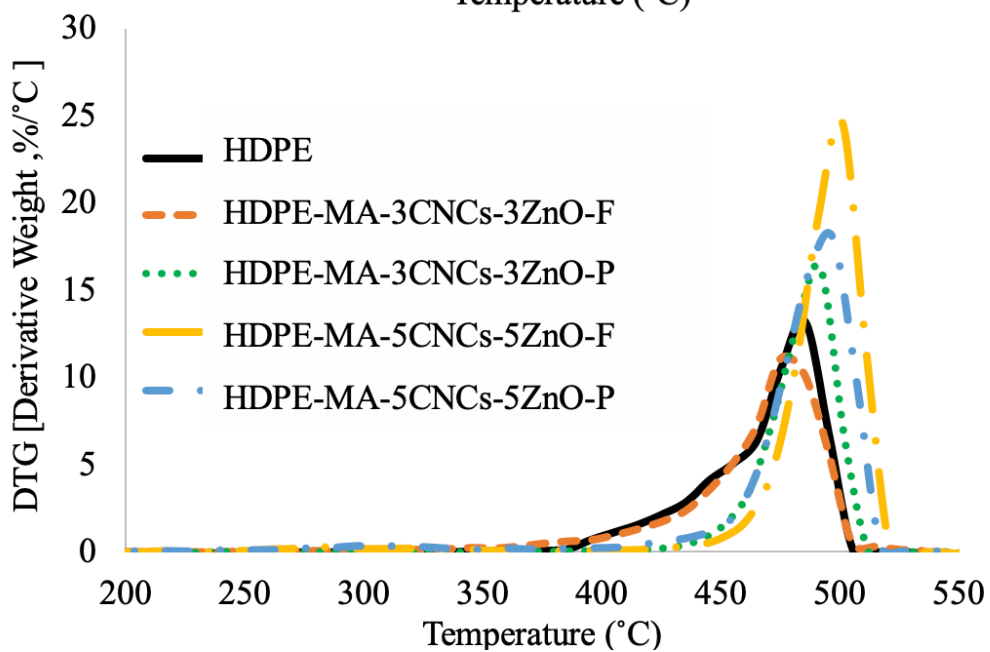
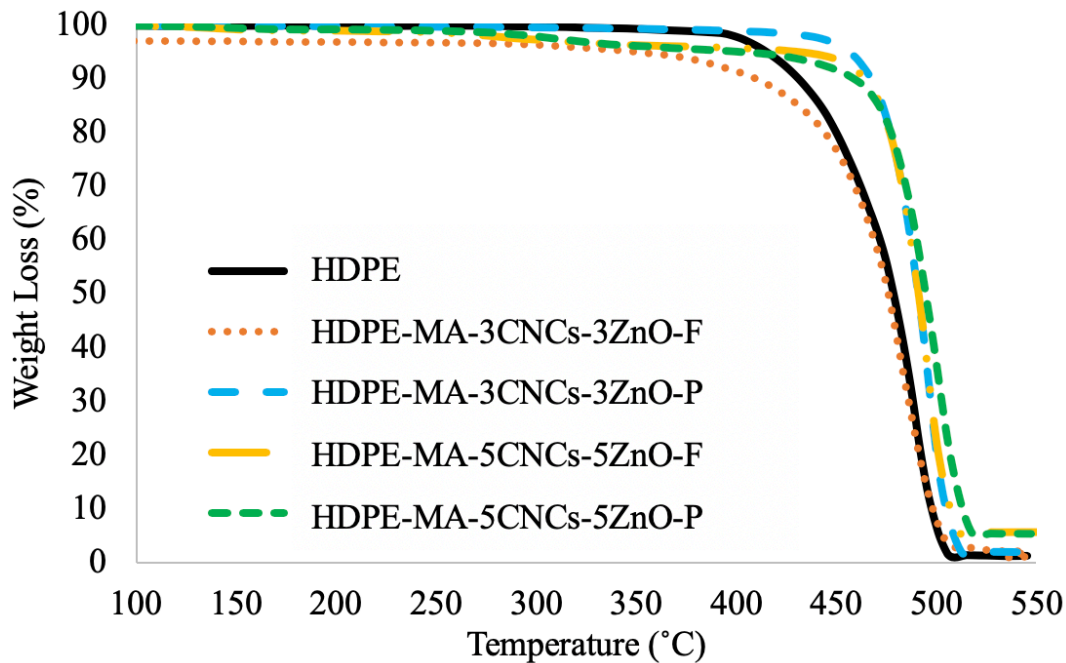


Figure 4.20. TGA and DTG curves for HDPE-MA composites.

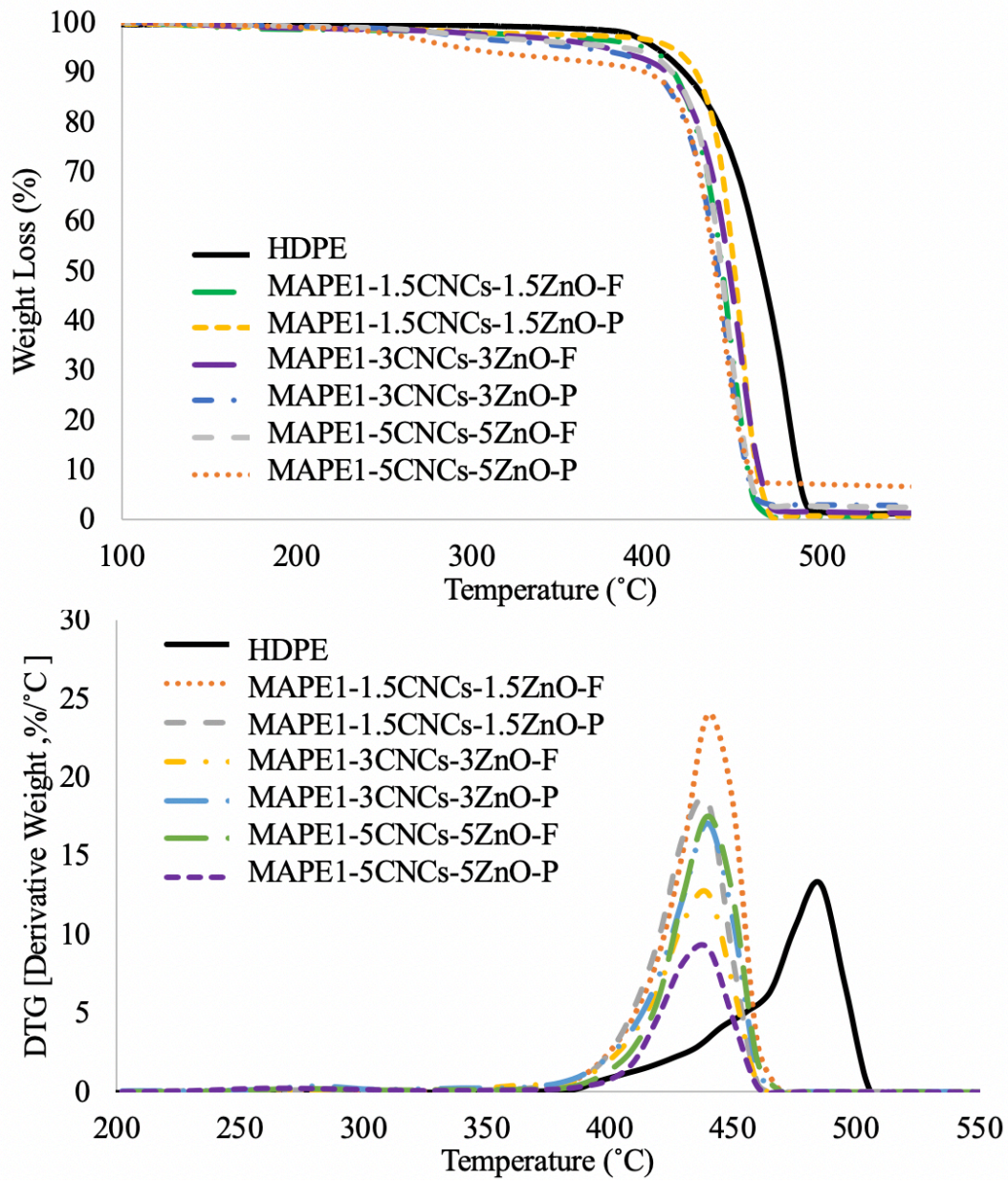


Figure 4.21. TGA and DTG curves for MAPE1 composites.

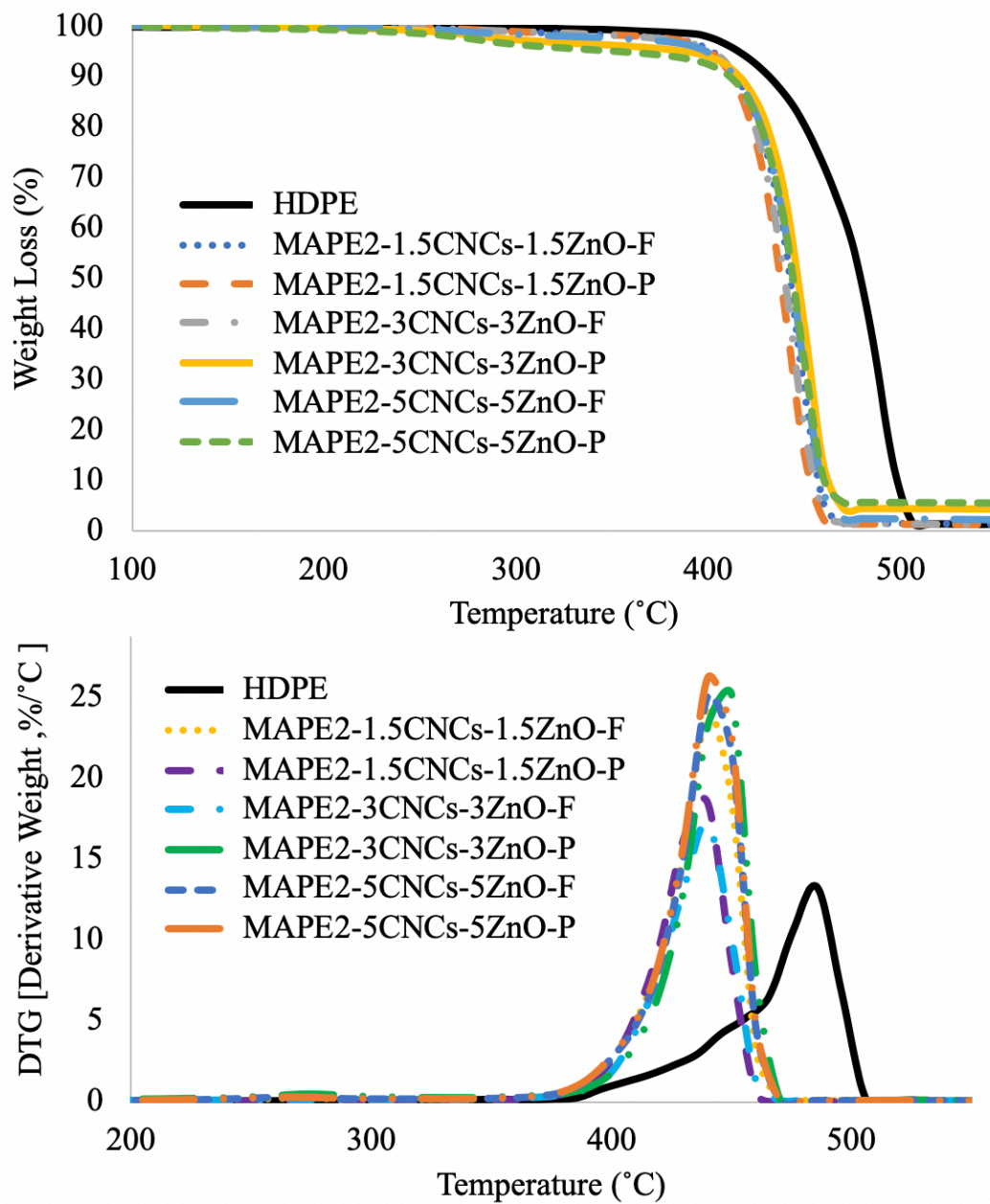


Figure 4.22. TGA and DTG curves for MAPE2 composites.

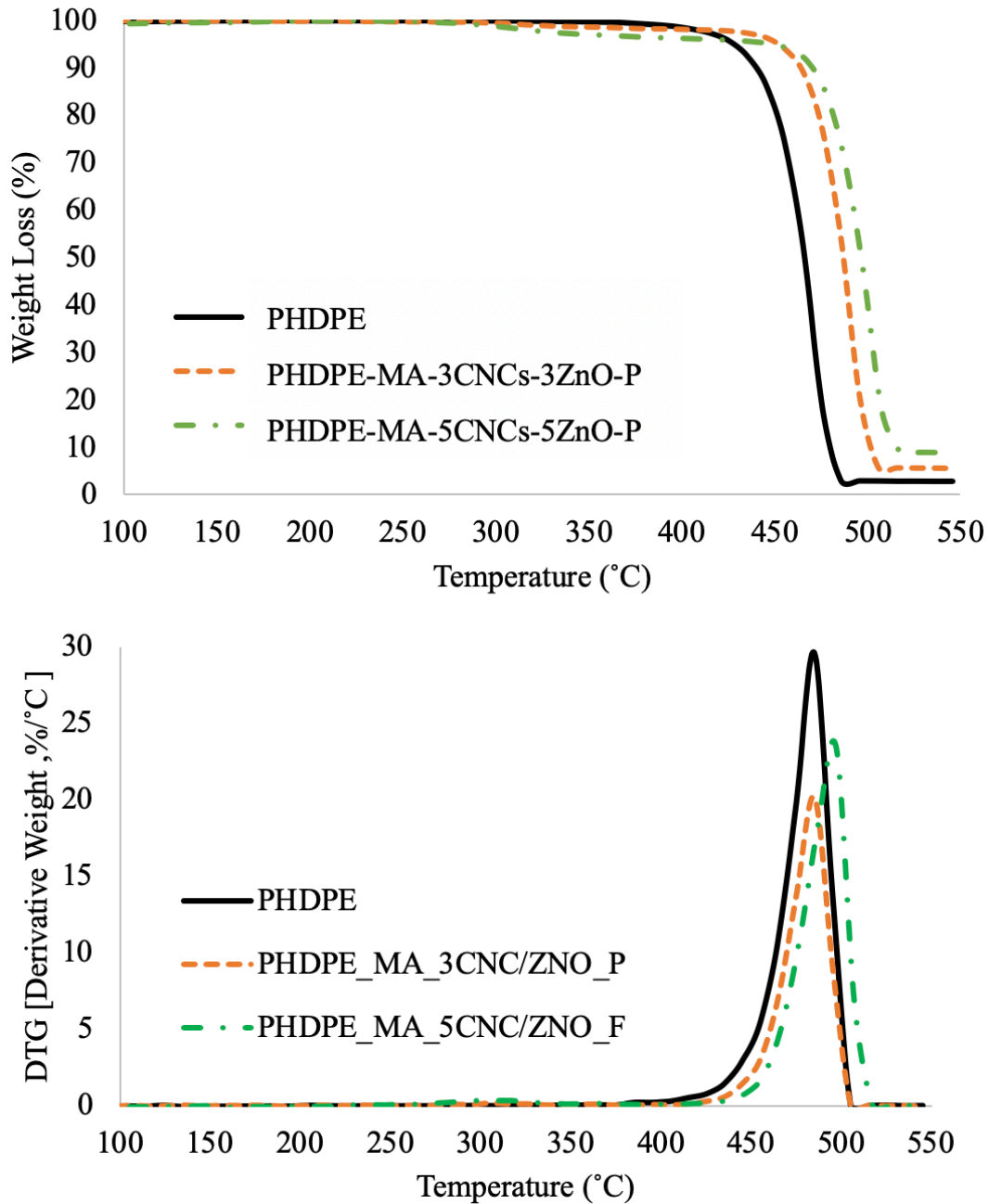


Figure 4.23. TGA and DTG curves for PHDPE composites.

4.2.8. Horizontal burn test

Horizontal burn test was conducted on the samples based on the ASTM D-635 standard. HDPE-MA composites with higher thermal stability in the TGA test displayed a relatively better performance in the fire test as shown in the following (Table 4.5 to Table 4.8). Weight-loss of the

HDPE-MA composites with 3wt% CNCs and 3 wt% ZnO in powder form decreased up to 34% compared to the virgin HDPE, which represents more thermal durability under combustion. Flame retardancy mechanism of CNCs and ZnO is the condensed phase char formation; the barrier charcoal layer inhibits the inner layers from burning excessively by diminishing the oxygen supply [14]. Also, up to 35% reduction was recorded in the flame spread rate (FSR) of the nanocomposite specimens with 3wt% CNCs-3wt% ZnO and 5wt% CNCs-5wt% ZnO in powder form. Lower FSR indicates the slower flame propagation throughout the samples and the resultant superior fire retardancy. This outcome highlighted that the presence of green fire retardants in the polymer matrix strengthened its fire resistance to a certain degree. Generally, nanofillers in the powder form showed better fire performance than nanofillers in the film form. This could be attributed to the improved distribution of the nanofillers in the polymer matrix and the resultant synergistic effect.

PHDPE-MA composites also had a decline up to 23% for both FSR and weight-loss in nanocomposites with 5wt% CNCs-5wt% ZnO compared to the virgin PHDPE. Increase in the concentration of the nanofillers resulted in improved fire retardancy. This observation could be assigned to improved interactions between composite component.

In MAPE1 formulations, a 37% decline in the weight-loss and 26% decline in the FSR was recorded. Minimum weight-loss happened in the maximum percentage of the CNCs and ZnO because of their charring effect. Nanocomposites with 3wt% CNCs-3wt% ZnO in film form exhibited the slowest FSR. Overall, poor dispersion of nanofillers in the HDPE matrix in these formulations would weaken the fire performance by degrading the CNCs during the processing steps. CNCs in powder form were believed to be more prone to this degradation compared to the film ones, and this could be the reason for better performance in film formulations for MAPE2 composites.

The performance of MAPE2 nanocomposites in the fire test was weaker than the other formulations. Minimum weight-loss happened in the formulation with 1.5wt% CNCs-1.5wt% ZnO in powder form. The decline in weight-loss can be attributed to the charring and shielding effect of the CNCs-ZnO, which were randomly distributed throughout the samples. FSR was decreased up to 11% in the formulation with 1.5wt% CNCs-1.5wt% ZnO in film form. In these composites, the oxidation caused by the presence of the peroxide can further reduce the fire performance.

Generally, HDPE-MA nanocomposites showed the best performance in the burn test among all the formulations. Overall, the dripping of the nanocomposite samples was significantly lower in volume compared to the virgin polymer, which can be assigned to the decrease in the weight-loss for composite formulations due to the formation of the barrier char layer. Moreover, dripping in the virgin polymer was fast and in a continuous manner, whereas dripping was much slower, non-continuous and intermittent in the nanocomposites, especially HDPE-MA formulations. This physical observation was most likely due to the slower flame propagation rate in these samples and improved heat absorption as a result of flame retardancy effect of CNCs and ZnO nanoparticles. Virgin HDPE samples burned showing a blue flame with an orange tip and a paraffin-like smell. However composite samples containing CNCs and ZnO produced a smoke with a black soot and a sweet odor. None of the samples showed self-extinguish properties and they all continued to burn after removing the flame resource.

Table 4.5. Fire characteristic of composite samples with HDPE-MA from horizontal burn test.

Sample code	WL (%) in 1 min	% change in WL%	FSR (mm/s)	% change in FSR
Virgin HDPE	30.00	-	0.35	-
HDPE + 3ZnO	29.00	3.33	0.33	5.71
HDPE + 3CNCs	27.00	10.00	0.35	0.00
HDPE-MA-3CNCs-3ZnO-P	19.50	35.00	0.23	34.29
HDPE-MA-5CNCs-5ZnO-P	20.00	33.33	0.23	34.29
HDPE-MA-3CNCs-3ZnO-F	21.00	30.00	0.27	22.86
HDPE-MA-5CNCs-5ZnO-F	19.00	35.00	0.25	28.57

WL: weight-loss, FSR: flame spread rate

Table 4.6. Fire characteristic of composite samples with MAPE1 from horizontal burn test.

Sample code	WL (%) in 1 min	% change in WL%	FSR (mm/s)	% change in FSR
MAPE1-1.5CNCs-1.5ZnO-P	27.00	10.00	0.35	0.00
MAPE1-3CNCs-3ZnO-P	21.00	30.00	0.35	0.00
MAPE1-5CNCs-5ZnO-P	20.00	33.33	0.27	22.86
MAPE1-1.5CNCs-1.5ZnO-F	21.00	30.00	0.26	25.71
MAPE1-3CNCs-3ZnO-F	25.00	16.67	0.25	28.57
MAPE1-5CNCs-5ZnO-F	19.00	36.67	0.30	14.29

WL: weight-loss, FSR: flame spread rate

Table 4.7. Fire characteristic of composite samples with MAPE2 from horizontal burn test.

Sample code	WL (%) in 1 min	% change in WL%	FSR (mm/s)	% change in FSR
MAPE2-1.5CNCs-1.5ZnO-P	18.00	40.00	0.35	0.00
MAPE2-3CNCs-3ZnO-P	20.00	33.33	0.34	2.85
MAPE2-5CNCs-5ZnO-P	21.00	30.00	0.34	2.85
MAPE2-1.5CNCs-1.5ZnO-F	20.00	33.33	0.31	11.42
MAPE2-3CNCs-3ZnO-F	22.00	26.67	0.35	0.00
MAPE2-5CNCs-5ZnO-F	23.00	23.33	0.34	2.85

WL: weight-loss, FSR: flame spread rate

Table 4.8. Fire characteristic of composite samples with PHDPE-MA from horizontal burn test.

Sample code	WL (%) in 1 min	% change in WL%	FSR (mm/s)	% change in FSR
Virgin PHDPE	30.00	-	0.39	-
PHDPE-MA-3CNCs-3ZnO-P	24.00	20.00	0.32	17.95
PHDPE-MA-5CNCs-5ZnO-P	23.00	23.33	0.30	23.07

WL: weight-loss, FSR: flame spread rate

CHAPTER 5. CONCLUSION AND FUTURE WORK

Designing a safe fire retardant system to prevent commodity polymers from combustion or at least lower their burning rate has been a field of interest recently. HDPE is one of the most popular commodity polymers because of its low cost, good mechanical behaviors, low permeability, and many other advantages. However, its low stability in high temperatures and susceptibility to combustion have limited its applications. This research has focused on developing an environmentally friendly fire retardant system for HDPE using scalable manufacturing techniques. In this study, HDPE composites were prepared by blending the cellulose nanocrystals and ZnO nanoparticles with HDPE using two different methods. PEO was used in the first method as a dispersion agent to enhance the interfacial bonding between the composite components. Unfortunately, PEO treatment did not improve the mechanical and physical properties since CNCs-ZnO nanofillers were not dispersed uniformly in the polymer matrix.

In the second method, MA was employed as a coupling agent to increase the uniform dispersion of nanofillers in the polymer matrix. HDPE-MA with different loadings of CNCs-ZnO showed a good mechanical performance, which was consistent or even better than the virgin HDPE. A relatively same trend was observed for PHDPE-MA nanocomposites. On the other hand, MAPE1 and MAPE2 caused a slight decrease in Young's modulus and did not perform as well as HDPE-MA formulations. HDPE-MA nanocomposites showed superior thermal properties compared to the virgin polymer. The fire spread rate of these HDPE-MA formulations was much slower than the virgin HDPE. PHDPE nanocomposites followed similar trends in terms of both thermal and fire performances. On the other hand, MAPE1 and MAPE2 exhibited lower thermal stability and relatively similar fire performance compared to the virgin polymer.

In addition to the tests conducted in this thesis, there are other tests that could be done to evaluate the fire performance of the nanocomposites, such as cone calorimetry test. Lu *et al.* reported the fire retardancy performance of HDPE composites in terms of peak and total heat release rate, using cone calorimetry [141]. To validate the fire test results in this research, cone calorimetry test is being conducted by U.S. Forest Products Lab, Madison WI. Moreover, studying the polymer molecular properties used in the nanocomposites may lead to a deeper understanding of their behaviors in the MFI, Rheology, and DMA tests [120].

Furthermore, there are some interesting works in the literature on the effect of other metal oxides instead of ZnO, such as Al(OH)₃ and boron on HDPE fire retardancy [142-144]. These metal oxides are reported to be also effective in augmenting the fire performance of HDPE composites especially in combination with other fire retardant systems. Bio-based fire retardants such as nanoclays, phloroglucinol, chitosan, DNA, proteins, and lignin can build a synergistic effect with CNCs and further enhance their shielding effect of char formation, as it has been reported by Costes *et al.* [10]. There are other methods of grafting MA on the HDPE backbone that can be used as an alternative, such as ball-milling, which have been proven to yield high grafting degrees [145]. Ball-milling process yields a fine powder and is considered to be an efficient mixing process in solid phase at low temperature; this in turn would improve the coupling effect of MA between HDPE and CNCs. Moreover, using a lower amount of peroxide (0.2 wt% or less) as an initiator in MAPE nanocomposites may inhibit the oxidation and degradation of the CNCs and subsequently, result in higher thermal stability.

Although these tests and materials may yield additional insights, this thesis has shown that, overall, HDPE-MA and PHDPE-MA nanocomposites likely have shown better thermal stability with a similar or better mechanical performance as the virgin HDPE. The proposed composite

fabrication method was fast, safe, and cost-effective with a minimum use of chemicals, and therefore could be scalable for commercial production.

REFERENCES

- [1] Kalam, A., Kamarudzaman, R., Hyie, K. M., Jumahat, A., and Rahman, N. L. A., 2017, "The Role of Secondary Filler on Fracture Toughness and Impact Strength of HDPE/Clay Nanocomposites," *Pertanika Journal of Science and Technology*, 25, pp. 95-104.
- [2] Müller, K., Bugnicourt, E., Latorre, M., Jorda, M., Echegoyen Sanz, Y., Lagaron, J., Miesbauer, O., Bianchin, A., Hankin, S., and Bölz, U., 2017, "Review on the processing and properties of polymer nanocomposites and nanocoatings and their applications in the packaging, automotive and solar energy fields," *Nanomaterials*, 7(4), p. 74.
- [3] Francisco, D. L., Paiva, L. B., and Aldeia, W., "Advances in polyamide nanocomposites: A review," *Polymer Composites*.
- [4] Coiai, S., Passaglia, E., Pucci, A., and Ruggeri, G., 2015, "Nanocomposites based on thermoplastic polymers and functional nanofiller for sensor applications," *Materials*, 8(6), pp. 3377-3427.
- [5] Lopez-Cuesta, J.-M., Longuet, C., and Chivas-Joly, C., 2014, "Thermal degradation, flammability, and potential toxicity of polymer nanocomposites," *Health and Environmental Safety of Nanomaterials*, Elsevier, pp. 278-310.
- [6] Levchik, S. V., 2007, "Introduction to flame retardancy and polymer flammability," *Flame retardant polymer nanocomposites*, pp. 1-29.
- [7] Irvine, D., McCluskey, J., and Robinson, I., 2000, "Fire hazards and some common polymers," *Polymer Degradation and Stability*, 67(3), pp. 383-396.
- [8] Fire-Administration, U. S., 2009, "Topical Fire Report Series (TFRS), Intentionally Set Vehicle Fires."
- [9] Fire-Administration, U. S., 2018, "Fire Estimate Summary, Residential Building Fire Trends (2007-2016)," U.S. Fire Administration.
- [10] Costes, L., Laoutid, F., Brohez, S., and Dubois, P., 2017, "Bio-based flame retardants: When nature meets fire protection," *Materials Science and Engineering: R: Reports*, 117, pp. 1-25.
- [11] Fallah, M. H., Fallah, S. A., and Zanjanchi, M. A., 2011, "Synthesis and Characterization of Nano-sized Zinc Oxide Coating on Cellulosic Fibers: Photoactivity and Flame-retardancy Study," *Chinese Journal of Chemistry*, 29(6), pp. 1239-1245.
- [12] Grand, A. F., and Wilkie, C. A., 2000, *Fire retardancy of polymeric materials*, CRC Press.
- [13] Harley, K. G., Marks, A. R., Chevrier, J., Bradman, A., Sjödin, A., and Eskenazi, B., 2010, "PBDE concentrations in women's serum and fecundability," *Environmental health perspectives*, 118(5), p. 699.

- [14] Sheshama, M., Khatri, H., Suthar, M., Basak, S., and Ali, W., 2017, "Bulk vs. Nano ZnO: Influence of fire retardant behavior on sisal fibre yarn," *Carbohydrate polymers*, 175, pp. 257-264.
- [15] Al Nuumani, R., Bolognesi, G., and Vladisavljevic, G. T., 2018, "Microfluidic production of poly (1, 6-hexanediol diacrylate)-based polymer microspheres and bifunctional microcapsules with embedded TiO₂ nanoparticles," *Langmuir*, 34(39), pp. 11822-11831.
- [16] Espitia, P., Otoni, C., and Soares, N., 2016, "Zinc Oxide Nanoparticles for Food Packaging Applications," *Antimicrobial Food Packaging*, Elsevier, pp. 425-431.
- [17] Agarwal, H., Kumar, S. V., and Rajeshkumar, S., 2017, "A review on green synthesis of zinc oxide nanoparticles—An eco-friendly approach," *Resource-Efficient Technologies*, 3(4), pp. 406-413.
- [18] Shojaeiarani, J., Bajwa, D., Jiang, L., Liaw, J., and Hartman, K., 2019, "Insight on the influence of nano zinc oxide on the thermal, dynamic mechanical, and flow characteristics of Poly (lactic acid)—zinc oxide composites," *Polymer Engineering & Science*, 59(6), pp. 1242-1249.
- [19] Tang, E., Cheng, G., Pang, X., Ma, X., and Xing, F., 2006, "Synthesis of nano-ZnO/poly (methyl methacrylate) composite microsphere through emulsion polymerization and its UV-shielding property," *Colloid and Polymer Science*, 284(4), pp. 422-428.
- [20] Inai, N., Lewandowska, A., Ghita, O., and Eichhorn, S., 2018, "Interfaces in polyethylene oxide modified cellulose nanocrystal-polyethylene matrix composites," *Composites Science and Technology*, 154, pp. 128-135.
- [21] Ben Azouz, K., Ramires, E. C., Van den Fonteyne, W., El Kissi, N., and Dufresne, A., 2011, "Simple method for the melt extrusion of a cellulose nanocrystal reinforced hydrophobic polymer," *ACS Macro Letters*, 1(1), pp. 236-240.
- [22] Azizi, S., Ahmad, M. B., Ibrahim, N. A., Hussein, M. Z., and Namvar, F., 2014, "Cellulose nanocrystals/ZnO as a bifunctional reinforcing nanocomposite for poly (vinyl alcohol)/chitosan blend films: fabrication, characterization and properties," *International journal of molecular sciences*, 15(6), pp. 11040-11053.
- [23] de Luna, M. S., Galizia, M., Wojnarowicz, J., Rosa, R., Lojkowski, W., Leonelli, C., Acierno, D., and Filippone, G., 2014, "Dispersing hydrophilic nanoparticles in hydrophobic polymers: HDPE/ZnO nanocomposites by a novel template-based approach," *Express Polymer Letters*, 8, pp. 362-372.
- [24] Shojaeiarani, J., Bajwa, D. S., and Hartman, K., 2019, "Esterified cellulose nanocrystals as reinforcement in poly (lactic acid) nanocomposites," *Cellulose*, 26(4), pp. 1-14.

- [25] Shojaeiarani, J., Bajwa, D., and Shirzadifar, A., 2019, "A review on cellulose nanocrystals as promising biocompounds for the synthesis of nanocomposite hydrogels," *Carbohydrate polymers*, 216, pp. 247-259.
- [26] Tang, W., Santare, M. H., and Advani, S. G., 2003, "Melt processing and mechanical property characterization of multi-walled carbon nanotube/high density polyethylene (MWNT/HDPE) composite films," *Carbon*, 41(14), pp. 2779-2785.
- [27] Lewandowska, A., and Eichhorn, S., 2016, "Raman imaging as a tool for assessing the degree of mixing and the interface between polyethylene and cellulose nanocrystals," *Proc. IOP Conference Series: Materials Science and Engineering*, IOP Publishing, p. 012030.
- [28] Felix, J. M., and Gatenholm, P., 1991, "The nature of adhesion in composites of modified cellulose fibers and polypropylene," *Journal of Applied Polymer Science*, 42(3), pp. 609-620.
- [29] Lu, B., and Chung, T., 2000, "Synthesis of maleic anhydride grafted polyethylene and polypropylene, with controlled molecular structures," *Journal of Polymer Science Part A: Polymer Chemistry*, 38(8), pp. 1337-1343.
- [30] Cutler, C. P., 2018, "Use of Metals in Our Society," *Metal Allergy*, Springer, pp. 3-16.
- [31] Alehosseini, A., Gómez-Mascaraque, L. G., Martínez-Sanz, M., and López-Rubio, A., 2019, "Electrospun curcumin-loaded protein nanofiber mats as active/bioactive coatings for food packaging applications," *Food Hydrocolloids*, 87, pp. 758-771.
- [32] Ching, Y. C., Gunathilake, T. U., Ching, K. Y., Chuah, C. H., Sandu, V., Singh, R., and Liou, N.-S., 2019, "Effects of high temperature and ultraviolet radiation on polymer composites," *Durability and Life Prediction in Biocomposites, Fibre-Reinforced Composites and Hybrid Composites*, Elsevier, pp. 407-426.
- [33] Ray, S., and Cooney, R. P., 2018, "Thermal degradation of polymer and polymer composites," *Handbook of Environmental Degradation of Materials (Third Edition)*, Elsevier, pp. 185-206.
- [34] Emmons, H., 1973, "Heat transfer in fire," *Journal of Heat Transfer*, 95(2), pp. 145-151.
- [35] Papazoglou, E. S., 2004, "Flame retardants for plastics," *Handbook of building materials for fire protection*, pp. 4.1-4.88.
- [36] Norouzi, M., Zare, Y., and Kiany, P., 2015, "Nanoparticles as effective flame retardants for natural and synthetic textile polymers: application, mechanism, and optimization," *Polymer Reviews*, 55(3), pp. 531-560.
- [37] Wang, X., Kalali, E. N., Wan, J.-T., and Wang, D.-Y., 2017, "Carbon-family materials for flame retardant polymeric materials," *Progress in Polymer Science*, 69, pp. 22-46.

- [38] Horacek, H., and Pieh, S., 2000, "The importance of intumescent systems for fire protection of plastic materials," *Polymer International*, 49(10), pp. 1106-1114.
- [39] Schmitt, E., 2007, "Phosphorus-based flame retardants for thermoplastics," *Plastics, Additives and Compounding*, 9(3), pp. 26-30.
- [40] Dasari, A., Yu, Z.-Z., Cai, G.-P., and Mai, Y.-W., 2013, "Recent developments in the fire retardancy of polymeric materials," *Progress in Polymer Science*, 38(9), pp. 1357-1387.
- [41] Laoutid, F., Bonnaud, L., Alexandre, M., Lopez-Cuesta, J.-M., and Dubois, P., 2009, "New prospects in flame retardant polymer materials: from fundamentals to nanocomposites," *Materials science and engineering: R: Reports*, 63(3), pp. 100-125.
- [42] Alaei, M., Arias, P., Sjödin, A., and Bergman, Å., 2003, "An overview of commercially used brominated flame retardants, their applications, their use patterns in different countries/regions and possible modes of release," *Environment international*, 29(6), pp. 683-689.
- [43] Lu, S.-Y., and Hamerton, I., 2002, "Recent developments in the chemistry of halogen-free flame retardant polymers," *Progress in polymer science*, 27(8), pp. 1661-1712.
- [44] Levchik, S. V., and Weil, E. D., 2006, "A review of recent progress in phosphorus-based flame retardants," *Journal of fire sciences*, 24(5), pp. 345-364.
- [45] Qu, L., Zhang, C., Li, P., Dai, X., Xu, T., Sui, Y., Gu, J., and Dou, Y., 2018, "Improved thermal properties of epoxy resin modified with polymethyl methacrylate-microencapsulated phosphorus-nitrogen-containing flame retardant," *RSC Advances*, 8(52), pp. 29816-29829.
- [46] Visakh, P., and Yoshihiko, A., 2015, *Flame retardants: Polymer blends, composites and nanocomposites*, Springer.
- [47] Jineesh, A. G., and Mohapatra, S., 2019, "Thermal Properties of Polymer–Carbon Nanocomposites," *Carbon-Containing Polymer Composites*, Springer, pp. 235-270.
- [48] Du, B., Ma, H., and Fang, Z., 2011, "How nano-fillers affect thermal stability and flame retardancy of intumescent flame retarded polypropylene," *Polymers for Advanced Technologies*, 22(7), pp. 1139-1146.
- [49] Ahmed, L., Zhang, B., Shen, R., Agnew, R. J., Park, H., Cheng, Z., Mannan, M. S., and Wang, Q., 2018, "Fire reaction properties of polystyrene-based nanocomposites using nanosilica and nanoclay as additives in cone calorimeter test," *Journal of Thermal Analysis and Calorimetry*, 132(3), pp. 1853-1865.
- [50] Isitman, N. A., and Kaynak, C., 2010, "Tailored flame retardancy via nanofiller dispersion state: Synergistic action between a conventional flame-retardant and nanoclay in high-impact polystyrene," *Polymer Degradation and Stability*, 95(9), pp. 1759-1768.

- [51] Aydođan, B., and Usta, N., 2019, "Fire behaviour assessment of rigid polyurethane foams containing nanoclay and intumescent flame retardant based on cone calorimeter tests," *Journal of Chemical Technology & Metallurgy*, 54(1), pp. 55-63.
- [52] Wang, S., Gao, R., and Zhou, K., 2019, "The influence of cerium dioxide functionalized reduced graphene oxide on reducing fire hazards of thermoplastic polyurethane nanocomposites," *Journal of colloid and interface science*, 536, pp. 127-134.
- [53] Lee, S., min Kim, H., Seong, D. G., and Lee, D., 2019, "Synergistic improvement of flame retardant properties of expandable graphite and multi-walled carbon nanotube reinforced intumescent polyketone nanocomposites," *Carbon*, 143, pp. 650-659.
- [54] Guo, J., Liu, G., Guo, Y., Tian, L., Bao, X., Zhang, X., Yang, B., and Cui, J., 2019, "Enhanced flame retardancy and smoke suppression of polypropylene by incorporating zinc oxide nanowires," *Journal of Polymer Research*, 26(1), p. 19.
- [55] Liu, J., Wang, W., Yuen, R. K., Gui, Z., and Hu, Y., 2018, "1/2D SnO₂ nanowires on MnO₂ nanosheets hybrid architecture for reducing fire hazards of epoxy nanocomposites," *Composites Part A: Applied Science and Manufacturing*, 107, pp. 461-470.
- [56] Yurddaskal, M., and Celik, E., 2018, "Effect of halogen-free nanoparticles on the mechanical, structural, thermal and flame retardant properties of polymer matrix composite," *Composite Structures*, 183, pp. 381-388.
- [57] Wu, Z. H., Wang, Q., Fan, Q. X., Cai, Y. J., and Zhao, Y. Q., 2018, "Synergistic effect of Nano-ZnO and intumescent flame retardant on flame retardancy of polypropylene/ethylene-propylene-diene monomer composites using elongational flow field," *Polymer Composites*, 19(1), pp. 50-60.
- [58] Gan, I., and Chow, W. S., 2018, "Synthesis of phosphoric acid-treated sugarcane bagasse cellulose nanocrystal and its thermal properties enhancement for poly (lactic acid) nanocomposites," *Journal of Thermoplastic Composite Materials*, p. 0892705718772866.
- [59] Tang, Y., and Lewin, M., 2008, "New aspects of migration and flame retardancy in polymer nanocomposites," *Polymer Degradation and Stability*, 93(11), pp. 1986-1995.
- [60] Wang, X. C., Geng, T., Han, J., Liu, C. T., Shen, C. Y., Turng, L. S., and Yang, H. E., 2018, "Effects of nanoclays on the thermal stability and flame retardancy of microcellular thermoplastic polyurethane nanocomposites," *Polymer Composites*, 39(S3), pp. E1429-E1440.
- [61] Shan, G., Jin, W., Chen, H., Zhao, M., Surampalli, R., Ramakrishnan, A., Zhang, T., and Tyagi, R. D., 2015, "Flame-retardant polymer nanocomposites and their heat-release rates," *Journal of Hazardous, Toxic, and Radioactive waste*, 19(4), p. 04015006.
- [62] Uddin, F., 2013, "Studies in finishing effects of clay mineral in polymers and synthetic fibers," *Advances in Materials Science and Engineering*, 2013.

- [63] Kaynak, C., and Polat, O., 2015, "Influences of nanoclays on the flame retardancy of fiber-filled and unfilled polyamide-6 with and without aluminum diethylphosphinate," *Journal of Fire Sciences*, 33(2), pp. 87-112.
- [64] Kaynak, C., and Ibibikcan, E., 2014, "Contribution of nanoclays to the flame retardancy of polyethylene-based cable insulation materials with aluminum hydroxide and zinc borate," *Journal of Fire Sciences*, 32(2), pp. 121-144.
- [65] Lu, C., Gao, X.-p., Yao, D.-h., Cao, C.-l., and Luo, Y.-j., 2018, "Improving flame retardancy of linear low-density polyethylene/nylon 6 blends via controlling localization of clay and intumescent flame-retardant," *Polymer degradation and stability*, 153, pp. 75-87.
- [66] Aziz, A. A. A., Alauddin, S. M., Salleh, R. M., and Sabet, M., 2012, "Influence of Magnesium Hydroxide/Aluminum Tri-Hydroxide Particle Size on Polymer Flame Retardancy: An Overview," *International Journal of Chemical Engineering and Applications*, 3(6), p. 437.
- [67] Palacios, E., Leret, P., De La Mata, M. J., Fernández, J. F., De Aza, A. H., Rodríguez, M. A., and Rubio-Marcos, F., 2016, "Self-forming 3D core-shell ceramic nanostructures for halogen-free flame retardant materials," *ACS applied materials & interfaces*, 8(14), pp. 9462-9471.
- [68] Xi, W., Qian, L., and Li, L., 2019, "Flame Retardant Behavior of Ternary Synergistic Systems in Rigid Polyurethane Foams," *Polymers*, 11(2), p. 207.
- [69] Lou, F., Wu, K., Wang, Q., Qian, Z., Li, S., and Guo, W., 2019, "Improved Flame-Retardant and Ceramifiable Properties of EVA Composites by Combination of Ammonium Polyphosphate and Aluminum Hydroxide," *Polymers*, 11(1), p. 125.
- [70] Dumazert, L., Rasselet, D., Pang, B., Gallard, B., Kennouche, S., and Lopez-Cuesta, J. M., 2018, "Thermal stability and fire reaction of poly (butylene succinate) nanocomposites using natural clays and FR additives," *Polymers for Advanced Technologies*, 29(1), pp. 69-83.
- [71] Lam, Y., Kan, C., and Yuen, C., 2011, "Effect of zinc oxide on flame retardant finishing of plasma pre-treated cotton fabric," *Cellulose*, 18(1), pp. 151-165.
- [72] Samanta, A. K., Bhattacharyya, R., Jose, S., Basu, G., and Chowdhury, R., 2017, "Fire retardant finish of jute fabric with nano zinc oxide," *Cellulose*, 24(2), pp. 1143-1157.
- [73] Termine, J. D., Kleinman, H. K., Whitson, S. W., Conn, K. M., McGarvey, M. L., and Martin, G. R., 1981, "Osteonectin, a bone-specific protein linking mineral to collagen," *Cell*, 26(1), pp. 99-105.
- [74] Qu, H., Wu, W., Jiao, Y., and Xu, J., 2005, "Thermal behavior and flame retardancy of flexible poly (vinyl chloride) treated with Al (OH) 3 and ZnO," *Polymer international*, 54(11), pp. 1469-1473.

- [75] Czimeczik, C. I., Preston, C. M., Schmidt, M. W., Werner, R. A., and Schulze, E.-D., 2002, "Effects of charring on mass, organic carbon, and stable carbon isotope composition of wood," *Organic Geochemistry*, 33(11), pp. 1207-1223.
- [76] Shen, D., Xiao, R., Gu, S., and Zhang, H., 2013, "The overview of thermal decomposition of cellulose in lignocellulosic biomass," *Cellulose-Biomass Conversion*, InTech.
- [77] Chen, L., Wang, Q., Hirth, K., Baez, C., Agarwal, U. P., and Zhu, J., 2015, "Tailoring the yield and characteristics of wood cellulose nanocrystals (CNC) using concentrated acid hydrolysis," *Cellulose*, 22(3), pp. 1753-1762.
- [78] Wooten, J. B., Seeman, J. I., and Hajaligol, M. R., 2004, "Observation and characterization of cellulose pyrolysis intermediates by ^{13}C CPMAS NMR. A new mechanistic model," *Energy & fuels*, 18(1), pp. 1-15.
- [79] Hajaligol, M., Waymack, B., and Kellogg, D., 2001, "Low temperature formation of aromatic hydrocarbon from pyrolysis of cellulosic materials," *Fuel*, 80(12), pp. 1799-1807.
- [80] Khelfa, A., Fingueneisel, G., Auber, M., and Weber, J., 2008, "Influence of some minerals on the cellulose thermal degradation mechanisms," *Journal of Thermal Analysis and Calorimetry*, 92(3), pp. 795-799.
- [81] Broido, A., "Kinetics of solid-phase cellulose pyrolysis," *Proc. Symposium on Thermal Uses and Properties of Carbohydrates and Lignins*, San Francisco, Calif.(USA), 1976, Academic Press.
- [82] Boday, D. J., Kuczynski, J., and Wertz, J. T., 2017, "Flame retardant modified cellulosic nanomaterials (FR-CNs) prepared using phosphorus-containing monomers," Google Patents.
- [83] Hao, X., Mou, K., Jiang, X., and Cha, R., 2017, "High-value Applications of Nanocellulose," *Paper and Biomaterials*, 2(4), pp. 58-64.
- [84] Farooq, M., Sipponen, M. H., Seppälä, A., and Österberg, M., 2018, "Eco-friendly Flame-Retardant Cellulose Nanofibril Aerogels by Incorporating Sodium Bicarbonate," *ACS applied materials & interfaces*, 10(32), pp. 27407-27415.
- [85] Carosio, F., Cuttica, F., Medina, L., and Berglund, L. A., 2016, "Clay nanopaper as multifunctional brick and mortar fire protection coating—Wood case study," *Materials & Design*, 93, pp. 357-363.
- [86] Fenimore, C. P., and Martin, F. J., 1966, "Flammability of polymers," *Combustion and Flame*, 10(2), pp. 135-139.
- [87] Gou, J., and Tang, Y., 2011, "Flame retardant polymer nanocomposites," *Multifunctional Polymer Nanocomposites*, pp. 309-336.

- [88] Morgan, A. B., and Bundy, M., 2007, "Cone calorimeter analysis of UL-94 V-rated plastics," *Fire and Materials: An International Journal*, 31(4), pp. 257-283.
- [89] Babrauskas, V., 2016, "The cone calorimeter," *SFPE handbook of fire protection engineering*, Springer, pp. 952-980.
- [90] Schartel, B., and Hull, T. R., 2007, "Development of fire-retarded materials—interpretation of cone calorimeter data," *Fire and Materials: An International Journal*, 31(5), pp. 327-354.
- [91] Seo, D. K., Park, S. S., Hwang, J., and Yu, T.-U., 2010, "Study of the pyrolysis of biomass using thermo-gravimetric analysis (TGA) and concentration measurements of the evolved species," *Journal of Analytical and Applied Pyrolysis*, 89(1), pp. 66-73.
- [92] He, Y., 2004, "Preparation of polyaniline/nano-ZnO composites via a novel Pickering emulsion route," *Powder Technology*, 147(1-3), pp. 59-63.
- [93] Xu, X., Liu, F., Jiang, L., Zhu, J., Haagenson, D., and Wiesenborn, D. P., 2013, "Cellulose nanocrystals vs. cellulose nanofibrils: a comparative study on their microstructures and effects as polymer reinforcing agents," *ACS applied materials & interfaces*, 5(8), pp. 2999-3009.
- [94] de Graaf, R. A., Karman, A. P., and Janssen, L. P., 2003, "Material properties and glass transition temperatures of different thermoplastic starches after extrusion processing," *Starch-Stärke*, 55(2), pp. 80-86.
- [95] Zhang, Q., Yi, W., Li, Z., Wang, L., and Cai, H., 2018, "Mechanical properties of rice husk biochar reinforced high density polyethylene composites," *Polymers*, 10(3), p. 286.
- [96] Chuah, K. P., Gan, S., and Chee, K., 1999, "Determination of Avrami exponent by differential scanning calorimetry for non-isothermal crystallization of polymers," *Polymer*, 40(1), pp. 253-259.
- [97] Pereira, A. G., Gouveia, R. F., de Carvalho, G. M., Rubira, A. F., and Muniz, E. C., 2009, "Polymer blends based on PEO and starch: Miscibility and spherulite growth rate evaluated through DSC and optical microscopy," *Materials Science and Engineering: C*, 29(2), pp. 499-504.
- [98] Nagalakshmaiah, M., Pignon, F., El Kissi, N., and Dufresne, A., 2016, "Surface adsorption of triblock copolymer (PEO-PPO-PEO) on cellulose nanocrystals and their melt extrusion with polyethylene," *RSC Advances*, 6(70), pp. 66224-66232.
- [99] Li, J., Song, Z., Li, D., Shang, S., and Guo, Y., 2014, "Cotton cellulose nanofiber-reinforced high density polyethylene composites prepared with two different pretreatment methods," *Industrial Crops and Products*, 59, pp. 318-328.
- [100] Samsudin, D., Ismail, H., Othman, N., and Hamid, Z. A. A., 2016, "Comparative study of glut palmitate salt and polyethylene grafted maleic anhydride compatibilizer on the properties of silica filled high-density polyethylene composites," *Polymer Testing*, 52, pp. 104-110.

- [101] Mehrabzadeh, M., Kamal, M. R., and Quintanar, G., 2009, "Maleic anhydride grafting onto HDPE by in situ reactive extrusion and its effect on intercalation and mechanical properties of HDPE/clay nanocomposites." *Iranian polymer journal*, 18(10), PP.833-842.
- [102] Manaila, E., Stelescu, M. D., Craciun, G., and Surdu, L., 2014, "Effects of benzoyl peroxide on some properties of composites based on hemp and natural rubber," *Polymer bulletin*, 71(8), pp. 2001-2022.
- [103] Guo, X.-X., Hu, W., Liu, Y., Sun, S.-Q., Gu, D.-C., He, H., Xu, C.-H., and Wang, X.-C., 2016, "Rapid determination and chemical change tracking of benzoyl peroxide in wheat flour by multi-step IR macro-fingerprinting," *Spectrochimica Acta Part A: Molecular and Biomolecular Spectroscopy*, 154, pp. 123-129.
- [104] Oromiehie, A., Ebadi-Dehaghani, H., and Mirbagheri, S., 2014, "Chemical modification of polypropylene by maleic anhydride: melt grafting, characterization and mechanism," *International Journal of Chemical Engineering and Applications*, 5(2), p. 117.
- [105] Sato, A., Kabusaki, D., Okumura, H., Nakatani, T., Nakatsubo, F., and Yano, H., 2016, "Surface modification of cellulose nanofibers with alkenyl succinic anhydride for high-density polyethylene reinforcement," *Composites Part A: Applied Science and Manufacturing*, 83, pp. 72-79.
- [106] Kai, X., Yang, T., Shen, S., and Li, R., 2019, "TG-FTIR-MS study of synergistic effects during co-pyrolysis of corn stalk and high-density polyethylene (HDPE)," *Energy Conversion and Management*, 181, pp. 202-213.
- [107] Hokkanen, S., Bhatnagar, A., and Sillanpää, M., 2016, "A review on modification methods to cellulose-based adsorbents to improve adsorption capacity," *Water research*, 91, pp. 156-173.
- [108] Zhang, K., Zong, L., Tan, Y., Ji, Q., Yun, W., Shi, R., and Xia, Y., 2016, "Improve the flame retardancy of cellulose fibers by grafting zinc ion," *Carbohydrate polymers*, 136, pp. 121-127.
- [109] Shojaeiarani, J., Bajwa, D. S., and Stark, N. M., 2018, "Green esterification: A new approach to improve thermal and mechanical properties of poly (lactic acid) composites reinforced by cellulose nanocrystals," *Journal of Applied Polymer Science*, p. 46468.
- [110] Lu, P., and Hsieh, Y.-L., 2010, "Preparation and properties of cellulose nanocrystals: rods, spheres, and network," *Carbohydrate polymers*, 82(2), pp. 329-336.
- [111] Grigoriadou, I., Pavlidou, E., Paraskevopoulos, K. M., Terzopoulou, Z., and Bikiaris, D. N., 2018, "Comparative study of the photochemical stability of HDPE/Ag composites," *Polymer degradation and stability*, 153, pp. 23-36.
- [112] Yatigala, N. S., Bajwa, D. S., and Bajwa, S. G., 2018, "Compatibilization improves physico-mechanical properties of biodegradable biobased polymer composites," *Composites Part A: Applied Science and Manufacturing*, 107, pp. 315-325.

- [113] Rimal, S., Rowe, R., and Bathurst, R., 2007, "Durability of fluorinated high density polyethylene (f-HDPE) geomembrane exposed to hydrocarbons in the arctic," 60th Canadian G.
- [114] Lu, J. Z., Wu, Q., and McNabb, H. S., 2007, "Chemical coupling in wood fiber and polymer composites: a review of coupling agents and treatments," *Wood and fiber science*, 32(1), pp. 88-104.
- [115] Bakkal, M., Bodur, M. S., Berkalp, O. B., and Yilmaz, S., 2012, "The effect of reprocessing on the mechanical properties of the waste fabric reinforced composites," *Journal of Materials Processing Technology*, 212(11), pp. 2541-2548.
- [116] Pinheiro, L., Chinelatto, M., and Canevarolo, S., 2004, "The role of chain scission and chain branching in high density polyethylene during thermo-mechanical degradation," *Polymer Degradation and Stability*, 86(3), pp. 445-453.
- [117] Johnston, R. T., and Morrison, E. J., 1993, "Thermal scission and cross-linking during polyethylene melt processing," *Polymer Durability: Degradation, Stabilization, and Lifetime Prediction*, pp. 651-682.
- [118] Hinsken, H., Moss, S., Pauquet, J.-R., and Zweifel, H., 1991, "Degradation of polyolefins during melt processing," *Polymer degradation and stability*, 34(1-3), pp. 279-293.
- [119] Muniyandi, S. K., Sohaili, J., and Hassan, A., 2016, "Accelerated weathering properties of compatibilized composites made from recycled HDPE and nonmetallic printed circuit board waste," *Journal of Applied Polymer Science*, 133(11).
- [120] Shojaeiarani, J., Bajwa, D. S., Stark, N. M., and Bajwa, S. G., 2019, "Rheological properties of cellulose nanocrystals engineered polylactic acid nanocomposites," *Composites Part B: Engineering*, 161, pp. 483-489.
- [121] Mohanty, S., Verma, S. K., and Nayak, S. K., 2006, "Dynamic mechanical and thermal properties of MAPE treated jute/HDPE composites," *Composites Science and Technology*, 66(3), pp. 538-547.
- [122] Mozumder, M. S., Mourad, A.-H. I., Mairpady, A., Pervez, H., and Haque, M. E., 2018, "Effect of TiO₂ Nanofiller Concentration on the Mechanical, Thermal and Biological Properties of HDPE/TiO₂ Nanocomposites," *Journal of Materials Engineering and Performance*, 27(5), pp. 2166-2181.
- [123] Iskoe, J., Lange, F., and Diaz, E., 1976, "Effect of selected impurities on the high temperature mechanical properties of hot-pressed silicon nitride," *Journal of Materials Science*, 11(5), pp. 908-912.
- [124] Wang, Y., Cheng, S., Wei, Q., Ma, E., Nieh, T., and Hamza, A., 2004, "Effects of annealing and impurities on tensile properties of electrodeposited nanocrystalline Ni," *Scripta Materialia*, 51(11), pp. 1023-1028.

- [125] Jun, D., Guomin, Z., Mingzhu, P., Leilei, Z., Dagang, L., and Rui, Z., 2017, "Crystallization and mechanical properties of reinforced PHBV composites using melt compounding: Effect of CNCs and CNFs," *Carbohydrate polymers*, 168, pp. 255-262.
- [126] Shojaeiarani, J., Hosseini-Farid, M., and Bajwa, D., 2019, "Modeling and Experimental Verification of Nonlinear Behavior of Cellulose Nanocrystals Reinforced Poly (Lactic Acid) Composites," *Mechanics of Materials*, 135, pp. 77-87.
- [127] da Silva, J. M., Coutinho, S. V., Diniz, R. K., Almeida, A. N., Lima, M. E., and de C. Fim, F., "Evaluation of the Mechanical and Thermal Properties of Blended (HDPE/UHMWPE) Nanocomposites with Graphite Nanosheets (GNS)," *Proc. Macromolecular Symposia*, Wiley Online Library, p. 1800017.
- [128] De Menezes, B., Ferreira, F., Silva, B., Simonetti, E., Bastos, T., Cividanes, L., and Thim, G., 2018, "Effects of octadecylamine functionalization of carbon nanotubes on dispersion, polarity, and mechanical properties of CNT/HDPE nanocomposites," *Journal of materials science*, 53(20), pp. 14311-14327.
- [129] Ferreira, F., Menezes, B., Franceschi, W., Ferreira, E., Lozano, K., Cividanes, L., Coutinho, A., and Thim, G., 2017, "Influence of carbon nanotube concentration and sonication temperature on mechanical properties of HDPE/CNT nanocomposites," *Fullerenes, Nanotubes and Carbon Nanostructures*, 25(9), pp. 531-539.
- [130] Oliveira de Castro, D., Frollini, E., Ruvolo-Filho, A., and Dufresne, A., 2015, "'Green polyethylene' and curauá cellulose nanocrystal based nanocomposites: Effect of vegetable oils as coupling agent and processing technique," *Journal of Polymer Science Part B: Polymer Physics*, 53(14), pp. 1010-1019.
- [131] da Cruz, K. Z. C., Casagrande, A. C., and Casagrande Jr, O. L., 2017, "High-density polyethylene/expanded graphite nanocomposites produced by polymerization-filling technique using an industrial heterogeneous catalyst," *Journal of Polymer Science Part A: Polymer Chemistry*, 55(7), pp. 1260-1267.
- [132] Novo, L. P., da Silva Curvelo, A. A., and Carvalho, A. J. F., 2018, "Nanocomposites of acid free CNC and HDPE: Dispersion from solvent driven by fast crystallization/gelation," *Journal of Molecular Liquids*, 266, pp. 233-241.
- [133] Salleh, F. M., Hassan, A., Yahya, R., Mohd Isa, M. R., and Lafia-Araga, R. A., 2018, "Physico-thermal properties of kenaf fiber/high-density polyethylene/maleic anhydride compatibilized composites," *High Performance Polymers*, 30(8), pp. 900-910.
- [134] Rezanavaz, R., Razavi Aghjeh, M., and Babaluo, A., 2010, "Rheology, morphology, and thermal behavior of HDPE/clay nanocomposites," *Polymer Composites*, 31(6), pp. 1028-1036.
- [135] Swain, S. K., and Isayev, A. I., 2007, "Effect of ultrasound on HDPE/clay nanocomposites: rheology, structure and properties," *Polymer*, 48(1), pp. 281-289.

- [136] Mir, S., Yasin, T., Siddiqi, H. M., and Murtaza, G., 2017, "Thermal, rheological, mechanical and morphological behavior of high density polyethylene and carboxymethyl cellulose blend," *Journal of Polymers and the Environment*, 25(4), pp. 1011-1020.
- [137] Ching, Y. C., Ali, M. E., Abdullah, L. C., Choo, K. W., Kuan, Y. C., Julaihi, S. J., Chuah, C. H., and Liou, N.-S., 2016, "Rheological properties of cellulose nanocrystal-embedded polymer composites: A review," *Cellulose*, 23(2), pp. 1011-1030.
- [138] Mir, S., Yasin, T., Halley, P. J., Siddiqi, H. M., and Nicholson, T., 2011, "Thermal, rheological, mechanical and morphological behavior of HDPE/chitosan blend," *Carbohydrate Polymers*, 83(2), pp. 414-421.
- [139] Shojaeiarani, J., Bajwa, D., Rehovsky, C., Bajwa, S., and Vahidi, G., 2019, "Deterioration in the Physico-Mechanical and Thermal Properties of Biopolymers Due to Reprocessing," *Polymers*, 11(1), p. 58.
- [140] Shojaeiarani, J., Bajwa, D. S., and Stark, N. M., 2018, "Spin-coating: A new approach for improving dispersion of cellulose nanocrystals and mechanical properties of poly (lactic acid) composites," *Carbohydrate polymers*, 190, pp. 139-147.
- [141] Liu, W., Wang, D., Zhang, Y., Bai, T., and Li, J., 2018, "Flammability and flame-retardant mechanism of high density polyethylene/wood fiber/modified ammonium polyphosphate composite," *Polymer Composites*, 39(4), pp. 1192-1199.
- [142] Yang, X., and Zhang, W., 2019, "Flame Retardancy of Wood-Polymeric Composites," *Polymer-Based Multifunctional Nanocomposites and Their Applications*, Elsevier, pp. 285-317.
- [143] Apostolopoulou, N., Romeos, A., Hinopoulos, G., Perrakis, K., and Panidis, T., 2018, "Considerations on reaction to fire tests of polyethylene foam with a cone calorimeter apparatus," *Journal of Fire Sciences*, 36(3), pp. 240-255.
- [144] Zhang, J., Mei, C., Huang, R., Xu, X., Lee, S., Kim, B. J., and Wu, Q., 2018, "Comparative mechanical, fire-retarding, and morphological properties of high-density polyethylene/(wood flour) composites with different flame retardants," *Journal of Vinyl and Additive Technology*, 24(1), pp. 3-12.
- [145] Qiu, W., Endo, T., and Hirotsu, T., 2005, "A novel technique for preparing of maleic anhydride grafted polyolefins," *European polymer journal*, 41(9), pp. 1979-1984.